ChemInform Abstract: Gas Solubility in Ionic Liquids

ARTICLE *in* CHEMINFORM · MARCH 2014

Impact Factor: 0.74 · DOI: 10.1002/chin.201410266

3 AUTHORS:

Zhigang Lei

Beijing University of Chemical Technology

106 PUBLICATIONS **1,486** CITATIONS

SEE PROFILE

Chengna Dai

Beijing University of Chemical Technology

26 PUBLICATIONS **216** CITATIONS

SEE PROFILE

Biaohua Chen

Beijing University of Chemical Technology

170 PUBLICATIONS **1,793** CITATIONS

SEE PROFILE

CHEMICAL REVIEWS

Review

pubs.acs.org/CR

Gas Solubility in Ionic Liquids

Zhigang Lei, Chengna Dai, and Biaohua Chen*

State Key Laboratory of Chemical Resource Engineering, Beijing University of Chemical Technology, Box 266, Beijing, 100029, China

Supporting Information

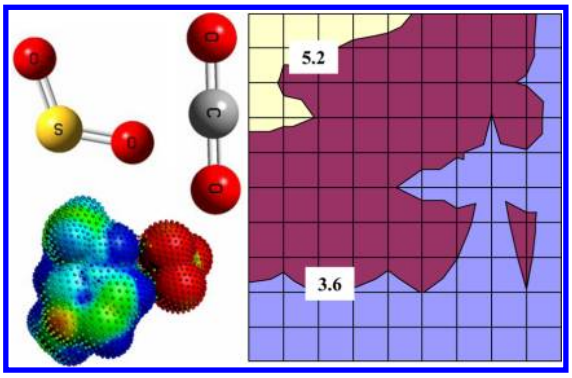

CONTENTS

Received: December 13, 2012
Published: November 6, 2013

   dx.doi.org/10.1021/cr300497a | *Chem. Rev.* 2014, 114, 1289–1326

1. INTRODUCTION

In 1966 and 1977, *Chemical Reviews* published two reviews on the subject of "Gas Solubility in Liquids".[1,2] However, the term "Liquids" did not include ionic liquids (ILs) because at that time there were very few chemists who had ever heard of ILs. Recently, ILs have received significant attention due to their unique properties, such as nonvolatility, high chemical stability, and easy operation at liquid state, and thus become good alternatives to traditional liquid solvents.[3−10] Accordingly, solubility data of gases in ILs are very important in assessing a variety of chemical processes. For instance, in gas separations, the amount of cycled ILs and the number of theoretical stages required for fulfilling a specific separation in an absorption column can be derived from the solubility data. In many gas−liquid reactions such as alkylation, hydrogenation, hydroformylations, and Diels−Alder addition involving mass transfer of gases into the IL phase, gas solubility data are also needed to incorporate into the reaction kinetic equations which are necessary for design, optimization, and controlling the chemical reactor.[11−18] Other potential applications requiring knowledge of pertinent gas solubility in ILs are the gas antisolvent (GAS) process where a condensable gas alters the IL strength that leads to precipitation of a dissolved solute,[19−22] absorbing refrigerant gases (e.g., hydrofluorocarbons) in the absorption cooling cycles,[23−27] material processing as supported liquid membranes (SLMs),[28−40] and so forth.

In the past decade, more and more ILs with different types of cations and anions have been synthesized in the laboratory, and the solubility data of gases in ILs have also been tested individually by many researchers but not systemically. Therefore, a comprehensive database on the solubility data of various gases in ILs exhaustively colleted from references by the end of August 2013 is provided in the Supporting Information as a spreadsheet file that allows any reader to use conveniently. In this review, the impetus for establishing the database is 3-fold. First, we can identify the structure−property relation between molecular structures of ILs (or gases) and gas solubility, thus understanding the molecular interactions like electrostatic, hydrogen-bonding, and van der Waals forces. Second, we are aware that for a given system not all of the solubility data coming from different data sources are reliable. In particular for gases like oxygen, nitrogen, and hydrogen, solubility discrepancies were found to be very large, sometimes more than 100%.[41−43] In this case data accuracy should be evaluated. Third, extensive experimental data can be used to correlate and expand the group parameters of predictive thermodynamic models. As we know, typical ILs are composed of a large organic cation and an inorganic polyatomic anion, and thus, there is virtually no limit in the possible combinations of cations and anions. It is time consuming and expensive to measure the solubility data for every new system only through experiments. Therefore, the aspiration for predictive thermodynamic models is so great for scientists and engineers attempting to conduct research and applications on ILs.

The predictive thermodynamic models mean that physical properties of ILs in the mixtures, such as vapor−liquid equilibria (VLE), solubility, and selectivity can be predicated provided that molecular structures or physical properties of pure ILs are known. From a scientific viewpoint, it is highly desirable to develop predictive thermodynamic models to identify the structure−property relation and rapidly screen suitable ILs so as to decrease the amount of experimental work; from a technological viewpoint, predictive thermodynamic models can provide the information on the PVT (pressure−volume−temperature) relation or phase equilibria of the systems, which are necessary for establishing the rigorous process models for specific application. Predictive thermodynamic models are divided into two types:

(i) Activity coefficient models including UNIFAC (universal quasichemical functional-group activity coefficients)-based models, COSMO (conductor-like screening model)-based models, and the RST (regular solution theory) model;

(ii) Equations of state models including GCNLF EOS (group contribution nonrandom lattice−fluid equation of state), GC EOS (group contribution equation of state), and SAFT-based EOS (statistical associating fluid theory-based equation of state). Equations of state are preferred over activity coefficient models for calculation of phase equilibria in that they can disclose the dependence of phase volume on pressure, which is especially important in estimating the volume expansion and solvent strength in the GAS process.

In this review, we would like to address the solubility of CO_2 (carbon dioxide) in ILs, which has been extensively studied in the past decade, and should arouse a common interest in the community of chemistry and chemical engineering. However, we will not simply seek to present these solubility data. The characteristics of this review are listed as follows.

(i) Not only is the focus on identifying the structure−property relation by combination of experiments and predictive thermodynamic models but also the factors influencing the CO_2 solubility (e.g., the existence of other gases and impurities) are addressed, reflecting the real situation in many chemical processes.

(ii) A discussion on the CO_2 solubility on mixed solvents containing IL (i.e., IL + IL, organic solvent + IL) which integrates the advantages of each solvent is covered, offering interested readers some useful introduction on multiplying the possibility of creating suitable solvents.

(iii) It is known that in the Rectisol process using methanol as the separating agent the operating temperature is as low as 228.15 K because the CO_2 content in syngas must be purged up to several ppm level.[44] Otherwise, side reactions will take place downstream.[45,46] Then, why cannot ILs be used at low temperatures? Actually, for some common ILs such as $[BMIM]^+[BF_4]^-$, $[OMIM]^+[PF_6]^-$, $[OMIM]^+[Cl]^-$, and so on, their melting points are very low. Moreover, when pressurized CO_2 is added into ILs, it will induce a melting point depression (MPD), leading to a large number of ILs suitable for this separation problem. The solubility of CO_2 in ILs at low temperatures down to 228.15 K is considered in this review. More importantly, we will compare CO_2 solubility between low and high temperatures and thus open a larger temperature window for application of ILs in separation and/or reaction processes. It is noted that a high CO_2 solubility at low

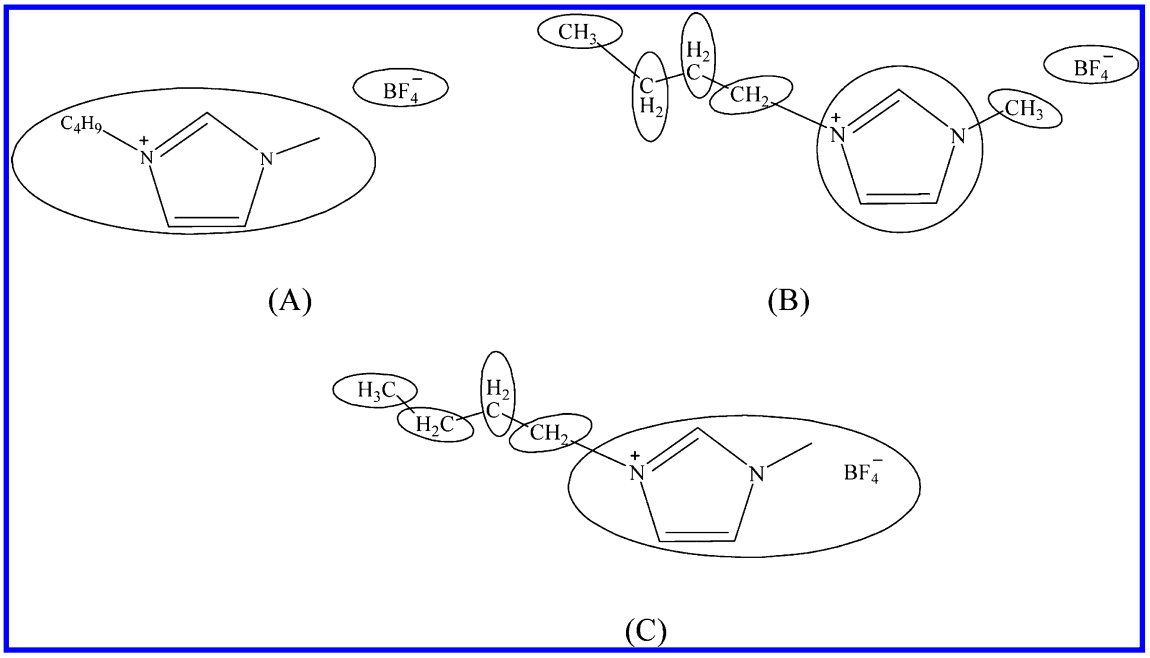

Figure 1. Decomposition of UNIFAC functional groups in three approaches.

temperatures may counteract the increase of viscosity of pure IL in the mixture.

(iv) Various microscopic solubility mechanisms are summarized to provide a deep insight into the nature of interaction of CO_2 with ILs at the molecular level.

(v) Information on solubility data, Henry's law constants, experimental methods, and references as well as predicted results by different predictive thermodynamic models is provided in detail in the database.

Compared with the hot topic on measuring the solubility of CO_2 in ILs, studies on SO_2 (sulfur dioxide) solubility seem to be fewer. However, this never means that these data are not important. Actually, SO_2 is so detrimental to the environment and humans that it should be captured from industrial flue gases. During solubility measurement, a series of special precautions should be taken carefully in laboratories, thus making it difficult to carry out the experimental study. Therefore, we feel that these data collected in this review are precious and discussed as a separate chapter, with a more detailed focus on clarifying the structure−property relation.

This is the first review devoted to providing an easy-to-read and comprehensive comment on the solubility of gases in ILs and covering the issues on experimental methods, experimental data, and predictive thermodynamic models. It is beyond our scope to review how to synthesize the specified ILs, and the ILs concerned in this review are confined to room-temperature ILs (RTILs), task-specific ILs (TSILs), and poly(ionic liquid)s (PILs) since they are commonly encountered in the family of ILs, while for SLMs the permeability of gases can be represented by solubility and diffusion coefficients in ILs regardless of the porous polymer or inorganic supports. The contents are arranged in the series of predictive thermodynamic models, experimental methods, CO_2 solubility, SO_2 solubility, and other gases' solubility in ILs step by step. We first introduce the predictive thermodynamic models developed in the past decade in section 2, and their applications have been extended from traditional organic solvents or polymers to ILs. Then, the static and dynamic experimental methods for measuring the solubility of gases in nonvolatile ILs are introduced in section 3 along with the thermodynamic consistency test for experimental solubility data. The structure−property relation for the solubility of CO_2 in ILs is emphasized by means of the combination of experiments and predictive thermodynamic models in section 4 as well as tuning the solubility by use of mixed solvents containing ILs. Afterward, the solubility of SO_2 in ILs is summarized as well as comparison with the predicted results by COSMO-RS (conductor-like screening model for real solvents) model to explore the structure−property relation, and the solubility mechanism is clarified in section 5. The solubility of other gases in ILs is affected by pressure, temperature, and the combination of anions and cations, and the general solubility trend is discussed in section 6. Finally, concluding remarks are given in section 7. The abbreviations, names, and chemical structure of cations, anions, and HFC family gases throughout this review are given in Table S1, Supporting Information.

2. PREDICTIVE THERMODYNAMIC MODELS

2.1. UNIFAC Model

2.1.1. Model Equations. Although the UNIFAC model is very familiar to many chemists and chemical engineers, it has been extended to the solute−IL and gas−IL systems only recently.[23,47−56] The model has a combinatorial contribution to the activity coefficient, i.e., $\ln \gamma_i^C$, essentially due to differences in the size and shape of the molecules, and a residual contribution, i.e., $\ln \gamma_i^R$, essentially due to energetic interactions, and is written as

$$\ln \gamma_i = \ln \gamma_i^C + \ln \gamma_i^R \quad (1)$$

The combinatorial part $\ln \gamma_i^C$ contains the group parameters R_k and Q_k and is derived by

$$\ln \gamma_i^C = 1 - V_i + \ln V_i - 5q_i\left(1 - \frac{V_i}{F_i} + \ln\left(\frac{V_i}{F_i}\right)\right) \quad (2)$$

dx.doi.org/10.1021/cr300497a | Chem. Rev. 2014, 114, 1289−1326

$$F_i = \frac{q_i}{\sum_j q_j x_j};\ V_i = \frac{r_i}{\sum_j r_j x_j} \tag{3}$$

$$r_i = \sum_k \nu_k^{(i)} R_k;\ q_i = \sum_k \nu_k^{(i)} Q_k \tag{4}$$

$$R_k = \frac{V_k \times N_A}{V_{VW}},\ Q_k = \frac{A_k \times N_A}{A_{VW}} \tag{5}$$

where $\nu_k^{(i)}$, always an integer, is the number of groups of type k in molecule i, V_k and A_k are group volume and surface area, respectively, V_{VW} (15.17 $cm^3 \cdot mol^{-1}$) and A_{VW} (2.5×10^9 $cm^2 \cdot mol^{-1}$) are standard segment volume and surface area as suggested by Bondi,[57] respectively, and N_A is Avogadro's number (6.023×10^{23} mol^{-1}).

The residual part $\ln \gamma_i^R$ can be obtained by

$$\ln \gamma_i^R = \sum_k \nu_k^{(i)} [\ln \Gamma_k - \ln \Gamma_k^{(i)}] \tag{6}$$

$$\ln \Gamma_k = Q_k [1 - \ln(\sum_m \theta_m \psi_{mk}) - \sum_m (\theta_m \psi_{km} / \sum_n \theta_n \psi_{nm})] \tag{7}$$

$$\theta_m = \frac{Q_m X_m}{\sum_n Q_n X_n};\ X_m = \frac{\sum_i \nu_m^{(i)} x_i}{\sum_i \sum_k \nu_k^{(i)} x_i} \tag{8}$$

where Γ_k is the group residual activity coefficient and $\Gamma_k^{(i)}$ is the residual activity coefficient of group k in a reference solution containing only molecules of type i. X_m is the fraction of group m in the mixture. The group interaction parameter ψ_{nm} is expressed as

$$\psi_{nm} = \exp[-(a_{nm}/T)] \tag{9}$$

where T is the absolute temperature, a_{nm} is the temperature-independent parameter for each pair of functional groups n and m, and $a_{nm} \neq a_{nm}$.

In order to apply the UNIFAC and other predictive thermodynamic models associated with the group contribution method it is required to divide one IL molecule into separate functional groups. By far, there have been three approaches for this purpose. (i) The IL molecule is divided into one cation group and one anion group (see Figure 1A).[49,50] Evidently, this approach does not reflect the influence of the structural variation of substitutents on the cations (or anions) on the thermodynamic properties. (ii) The IL molecule is divided into several groups with the imidazolium or pyrrolidinium ring as a functional group (see Figure 1B).[51−56] Although the structural variation of cations, anions, and substitutents are adequately considered in this approach, the functional groups with electric charge are introduced, and thus, a Debye−Hückel term accounting for long-rang (LR) electrostatic contributions should be added in eq 1 in the same manner as for solvent−solid salt systems described by some researchers.[58−61] (iii) The IL molecule is also divided into several groups, but the skeletons of the cation and anion are treated as an electrically neutral group.[48,62−66] For example, $[BMIM]^+[BF_4]^-$ is composed of one CH_3 group, three CH_2 groups, and one $[MIM][BF_4]$ group (see Figure 1C). Moreover, the main group $[MIM][BF_4]$ has two subgroups, i.e., $[MIM][BF_4]$ and $[IM][BF_4]$. The third approach is recommended by more researchers because it remains the original equation form of the UNIFAC model.

2.1.2. Model Parameters

In most cases, the group parameters R_k and Q_k for ILs cannot be directly obtained from the references and have to be determined by the following two methods.

(i) The correlation using molar volumes as proposed by Domańska and Mazurowska[67,68] was used

$$r_i = 0.029281 V_M,\ q_i = \frac{(z-2) r_i}{z} + \frac{2(1-l_i)}{z} \tag{10}$$

where V_M is the molar volume of ILs at 298.15 K, z is the coordination number, and l_i is the bulk factor. It is known that the molar volumes (or densities) of ILs can be well predicted by such group contribution methods as proposed by Valderrama and Zarricueta,[69] Paduszynski and Domańska,[70] and Ye and Shreeve[71] with an acceptable accuracy of less than 10%. Then, R_k and Q_k for ILs can be derived according to eqs 4 and 5.

(ii) Modern commercial software (e.g., COSMO-RS, ChemOffice, Gaussian 03, and GAMESS 7.1 package) can provide information on the group surface area and volume for ILs for the UNIFAC model.[72−75] Since one group (or molecule) has a charge distribution which forms an electric field, it will polarize the embedding medium which will result in another electric field, given by a charge distribution on the surface of the group shaped cavity. This charge distribution is generated by the quantum mechanical calculation (e.g., COSMO, polarizable continuum model, etc.) in which the surface of the group shaped cavity will be called the group surface, and the corresponding volume will be called the group volume. The concept of a solvent-accessible surface introduced by Delley[76] was used for modeling the cavity by continuous variation of all properties as a function of geometry. As an example, the COSMO surface of group $[BF_4]^-$ with the Delley type of cavity construction is shown in Figure 2, where the small spheres in the Delley surface represent the COSMO surface points that are used for construction of the COSMO surface.

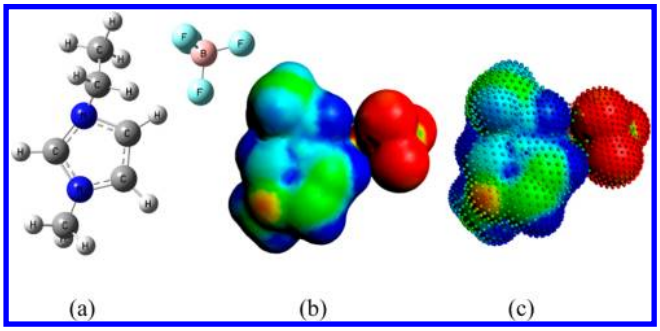

Figure 2. Optimized IL geometric structures (a), COSMO surface with the radius of small spheres equal to zero (b), and Delley surface (c) of $[EMIM]^+[BF_4]^-$. Red part represents positive COSMO charge density; the blue part representts negative COSMO charge density.

Parameters α_{nm} and α_{mn} are determined by fitting the solubility data of gases in ILs, and it is assumed that no appreciable amount of IL is solubilized into the vapor phase. The current UNIFAC parameter matrix is illustrated in Figure 3. In the future development more gas molecules should be added to extend the UNIFAC parameter matrix. The unique advantage of the UNIFAC model is that it can be readily incorporated into some famous simulation software (e.g.,

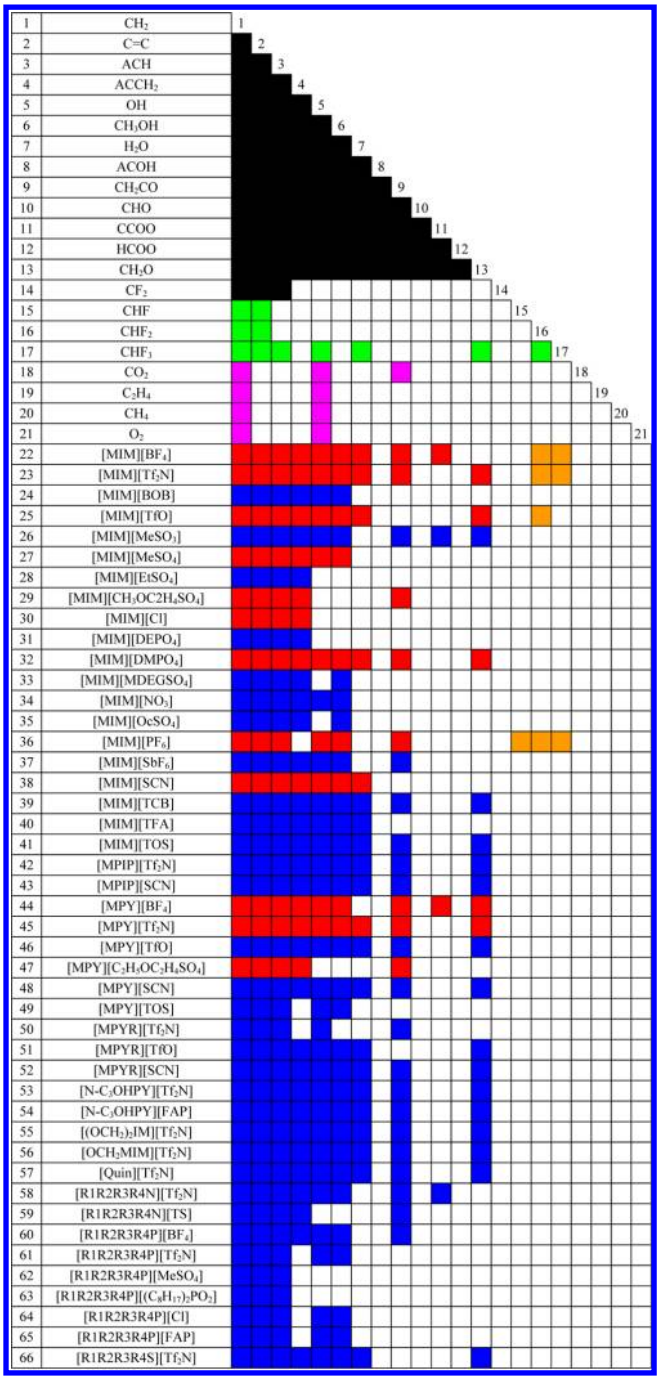

Figure 3. Current UNIFAC parameter matrix for ILs. (Black) Published in ref 77; (purple) published in ref 78; (green) published in ref 79; (red) published in ref 48; (blue) published in ref 80; (orange) published in ref 23; (white) no parameters available.

ASPEN PLUS and PROII) for process design and optimization but with the limitation of parameter availability. Besides, the calculation speed of the UNIFAC model is very quick even on a common computer. However, like all group contribution methods, the UNIFAC model cannot distinguish among isomers because the group proximity effect is not considered.

2.2. COSMO-Based Models

2.2.1. COSMO-RS Model. The COSMO-RS model developed by Klamt et al. is a novel method for predicting thermodynamic properties of pure and mixed liquids on the basis of unimolecular quantum chemical calculations for the respective individual molecules.[81−92] As a priori prediction method, it requires molecular structure as the only information and is independent of experimental data of the systems of interest. Therefore, the COSMO-RS model has received close attention for predicting the solubility of gases in ILs. In this case, the ions are normally treated separately as an electroneutral mixture, and the distinct COSMO files were generated. For a 1:1 IL (i.e., $[A]^+[B]^-$), the activity coefficient of the gas molecule at infinite dilution in IL should be converted by a scaling factor of 0.5 from the ternary system (cation + anion + gas) to the binary system (IL + gas). This also holds for the Henry's law constant, which reflects the magnitude of gas solubility and is calculated as

$$H_{gas} = \gamma^{\infty}_{gas} P^{s}_{gas} \tag{11}$$

where γ^{∞}_{gas} and P^{s}_{gas} are the activity coefficient at infinite dilution and the saturated vapor pressure of gas, respectively. It is worth mentioning that the saturated vapor pressure of gas can be estimated by the COSMO-RS calculation using the gas-phase energy information. Of course, the familiar Antoine and Wagner equations also suffice to calculate the vapor pressure below the critical temperature T_c. Above T_c, they can be extrapolated as a hypothetical vapor pressure.

In the COSMO-RS calculation, an IL molecule may be described either as a single compound or as discrete cation and anion. The latter is normally adopted in order to reduce the calculation time. Thus, the system of gas and IL will be treated as a hypothetical ternary mixture consisting of gas, cation, and anion. Structures of all ions are optimized prior to performing the COSMO-RS calculation. For a 1:1 IL, the solubility of gas in the hypothetical ternary system x^{T}_{gas} can be calculated by

$$x^{T}_{gas} = \frac{n_{gas}}{n_{gas} + n_{cation} + n_{anion}} = \frac{n_{gas}}{n_{gas} + 2n_{IL}} \tag{12}$$

where n_{gas}, n_{cation}, n_{anion}, and n_{IL} are the molar amounts of gas, cation, anion, and IL in the liquid phase, respectively. However, for a binary system of gas and IL, the gas solubility x is defined as

$$x = \frac{n_{gas}}{n_{gas} + n_{IL}} \tag{13}$$

Combining eqs 12 and 13 yields

$$x = \frac{2x^{T}_{gas}}{x^{T}_{gas} + 1} \tag{14}$$

where the gas solubility in the hypothetical ternary mixture is obtained by

$$x^{T}_{gas} = \frac{f_{gas}}{P^{s}_{gas}\gamma^{\infty}_{gas}} \tag{15}$$

where f_{gas} is the gas fugacity gas at the system temperature and pressure.

The predictive capability of the COSMO-RS model for 15 gases in 27 ILs was evaluated by Manan et al.[42] It was found that the predicted results by the COSMO-RS model are only qualitatively consistent with the experimental data collected from the IUPAC database, and a few predicted solubility data expressed in mole fraction of gas in IL even exceed 1.0! This demonstrates that the COSMO-RS model may be used as a tool to identify the structure−property relation and screen the

dx.doi.org/10.1021/cr300497a | Chem. Rev. 2014, 114, 1289−1326

Table 1. COSMO Parameters Used in Several Versions[a]

		COSMO-RS					
parameters	COSMO-SAC[101]	Grensemann and Gmehling[91]	Klamt and Eckert[87]	Klamt et al.[83]	ADF combi1998[103]	ADF (default)[103]	Banerjee et al.[102]
a_{eff}	7.50 Å^2	6.31 Å^2	6.25 Å^2	7.10 Å^2	7.62 Å^2	6.94 Å^2	7.55 Å^2
α'	5950 kJ/mol/Å^2	30.74 kJ/mol	5950 kJ/mol/Å^2	1288 kJ/mol/Å^2	1515 kJ/mol/Å^2	1510 kJ/mol/Å^2	5950 kJ/mol/Å^2
c_{hb}	35 772 kJ/mol/Å^2/e^2	36.52 kJ/mol@298 K	36 700 kJ/mol/Å^4/e^2	7400 kJ/mol/Å^4/e^2	8850 kJ/mol/Å^4/e^2	8850 kJ/mol/Å^2/e^2	34 984 kJ/mol/Å^4/e^2
		33.82 kJ/mol@313 K					
		31.35 kJ/mol@328 K					
σ_{hb}	0.0084 e/Å^2	0.0082 e/Å^2	0.0085 e/Å^2	0.0082 e/Å^2	0.0085 e/Å^2	0.0085 e/Å^2	0.0081 e/Å^2

[a]Reprinted with permission from ref 102 but with correction and addition. Copyright 2006 American Chemical Society.

Table 2. Several Versions of RST Model for Estimating the Gas Solubility[a]

model equation	application
(a) Prausnitz et al.[110]	(1) applied to nonpolar solvents, where δ_1 results from purely dispersion forces
$\frac{1}{x_2} = \frac{f_2^0}{P}\exp\left[\left(\frac{V_2\varphi_1^2}{RT}\right)(\delta_1 - \delta_2)^2\right]$, $\delta_1 = \left(\frac{E^{vap}}{V_1}\right)^{1/2}$	
(b) Scovazzo et al.[107] and Camper et al.[106]	(1) applied to RTILs, where δ_1 results from the product of the entropy of vaporization and melting point temperature
$\ln X_2 = -\frac{V_2(\delta_1 - \delta_2)^2\varphi_1^2}{RT} + \left[\ln\left(\frac{P}{f_2^0}\right) + \ln 2\right]$, $\delta_1 = (K_T T_m/V_1)^{1/2}$	(2) each cation and anion is considered to be an individual molecule in the gas−RTIL dilute solution
where X_2 is expressed as moles of gas per mole RTIL-atm and K_T is a correlation constant (Trounton's rule)	
(c) Camper et al.[111]	(1) applied to spherically symmetrical imidazolium RTILs (number of carbons in the alkyl chain is ≤4)
$\ln[H_{2,1}(\text{atm})] = a + b(\delta_1 - \delta_2)^2$	(2) δ_1 is estimated from the lattice energy densities
where $\delta_1 = [(2.56 \times 10^6(\text{J/mol})z_1z_2(\text{cm}^3/\text{mol})^{1/3}/(V_1)^{4/3})(1 - 0.367(\text{cm}^3/\text{mol})^{1/3}/(V_1)^{1/3})]^{1/2}$, z_1 and z_2 are the charges of the cation and anion, respectively, a and b are constants depending on the specific gas and IL	
(d) Kilaru et al.[109]	(1) applied to the imidazolium-, phosphonium-, and ammonium-based ILs and gases including CO_2, ethylene, propylene, 1-butene, and 1,3-butadiene
$-\ln X_2 = a + b(\delta_1 - \delta_2)^2$, $\delta_1 = \left(\frac{4.78 \times 10^{-8}N_A^{1/3}K_s\sigma}{V_1^{1/3}}\right)^{1/2}$	(2) δ_1 is estimated using surface tension
where σ is the surface tension of IL, V_1 is the molar volume of IL, and K_s is a proportionality constant	
(e) Kilaru and Scovazzo[112] and Moganty and Baltus[113]	(1) applied to the imidazolium-, phosphonium-, and ammonium-based ILs and gases including CO_2, ethylene, propylene, 1-butene, and 1,3-butadiene
$-\ln x_2 = a + b(\delta_1 - \delta_2)^2$, $\delta_1 = \left\{\frac{K_V RT}{V_1}\ln\left[\frac{(1 \times 10^{-9})\mu V_1}{hN_A}\right]\right\}^{1/2}$	(2) δ_1 is estimated using activation energy of viscosity
where x_2 is the mole fraction of gas in IL, μ is the viscosity of IL, h is Plank's constant, and K_V is a proportionality constant	

[a]Reprinted with permission from ref 109 but with addition. Copyright 2006 American Chemical Society.

potential ILs for a specific task. However, care should be taken on the structural variation of methyl substitution at the C(2) position on the 1-alkyl-3-methylimidazolium cations as well as ammonium- and triflate-based ILs due to the sigma profile definitions of these separate ions. The authors thought that the predicted results would be improved, where an IL defined with one ion pair generates only one COSMO file. In order to determine which kind of IL possesses the highest CO_2 solubility for physical absorption, the $[FEP]^-$ anion-based ILs were proposed by Zhang et al.[93] using the COSMO-RS model, while Maiti[94] found that the ILs with all-functionalized-guanidinium cation and $[BF_4]^-$ anion possess a higher CO_2 solubility than the best imidazolium-based IL previously studied.

Palomar et al.[95] went a further step to explore the molecular interaction between CO_2 and IL at the molecular level by means of the COSMO-RS model, which can be used to predict the excess enthalpy of the CO_2−IL liquid mixture expressed by summation of the following three terms which represent the contributions arising from hydrogen bonding, electrostatic interaction, and van der Waals force, respectively.

$$H_m^{E'} = H_m^{E'}(\text{H-bond}) + H_m^{E'}(\text{misfit}) + H_m^{E'}(\text{vdW}) \quad (16)$$

Among these contributions, the van der Waals force between gas and IL molecules is predominant, which is consistent with the previous finding by Monte Carlo (MC) and molecular dynamics (MD) simulations as for $[HMIM]^+[FEP]^-$−CO_2, $[HMIM]^+[Tf_2N]^-$−CO_2, and $[HMIM]^+[PF_6]^-$−CO_2 systems.[96−100]

2.2.2. COSMO-SAC Model. The COSMO-RS model provides better predictions for some systems but poorer predictions for others. In order to improve the prediction accuracy, the COSMO-SAC (COSMO segment activity coefficient) model[101] is proposed as a modification to the COSMO-based activity coefficient model with the same physical picture. The difference of the COSMO-SAC model

dx.doi.org/10.1021/cr300497a | Chem. Rev. 2014, 114, 1289−1326

from the COSMO-RS model is brought out in the following two aspects.

(i) The activity coefficient of solute i in the mixture is given by

$$\ln \gamma_i = n_i \sum_{\sigma_m} p_i(\sigma_m)[\ln \Gamma(\sigma_m) - \ln \Gamma_i(\sigma_m)] + \ln \gamma_i^{C} \quad (17)$$

where n_i is the number of surface segments in a single molecule i, p_i (σ_m) represents the probability of finding a charge segment σ_m, and $\Gamma(\sigma_m)$, and $\Gamma_i(\sigma_m)$ represent the segment activity coefficients in the mixture and pure solute, respectively. The last Staverman−Guggenheim combinatorial term, i.e., ln γ_i^C, which is not included in the COSMO-RS model, is introduced accounting for different sizes and shapes of the molecules.

(ii) The model parameters for the COSMO-SAC and COSMO-RS models with several versions are listed in Table 1, where the ADF default values are optimized parameters for ADF calculations.[104] By these modifications it was verified that the COSMO-SAC model conforms to the thermodynamic consistency better than the COSMO-RS model for the systems not involving ILs.

The influence of the cation and anion on the CO_2 solubility was investigated by Shimoyama and Ito[105] using the COSMO-SAC model. Involved cations are $[EMIM]^+$, $[BMIM]^+$, and $[HMIM]^+$, while the anions are $[BF_4]^-$, $[DCA]^-$, $[TfO]^-$, and $[Tf_2N]^-$. The predicted results by the COSMO-SAC model agree with the experiment data within the relative deviations 20%, and the anion has a much stronger influence on the CO_2 solubility than the cation.

In comparison with the UNIFAC model, COSMO-based models require only a few adjustable element-specific parameters and can distinguish various isomers. The weakness of COSMO-based models is that they often give poor predictions for some important thermodynamic properties.

2.3. RST Model

Scovazzo et al.[106,107] first reported that the RST model can describe the phase behavior of gases in ILs at low pressures satisfactorily and explained why solubility parameters can be reasonably related to the gas solubility in ILs instead of a curve-fitting exercise. This is due to the van der Waals force between gas and IL molecules being predominant, as mentioned above. Therefore, extension of the RST model to the application of gas−IL systems does not violate the assumption that the short-range attractive forces dominate in liquid solvents as imposed by Hildebrand and Scott[108] to define solubility parameters. Several versions of RST models and their corresponding model equations are summarized in Table 2, where subscripts 1 and 2 denote IL and gas molecules, respectively.

One advantage of the RST model is to help guide the molecular design of ILs so as to achieve the desirable gas solubility. It seems that solubility parameters of ILs δ_1 are important in determining the gas solubility when δ_2 is constant for a given gas, that is, as δ_1 decreases, gas solubility increases because $(\delta_1 - \delta_2)^2$ approaches zero, and δ_2 is generally lower than δ_1. Thus, the molecular structures of ILs can be tailored by adding or removing some functional groups to adjust the solubility parameters. An excellent example was demonstrated by Carlisle et al.,[114] who synthesized two types of imidazolium-based ILs containing nitrile and alkyn functional substituents, respectively, and found that inclusion of new functional groups does not increase CO_2 solubility but improves the selectivity of CO_2 to N_2 and CO_2 to CH_4 in some degrees when compared to their nonfunctionalized analogues. On the other hand, since it is tedious to tailor a certain IL through complicated chemical synthesis, we can resort to the mixed ILs which are easier to be bought from chemical markets. In this case, the solubility parameter of a mixed IL is defined as

$$\delta_{mix} = \sum_i \varphi_i \delta_i \quad (18)$$

where ϕ_i is the volume fraction of each IL. The RST model offers a simple method to predict and interpret the gas solubility in ILs as a semiquantitative model at low pressures and near ambient temperature. In this regard, more details have been comprehensively discussed by Bara et al.[115]

Another advantage is giving some theoretical insight into the solute/solvent interactions for CO_2/IL systems. The RST model using the activation energy of viscosity supports the free volume effect rather than the anion effect which is commonly taken on as a primary factor in determining the CO_2 solubility in ILs, because a high coefficient of determination in the linear correlation was obtained by Kilaru and Scovazzo,[112] who investigated a series of ILs with anions having a wide range of electron-donor potential from $[Cl]^-$ to $[BETI]^-$, and the interaction between gas and IL molecules may be negligible when compared to other gas−gas and IL−IL molecular interactions.

2.4. GCNLF EOS

You et al.[116,117] first proposed an approximate nonrandom lattice fluid model for describing phase equilibria of either pure fluids or binary mixtures consisting of simple and complex molecules. Park et al.[118] extended this model to the components which can form a strong hydrogen bond such as amino acids plus water. Later, it was successfully applied to predict the solubility of CO_2 in ILs in conjunction with the group contribution method.[62,63] The equation form of GCNLF EOS is written as

$$\frac{PV_H}{RT} = \frac{z}{2}\ln\left[1 + \left(\frac{q_M}{r_M} - 1\right)\rho\right] - \ln(1-\rho) + \frac{z\beta}{2}\varepsilon_M\theta^2 \quad (19)$$

For a c-component mixture, the following mixing rules are introduced

$$\varepsilon_M = \frac{1}{\theta^2}\left[\sum\sum \theta_i\theta_j\varepsilon_{ij} + \left(\frac{\beta}{2}\right)\sum\sum\sum\sum \theta_i\theta_j\theta_k\theta_l\varepsilon_{ij} \times (\varepsilon_{ij} + 3\varepsilon_{kl} - 2\varepsilon_{ik} - 2\varepsilon_{jk})\right] \quad (20)$$

$$r_M = \sum_{i=1}^{c} x_i r_i, \quad q_M = \sum_{i=1}^{c} x_i q_i \quad (21)$$

When ILs are decomposed into functional groups, the group mixing rules are

$$r_i = \sum_q \nu_i^q r_q^G \quad (22)$$

$$\varepsilon_{ij} = \sum_q \sum_r \theta_i^q \theta_j^r \varepsilon_{qr}^G \quad (23)$$

dx.doi.org/10.1021/cr300497a | Chem. Rev. 2014, 114, 1289−1326

$$\frac{\varepsilon_{qr}^{G}}{k} = \varepsilon_a^G + \varepsilon_b^G(T - T_0) + \varepsilon_c^G\left[T\ln\left(\frac{T_0}{T}\right) + T - T_0\right] \quad (24)$$

$$r_q^G = r_a^G + r_b^G(T - T_0) + r_c^G\left[T\ln\left(\frac{T_0}{T}\right) + T - T_0\right] \quad (25)$$

where T_0, V_H, and z are set to be 298.15 K, 9.75 $cm^3 \cdot mol^{-1}$, and 10, respectively, $\beta = kT$ (k is the Boltzmann constant), ρ is the reduced density, θ is the surface area fraction, ν_i^q is the number of group q in component i, r_q^G is the group segment number, and ε_{qr}^G is the group interaction energy.

Group parameters (ε_a^G, ε_b^G, ε_c^G, l_q^G, r_a^G, r_b^G, and r_b^G) for CH_2, CH_3, CO_2, [MIM][PF_6], [MIM][BF_4], and [MIM][Tf_2N] groups have been included in the current state of the art of GCNLF EOS and can give better prediction for CO_2 solubility in ILs at temperatures of 298.15−393.15 K and pressures up to 9.40 MPa. Furthermore, it is interesting to find that this model can predict the solubility of mixed gases of CO_2/N_2 and CO_2/C_3H_8 in $[HMIM]^+[Tf_2N]^-$ satisfactorily.[119]

2.5. GC EOS

Breure et al.[64] extened the application of GC EOS to prediction of gas solubility in ILs, not limited to traditional solvents any more. GC EOS is based on the generalized van der Waals function and the local composition principle[120,121] and is expressed implicitly by the residual Helmholtz energy

$$\left(\frac{A^R}{RT}\right)_{T,V,n} = \left(\frac{A^R}{RT}\right)_{att} + \left(\frac{A^R}{RT}\right)_{fv} \quad (26)$$

where subscripts "att" and "fv" represent the attractive and free volume terms, respectively. The free volume term contains the following parameter: group volume R_k and group surface area Q_k, normally obtained from van der Waals volume and surface area as given by Bondi,[57] critical hard sphere diameter d_c, and critical temperature T_c. The attractive term contains pure group constants (T_i*, q_i), pure group energy parameters (g^{ii}*, g_{ii}', g_{ii}''), and group−group interaction parameters (k_{ij}*, k_{oj}', α_{ij}, α_{ji}). Therefore, there are so many parameters to be derived in GC EOS for ILs, which is unfavorable for its wide application. The concerned cations are only $[RMIM]^+$ and $[OH-RMIM]^+$, and the anions are $[BF_4]^-$, $[PF_6]^-$, and $[NO_3]^-$. However, the prediction capacity of GC EOS is robust for CO_2 solubility in ILs and IL solubility in CO_2 at pressures up to 100 MPa.[64,65]

2.6. SAFT-Based EOS

2.6.1. tPC-PSAFT EOS. tPC-PSAFT EOS is a truncated version of PC-PSAFT (perturbed chain statistical associating fluid theory) EOS[122] and developed by Karakatsani et al.[123,124] from dipolar and quadrupolar molecular fluids to gas−IL systems. Like GC EOS, the residual Helmholtz energy is given by the sum of several contributions

$$\frac{A^{res}(T,\rho)}{RT} = \frac{A^{hs}(T,\rho)}{RT} + \frac{A^{chain}(T,\rho)}{RT} + \frac{A^{assoc}(T,\rho)}{RT} + \frac{A^{disp}(T,\rho)}{RT} + \frac{A^{polar}(T,\rho)}{RT} \quad (27)$$

where superscripts hs, chain, assoc, disp, and polar represent the contributions of hard sphere, hard chain, association, dispersion, and polar terms, respectively. This model contains six pure-component parameters of physical meaning, i.e., segment number m, temperature-independent segment volume v^∞, segment dispersive energy parameter u/k, association energy ε^{AB}, association volume κ^{AB}, and effective polar interaction parameter σ_p, as well as one temperature-dependent binary interaction parameter k_{ij}.

Since tPC-PSAFT EOS is deduced based on statistical mechanics, the solubility behavior of CO_2 in ILs at high pressures of up to100 MPa can be well explained. As pressure increases, CO_2 solubility in $[RMIM]^+[BF_4]^-$ and $[RMIM]^+[BF_4]^-$ (R = ethyl, butyl, hexyl, and octyl) first increases linearly but then levels off at a certain high pressure, as demonstrated by the experimental data and predicted results.[125] Karakatsani et al.[126] used this model to predict the marginal vapor pressure of pure ILs and the solubility of CO_2, CO, N_2, and CHF_3 in $[BMIM]^+[PF_6]^-$ and found good agreement.

2.6.2. soft-SAFT EOS. Andreu and Vega[127,128] proposed the soft-SAFT EOS which retains the main features of the original SAFT and tried to describe the solubility of CO_2, H_2, and Xe in three different imidazolium-based IL families of $[RMIM]^+[BF_4]^-$, $[RMIM]^+[PF_6]^-$, and $[RMIM]^+[Tf_2N]^-$ (R = ethyl, butyl, hexyl, and octyl) at pressures up to 100 MPa. The residual Helmholtz energy is of the similar form as other SAFT-type equations

$$\frac{A^{res}(T,\rho)}{RT} = \frac{A^{LJ}(T,\rho)}{RT} + \frac{A^{chain}(T,\rho)}{RT} + \frac{A^{assoc}(T,\rho)}{RT} + \frac{A^{polar}(T,\rho)}{RT} \quad (28)$$

where a Lennard−Jones (LJ) spherical fluid is selected in the reference term. The model parameters for gas molecules include chain length m, segment size σ, segment energy parameter ε, quadrupole moment Q, and $x_p = 1/3$, while for IL molecules these are chain length m, sphere diameter σ, interaction energy ε, association volume k_{HB}, and association energy ε_{HB}.

In order to keep the model in a simple manner, the binary interaction parameter between CO_2 and IL in macroscopic thermodynamics k_{ij} is not needed, and the predicted results are in quantitative agreement with the experimental data. In this sense, soft-SAFT EOS is a purely predictive model. However, in the case of the BF_3−$[BMIM]^+[BF_4]^-$ system, a reversible complexation between them occurs, and thus, a cross-association interaction should be taken into account based on soft-SAFT EOS to revise the large deviation from experimental data.[129]

2.6.3. Heterosegmented-SAFT EOS. The heterosegmented-SAFT EOS is defined as in the ion-based SAFT2[130−133]

$$\frac{A^{res}(T,\rho)}{RT} = \frac{A^{hs}(T,\rho)}{RT} + \frac{A^{disp}(T,\rho)}{RT} + \frac{A^{chain}(T,\rho)}{RT} + \frac{A^{assoc}(T,\rho)}{RT} \quad (29)$$

where CO_2 is taken on as a molecule and IL molecule is decomposed into several alkyl, cation head, and anion groups. The model parameters for each group include segment number m, segment volume v^{00}, segment energy u/k, reduced range of the potential well λ, and group bond number n_B. Meanwhile, the binary interaction parameters between CO_2 and the IL group as well as the cross-association parameter between CO_2 and anion are also required. Ji and Adidharma[134] compared the

dx.doi.org/10.1021/cr300497a | Chem. Rev. 2014, 114, 1289−1326

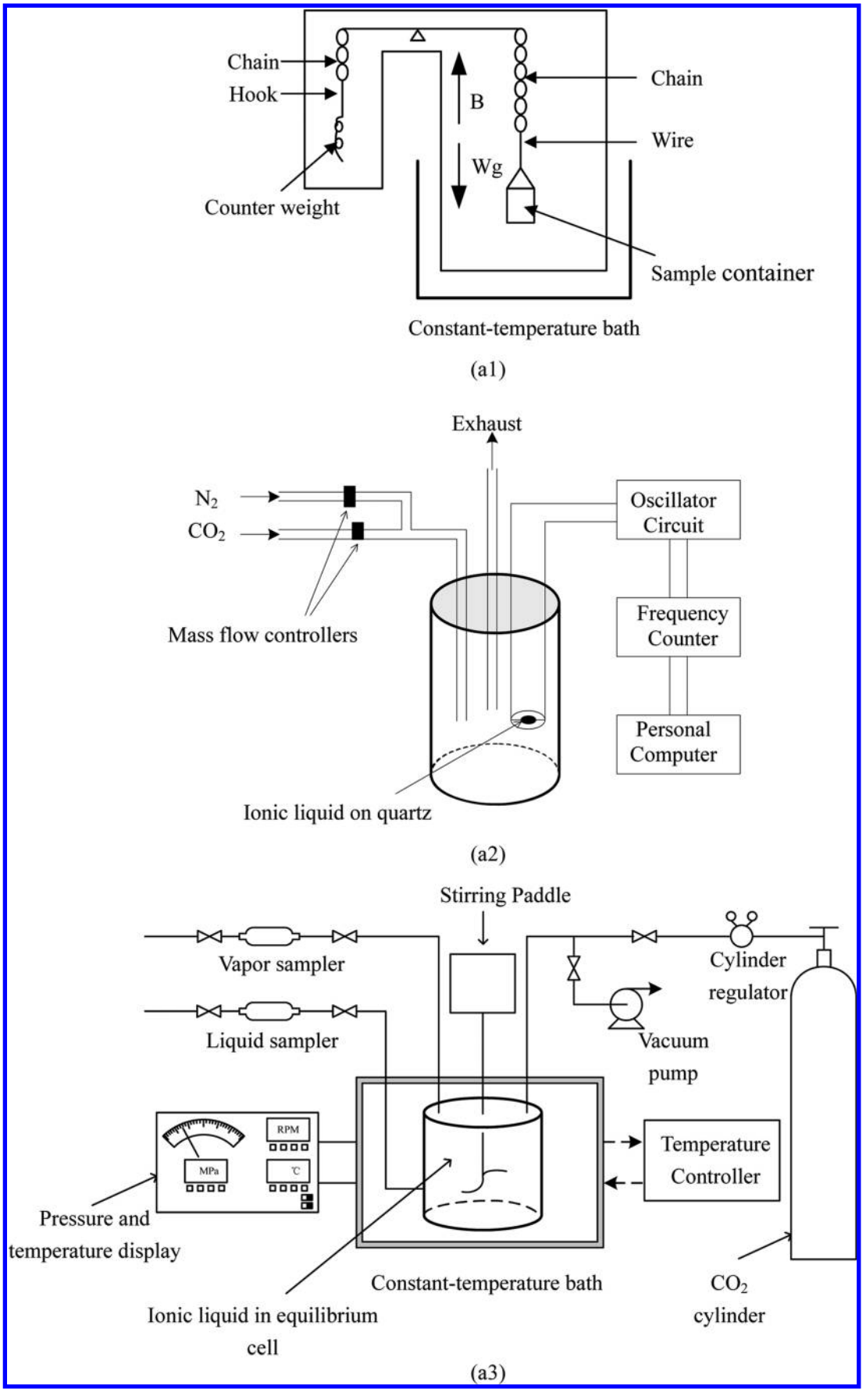

Figure 4. continued

dx.doi.org/10.1021/cr300497a | *Chem. Rev.* 2014, 114, 1289−1326

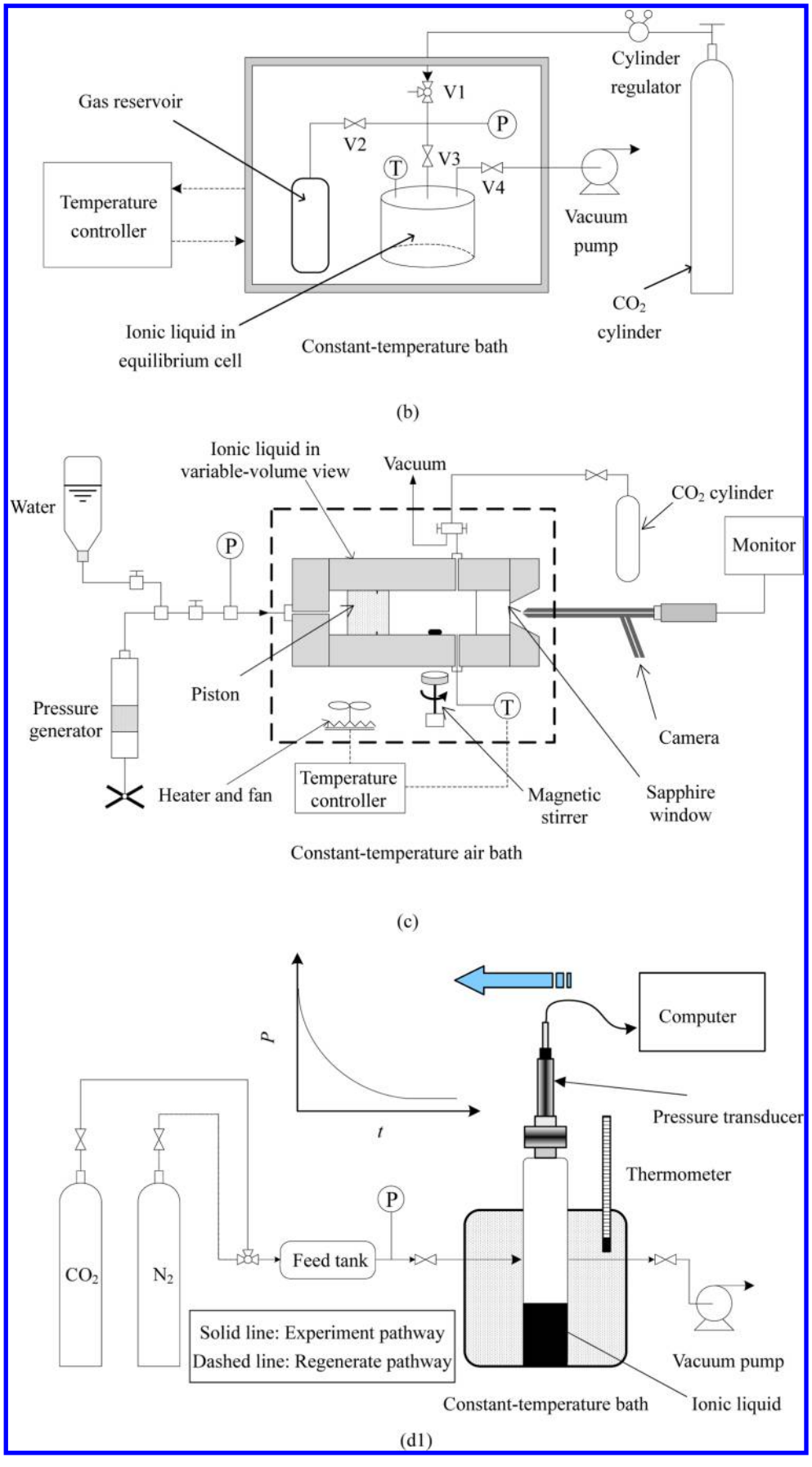

Figure 4. continued

dx.doi.org/10.1021/cr300497a | *Chem. Rev.* 2014, 114, 1289−1326

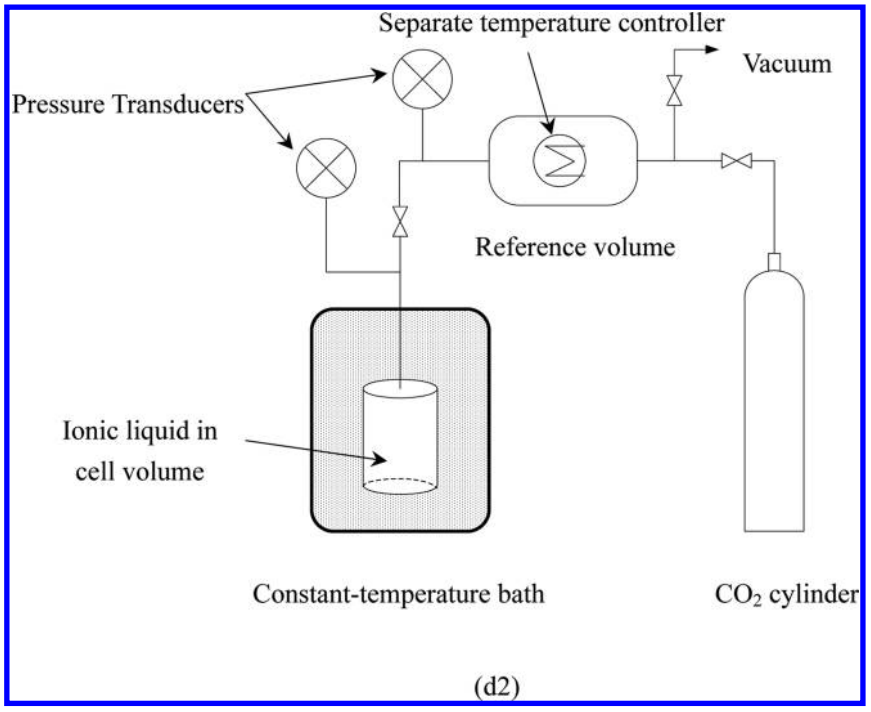

Figure 4. Schematic diagram of experimental methods and apparatus for measuring the solubility of CO_2 in ILs. (a1) Gravimetric microbalance method: B and Wg indicate the direction due to buoyancy and gravity on the sample side of the balance, respectively. Reprinted with permission from ref 149. Copyright 2005 American Chemical Society. (a2) Quartz crystal microbalance method. Reprinted with permission from ref 157. Copyright 2004 American Chemical Society. (a3) Weight method. Reprinted with permission from ref 158. Copyright 2013 American Institute of Chemical Engineers. (b) Isochoric saturation method. Reprinted with permission from ref 62. Copyright 2005 Elsevier. (c) Synthetic (bubble point) method. Reprinted with permission from ref 167. Copyright 2010 Elsevier. (d1) Transient thin-film method. Reprinted with permission from ref 173. Copyright 2007 American Chemical Society. (d2) Semi-infinite volume method. Reprinted with permission from ref 18. Copyright 2006 American Chemical Society.

experimental data with the calculated results for the solubility of CO_2 in $[RMIM]^+[BF_4]^-$, $[RMIM]^+[PF_6]^-$, and $[RMIM]^+[Tf_2N]^-$ (R = ethyl, butyl, hexyl, and octyl) at temperatures up to 423 K and pressures up to 200 bar and found that both agree well, especially at low pressures.

In summary, the equation forms of EOS are more complicated than the aforementioned activity coefficient models, which will limit their engineering applications. Future development should be to pay more attention to simplifying the model equations with fewer model parameters.

3. EXPERIMENTAL METHODS FOR MEASURING THE SOLUBILITY OF GASES IN ILS

There are various experimental methods (primarily physical methods) available to measure the solubility of gases in ILs. Among others, the gravimetric microbalance method, synthetic (bubble point) method, and isochoric saturation method have the most frequency to be used by researchers. The experimental procedures range in time from several minutes to 1 week, in temperature from 228 to 453 K, and in pressure from ~0 to 971 bar. These measurements will be discussed in this section. However, it is noted that no appreciable amount of ILs is assumed to be solubilized into the gas phase in all experimental methods.

3.1. Gravimetric Method

3.1.1. Gravimetric Microbalance. The gravimetric microbalance method was first used to measure the solubility of gases in polymers[135−138] and then extended to measure both gas solubility and diffusivity in ILs. A schematic diagram of this method is shown in Figure 4a1, which mainly consists of a sample container and a counter weight.

The mass of gas dissolved into IL is determined by the following force balance equation

$$W_g = W_F(P, T) - W_0(0, T) + \rho(P, T)\cdot [V_{IL}(P, T) + V_{SW}(P, T) + V_B] \quad (30)$$

where W_F is the balance readout for IL and gas at temperature T and pressure P, W_0 is the balance readout for IL at zero pressure, ρ is gas density obtained from the NIST Web site,[139] V_{IL} and V_B are the volumes of original IL and rod-basket assembly, respectively, and V_{SW} is the IL volume change due to swelling, which is the most important term in solubility measurement accounting for buoyancy correction. By far, there have been two approaches to deal with the volume expansion V_{SW}.

(i) V_{SW} is set to be zero.[140−146] In this case, the measured solubility is called "apparent solubility". Blasig et al.[147] thought that at low pressures (≤15 bar) V_{SW} can be neglected due to small swelling. Muldoon et al.[148] further confirmed that a 5% volume expansion has almost no influence on the CO_2 solubility in ILs.

(ii) The molar volume V_m of the mixture of IL and gas is taking the form of mole fraction average to make a buoyancy correction[26,149−154]

$$V_m(T, P) = V_{IL}(1 - x) + V_g x \quad (31)$$

dx.doi.org/10.1021/cr300497a | Chem. Rev. 2014, 114, 1289−1326

where x is the gas solubility expressed in mole fraction. Shiflett and Yokozeki[149] emphasized the importance for precise buoyancy correction and justified the assumption of eq 31.

The gravimetric microbalance method allows the user to monitor the mass change as time progresses. Once the mass no longer changes, the sample is at equilibrium. Thus, it can be clearly ensured when the equilibrium has been reached. In addition, the ability to monitor the mass change as time progresses allows the user to ensure that the initial liquid has been fully degassed prior to the measurement, which is also an important factor to determine how much gas is dissolved in the sample. The slight mass change of the sample can be monitored, indicating that this method can be efficiently applied in the case of very small gas solubility at a very low pressure range. This method is usually applied at low and middle pressures (<20 bar) and above room temperatures.

Note that during the measurement the volume expansion upon addition of gas into IL should be accurately predicted by equations of state that are suitable for gas−IL systems or by a simple linear relationship of volume expansion versus gas solubility for a wide range of imidazolium-based ILs, as proposed by Aki et al.[155] In addition, Anthony et al.[16,156] reported that the gases, e.g., CO, H_2, and N_2, have solubility in ILs below the detection limit of this apparatus, which have to be detected by other methods.

3.1.2. Quartz Crystal Microbalance. When gas is dissolved into IL, the frequency shift Δf, detected by a quartz crystal microbalance (QCM), is proportional to the mass change of IL film coated onto a quartz resonator

$$\Delta f = -C_1 \Delta m \tag{32}$$

where C_1 is a proportionality constant depending on the apparatus.

A schematic diagram of the QCM apparatus is shown in Figure 4a2, which consists of an oscillator and a frequency counter. Detailed information can be found in the ref 157. The quartz crystal microbalance measures the mass change by recording the change in frequency. In this way, a high precision (nanogram-level changes in mass) can be reached. Meanwhile, the frequency may be disturbed by the environment. Thus, rigorous operating conditions have to be required during the experimental procedure.

Baltus et al.[157] used this experimental technique to measure the solubility data of CO_2 in nine common RTILs and poly(ILs) at low pressures close to 1 bar and found that addition of an imine polymer to $[BMIM]^+[Tf_2N]^-$ does not increase the CO_2 solubility evaluated by Henry's law constants.

3.1.3. Weight Method. The apparatus for measuring the CO_2 solubility in ILs using the weight method is schematically diagrammed in Figure 4a3. A small amount of gas and liquid samples is, respectively, extracted from a high-pressure gas−liquid equilibrium cell, and the equilibrium temperature and pressure may be slightly changed within a tolerable range. The gas sample consisting of a gas mixture or gas plus organic solvent was analyzed by gas chromatography, while the composition in the liquid sample was determined by measuring the change in mass with and without CO_2. We used this method to measure the solubility of CO_2 in binary mixtures of IL plus IL and organic solvent plus IL, and the corresponding Henry's law constants were also derived.[159,160] Recently, this method in conjunction with a low-temperature equilibrium technique has been extended to measure the solubility of CO_2 in ILs at low temperatures down to 228 K.[158]

3.2. Isochoric Saturation Method

The measurement principle of the isochoric saturation method is similar to the pressure drop or pressure decay method, which is based on a known amount of gas contacting with the degassed IL in a closed equilibrium cell at constant temperature.[62,161−165] A typical schematic diagram of the isochoric saturation method is shown in Figure 4b. The mass of IL and the total cell volume are also known beforehand. As time goes on, the system pressure first decreases and then remains invariable. The solubility of gas (2) in IL (1) expressed in mole faction is derived by

$$x_2 = \frac{n_2^{\mathrm{liq}}}{n_1^{\mathrm{liq}} + n_2^{liq}} \tag{33}$$

where n_1^{liq} is the amount of IL predetermined before VLE and n_2^{lip} is the amount of gas dissolved into IL calculated from the PVT relation.

Compared to the gravimetric and quartz crystal microbalances, the isochoric saturation method is much simpler in design but can be used in a wider pressure range from 0.10 to 700 bar. Moreover, during measurement the liquid volume before and after gas dissolution may change, which is similar to the status of the aforementioned gravimetric microbalance method. With respect to the determination of volume expansion, the following three approaches were recommended by the researchers.

(i) It was simply assumed that no volume expansion occurs, that is, the volume of saturated solution is equal to that of pure IL.

(ii) Volume expansion as a function of pressure at a given temperature was directly measured using a cathetometer.[17,148,155]

(iii) Volume expansion was simply estimated by a linear relationship with mole fraction of CO_2 in IL.[63]

(iv) Unfortunately, no comparison of solubility data among these three approaches has been done. However, it seems that the correction to volume expansion is not so important, especially at low pressures.

3.3. Synthetic (Bubble Point) Method

The synthetic method is commonly performed in a Cailletet apparatus at middle pressures up to 14 MPa or in an autoclave apparatus at higher pressure up to 100 MPa. It can be used to measure the solubility of single gases such as CO_2, CO, H_2, and O_2 in ILs. Figure 4c shows a representative diagram of synthetic method, which mainly consists of a variable-volume view cell equipped with a sapphire window, a pressure generator, a borescope, a video monitor, a magnetic stirring system, and a constant-temperature bath. In the case of desirable liquid composition and temperature, the system pressure is increased by a pressure generator until a phase transition occurs visually. The bubble point pressure is defined as the pressure at which the first bubble is observed from a single homogeneous phase by decreasing pressure slowly[166−168] or at which the last bubble disappears from a gas−liquid two phase by increasing pressure slowly.[169−172] Therefore, in this sense, it is also called the bubble point method. However, during the experiments, Shin et al.[168] observed a cloudy point phenomenon as well due to the liquid−liquid phase split at high gas mole fractions. The advantages of this method are the short measurement time and the suitability at very high pressures.

3.4. Other Methods

3.4.1. Transient Thin-Film Method. IL was fabricated as a thin film in a small closed chamber. Pressure decay as a function of time was recorded as soon as gas entered into the chamber, as shown in Figure 4d1. The Henry's law constant and gas diffusivity were solved simultaneously by means of correlating the experimental data at low pressures of about 1−2 bar with a one-dimensional diffusion model using a nonlinear least-squares method. Hou and Baltus[173] reported that this method can give more accurate results than the semi-infinite volume method as described below because the entire pressure decay curve over a longer time was carefully recorded when measuring the CO_2 solubility and diffusivity in five imidazolium-based and pyridinium-based ILs, while Monganty and Baltus[113] measured the CO_2 solubility in eight imidazolium-based ILs by this method.

3.4.2. Semi-Infinite Volume Method. The semi-infinite volume method is different from the transient thin-film method in that the diffusion measurement was made in the first 20 min without agitation in the equilibrium cell while the solubility measurement was done after that time with vigorous agitation so as to reduce the equilibrium time. In addition, a larger amount of IL sample was needed because it was assumed that the IL volume is infinite when solving the mass transfer equations. The apparatus mainly consists of two parts: one is the reference volume serving as a space for the injected gas to come to thermal equilibrium and the other is the cell volume containing IL, as shown in Figure 4d2. Camper et al.[18] used this method to measure the solubility of CO_2, ethane, ethane, propene, and propane in $[EMIM]^+[Tf_2N]^-$, while Shokouhi et al.[174] measured the solubility of H_2S and CO_2 in $[HEMIM]^+[BF_4]^-$ at low pressures.

3.4.3. Gas Chromatography Method

According to eq 11, the Henry's law constants of gases are related to activity coefficients at infinite dilution. This means that the gas chromatography method, which is commonly used to measure the activity coefficients at infinite dilution of volatile solutes in nonvolatile solvents, is possible to be extended to measure the Henry's law constants of gases in ILs. However, only one paper reported the Henry's law constants of ethane and CO_2 in several imidazolium-based ILs by this method,[175] some of which are consistent with the experimental results by the gravimetric microbalance method.

3.5. Thermodynamic Consistency Test

The thermodynamic consistency test of experimental phase equilibrium data is important but often neglected by many researchers. The theoretical foundation is the Gibbs−Duhem equation, which should be transformed into a calculable form. For gas−IL systems, an equation of state and the corresponding mixing rule are incorporated into the Gibbs−Duhem equation to derive the integral areas A_p and A_φ in both sides. The average relative deviations (ARDs) of areas between A_p and A_φ and of pressures between experimental data and calculated results are used as the index of the thermodynamic consistency test. If the ARDs of areas and pressures are less than 20% and 10%, respectively, the experimental data are considered as thermodynamic consistent (TC), as proposed by Valderrama et al.[176] Otherwise, they are thermodynamic inconsistent (TI) or not fully consistent (NFC). In this way, the thermodynamic consistent solubility data of gases in ILs reported in the references have been checked by Alvarez and Aznar,[74,170,177] who found that some published data are NFC or even TI. Therefore, readers should carefully identify the reliability of gas solubility data coming from different sources.

Figure 5 shows the solubility data of CO_2 in $[BMIM]^+[PF_6]^-$ at 313.2 K and $[BMIM]^+[BF_4]^-$ at 298.2 K collected from the

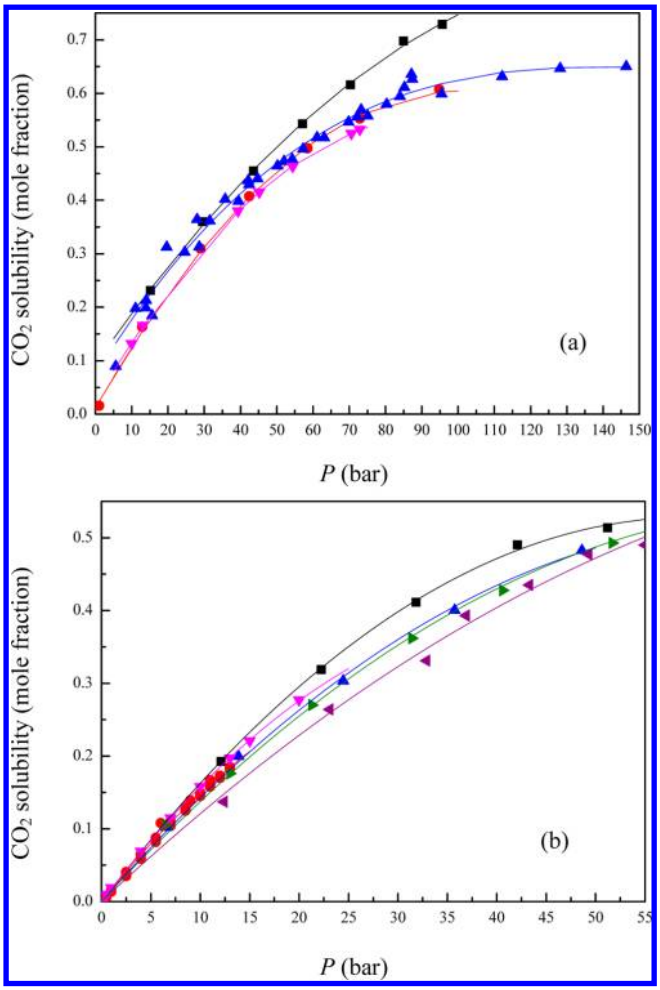

Figure 5. Solubility of CO_2 in $[BMIM]^+[PF_6]^-$ at 313.2 K and $[BMIM]^+[BF_4]^-$ at 298.2 K. (a) $[BMIM]^+[PF_6]^-$: (■) weight method,[17] (red ●) synthetic (bubble point) method,[178] (blue ▲) isochoric saturation method,[155] (pink ▼) weight method (at 314.25 K[179]; (b) $[BMIM]^+[BF_4]^-$: (■) synthetic (bubble point) method,[155] (red ●) gravimetric microbalance method,[16] (blue ▲) synthetic (bubble point) method,[180] (pink ▼) gravimetric microbalance method,[152] (brown side triangle pointing left) weight method,[181] (green side triangle pointing right) weight method.[182]

references. It can be seen that significant discrepancy arises among these data measured by different authors. The reasons may be summarized as follows.

(i) Different experimental methods. For example, the synthetic method may bring some random error through observing the bubble point of mixtures visually in a variable-volume view cell.[43]

(ii) Difficulty in measurement of very low gas solubility with an order of magnitude of 10^{-4} in mole fraction.[41]

(iii) Sample purity. Some authors pointed out that small amounts of water and other impurities may influence the gas solubility in ILs.[16,20,151,155,183]

(iv) No thermodynamic consistency test due to the complexity in mathematics.

dx.doi.org/10.1021/cr300497a | Chem. Rev. 2014, 114, 1289−1326

Table 3. Summary of Solubility Data of CO_2 in ILs

no. of IL	ILs	T range (K)	P range (bar)	no. of data points	experimental method	refs
1	$[(ETO)_2IM]^+[Tf_2N]^-$	302.85−363.15	21.50−328.60	36	synthetic (bubble point) method	189
2	$[b2\text{-}Nic]^+[Tf_2N]^-$	333.30−333.30	12.00−87.00	7	isochoric saturation method	148
3	$[BBIM]^+[MeSO_3]^-$	296.95−343.35	15.00−342.00	72	synthetic (bubble point) method	190
4	$[bhea]^+[Ac]^-$	298.15−328.15	1.25−15.15	18	isochoric saturation method	165
5	$[bhea]^+[L]^-$	298.15−328.15	1.21−15.98	18	isochoric saturation method	165
6	$[BMIM]^+[Ac]^-$	283.10−348.20	0.10−19.99	32	gravimetric microbalance method	191
		298.00−298.30	0.10−19.99	9	gravimetric microbalance method	152
		313.04−353.24	2.30−755.26	40	synthetic (bubble point) method	192
			total no.	**81**		
7	$[BMIM]^+[BF_4]^-$	303.72−344.49	0.18−0.84	21	isochoric saturation method	193
		298.20−333.30	10.50−246.00	20	isochoric saturation method	155
		283.15−323.15	0.02−13.00	90	gravimetric microbalance method	16
		278.47−368.22	5.87−467.20	104	synthetic (bubble point) method	180
		282.75−348.15	0.10−20.00	36	gravimetric microbalance method	149
		303.38−344.27	0.22−0.92	11	isochoric saturation method	163
		307.55−322.15	6.50−60.70	40	weight method	194
		298.00−298.20	0.10−20.00	9	gravimetric microbalance method	152
		293.15−383.15	10.50−246.00	59	synthetic (bubble point) method	189
		298.15−298.15	6.50−60.70	7	weight method	182
		313.20−333.20	11.20−53.90	12	weight method	160
		298.20−333.20	8.29−47.86	23	weight method	181
		323.15−323.15	3.80−39.70	6	isochoric saturation method	195
		298.40−354.20	0.46−1.92	15	isochoric saturation method	196
			total no.	**453**		
8	$[BMIM]^+[C_3F_7CO_2]^-$	303.15−333.15	5.50−42.70	28	isochoric saturation method	195
9	$[BMIM]^+[C_7F_{15}CO_2]^-$	333.23−333.23	14.90−84.10	7	isochoric saturation method	148
10	$[BMIM]^+[Cl]^-$	353.15−373.15	24.54−369.46	45	synthetic (bubble point) method	197
11	$[BMIM]^+[DBPO_4]^-$	313.15−333.15	0.22−1.75	16	isochoric saturation method	164
12	$[BMIM]^+[DCA]^-$	298.20−333.30	12.71−115.29	21	isochoric saturation method	155
		293.36−363.25	10.18−736.40	40	synthetic (bubble point) method	170
			total no.	**61**		
13	$[BMIM]^+[eFAP]^-$	303.16−343.27	0.66−0.77	15	isochoric saturation method	198
14	$[BMIM]^+[IAAc]^-$	298.10−298.10	0.10−20.00	9	gravimetric microbalance method	152
15	$[BMIM]^+[ISB]^-$	298.10−298.20	0.10−20.00	9	gravimetric microbalance method	152
16	$[BMIM]^+[LEV]^-$	298.10−298.10	0.10−20.00	9	gravimetric microbalance method	152
17	$[BMIM]^+[MDEGSO_4]^-$	313.31−333.36	14.30−91.20	11	isochoric saturation method	148
		313.15−363.15	22.60−264.80	65	synthetic (bubble point) method	199
			total no.	**76**		
18	$[BMIM]^+[MeSO_3]^-$	302.35−343.15	5.50−357.00	60	synthetic (bubble point) method	190
19	$[BMIM]^+[MeSO_4]^-$	293.20−413.10	9.08−98.05	54	isochoric saturation method	200
20	$[BMIM]^+[methide]^-$	298.20−333.30	12.58−114.27	21	isochoric saturation method	155
21	$[BMIM]^+[NO_3]^-$	313.15−333.15	15.47−93.17	21	weight method	17
		298.20−333.20	10.31−93.16	17	isochoric saturation method	155
		293.13−368.24	3.68−128.32	66	synthetic (bubble point) method	201
			total no.	**104**		
22	$[BMIM]^+[PF_6]^-$	313.15−323.15	15.17−95.67	21	weight method	17
		283.15−323.15	0.03−12.99	158	gravimetric microbalance method	156
		293.15−393.15	1.05−96.85	43	synthetic (bubble point) method	178
		298.20−333.40	5.60−146.39	70	isochoric saturation method	155
		283.15−323.15	0.00−13.00	160	gravimetric microbalance method	16
		293.29−363.54	4.30−735.00	99	synthetic (bubble point) method	202
		282.05−348.25	0.10−20.00	36	gravimetric microbalance method	149
		297.56−322.52	7.90−80.80	42	weight method	179
		298.15−298.15	5.29−6.67	4	isochoric saturation method	62
		283.15−343.04	0.41−0.92	14	isochoric saturation method	41
		298.00−298.20	0.11−20.00	9	gravimetric microbalance method	152
		298.15−298.15	2.60−40.20	9	isochoric saturation method	63
		312.30−354.90	0.64−1.86	20	isochoric saturation method	196
		318.00−338.00	4.95−199.95	33	gravimetric microbalance method	203
			total no.	**718**		
23	$[BMIM]^+[Pro]^-$	298.10−298.20	0.10−19.99	9	gravimetric microbalance method	152

dx.doi.org/10.1021/cr300497a | *Chem. Rev.* 2014, 114, 1289−1326

Table 3. continued

no. of IL	ILs	T range (K)	P range (bar)	no. of data points	experimental method	refs
24	$[BMIM]^+[SCN]^-$	292.35−384.15	10.50−315.00	56	synthetic (bubble point) method	189
25	$[BMIM]^+[SUC]^-$	298.10−298.10	0.10−20.00	9	gravimetric microbalance method	152
26	$[BMIM]^+[Tf_2N]^-$	298.10−333.30	11.38−132.43	55	isochoric saturation method	155
		283.15−323.15	0.01−13.00	100	gravimetric microbalance method	16
		279.98−339.97	2.92−48.00	16	isochoric saturation method	204
		283.36−343.78	0.68−1.12	14	isochoric saturation method	205
		293.35−344.55	10.70−428.00	84	synthetic (bubble point) method	168
		313.15−453.15	4.20−142.61	133	synthetic (bubble point) method	206
		292.65−363.26	6.29−499.90	68	synthetic (bubble point) method	170
		313.20−323.20	80.80−199.40	8	isochoric saturation method	207
		318.00−338.00	5.00−199.97	32	gravimetric microbalance method	208
		323.15−323.15	3.80−40.80	7	isochoric saturation method	195
			total no.	**517**		
27	$[BMIM]^+[TFA]^-$	298.17−333.41	11.70−92.60	19	isochoric saturation method	148
		298.00−298.20	0.11−20.00	9	gravimetric microbalance method	152
		293.25−363.18	9.79−624.73	52	synthetic (bubble point) method	192
			total no.	**80**		
28	$[BMIM]^+[TFES]^-$	298.00−298.20	0.10−20.00	9	gravimetric microbalance method	152
29	$[BMIM]^+[TfO]^-$	298.20−333.30	10.44−114.77	27	isochoric saturation method	155
		303.85−344.55	8.50−375.00	65	synthetic (bubble point) method	166
		303.20−343.20	2.15−65.21	35	gravimetric microbalance method	142
			total no.	**127**		
30	$[BMIM]^+[TMA]^-$	298.10−298.10	0.10−20.00	9	gravimetric microbalance method	152
31	$[BMIM]_2^+[IDA]^{2-}$	298.10−298.10	0.10−20.00	9	gravimetric microbalance method	152
32	$[BMPYR]^+[Ac]^-$	353.18−353.55	0.43−0.89	2	isochoric saturation method	208
33	$[BMPYR]^+[TfO]^-$	303.15−373.25	18.80−702.00	64	isochoric saturation method	209
34	$[BMPYR]^+[eFAP]^-$	283.50−323.30	0.30−18.00	42	weight method	93
		303.16−343.38	0.64−0.75	15	isochoric saturation method	210
			total no.	**57**		
35	$[BMPYR]^+[LEV]^-$	303.16−333.41	0.63−0.75	10	isochoric saturation method	208
36	$[BMPYR]^+[MeSO_4]^-$	303.15−373.15	30.70−973.00	40	synthetic (bubble point) method	211
37	$[BMPYR]^+[Tf_2N]^-$	283.15−323.15	0.02−13.00	52	gravimetric microbalance method	16
		303.78−344.15	0.49−0.57	11	isochoric saturation method	162
		293.10−413.20	2.80−108.13	26	isochoric saturation method	212
		303.15−373.15	6.80−627.70	72	synthetic (bubble point) method	211
		313.20−323.20	80.60−200.60	8	isochoric saturation method	207
			total no.	**169**		
38	$[BPY]^+[BF_4]^-$	313.15−333.15	15.47−95.80	21	weight method	17
39	$[C_2OMIM]^+[BF_4]^-$	303.15−323.15	0.10−1.60	18	isochoric saturation method	213
40	$[C_2OMIM]^+[DCA]^-$	303.15−323.15	0.10−1.60	18	isochoric saturation method	213
41	$[C_2OMIM]^+[PF_6]^-$	303.15−323.15	0.10−1.60	18	isochoric saturation method	213
42	$[C_2OMIM]^+[Tf_2N]^-$	303.15−323.15	0.10−1.60	18	isochoric saturation method	213
43	$[C_2OMIM]^+[TfO]^-$	303.15−323.15	0.10−1.60	18	isochoric saturation method	213
44	$[C_3MPYR]^+[Tf_2N]^-$	303.15−373.15	5.20−471.00	56	synthetic (bubble point) method	214
45	$[C_5MIM]^+[bFAP]^-$	298.14−333.40	0.01−87.60	58	isochoric saturation method	148
46	$[C_5MIM]^+[Tf_2N]^-$	293.30−363.29	6.18−598.05	144	synthetic (bubble point) method	171
47	$[C_5MPYR]^+[Tf_2N]^-$	303.15−373.15	2.70−551.00	64	synthetic (bubble point) method	214
48	$[C_6F_9MIM]^+[Tf_2N]^-$	298.13−333.30	0.01−99.90	58	isochoric saturation method	148
49	$[C_7MPYR]^+[Tf_2N]^-$	303.15−373.15	1.60−722.40	64	synthetic (bubble point) method	214
50	$[C_8F_{13}MIM]^+[Tf_2N]^-$	298.16−333.05	0.03−36.20	38	isochoric saturation method	148
51	$[DMFH]^+[Tf_2N]^-$	298.15−333.15	9.79−100.00	31	weight method	215
52	$[DMIM]^+[Tf_2N]^-$	298.15−343.15	14.74−148.47	22	synthetic (bubble point) method	216
		313.15−313.15	20.00−144.00	14	isochoric saturation method	217
		313.20−323.20	80.70−201.50	8	isochoric saturation method	207
			total no.	**44**		
53	$[EMIM]^+[Ac]^-$	298.10−298.10	0.10−20.00	9	gravimetric microbalance method	152
		298.10−348.20	0.10−20.00	27	gravimetric microbalance method	150
			total no.	**36**		
54	$[EMIM]^+[BF_4]^-$	298.15−298.15	2.51−8.75	9	isochoric saturation method	62
		303.20−343.20	4.96−43.29	25	gravimetric microbalance method	143
		298.20−313.20	5.30−40.60	17	weight method	159

dx.doi.org/10.1021/cr300497a | Chem. Rev. 2014, 114, 1289−1326

Table 3. continued

no. of IL	ILs	T range (K)	P range (bar)	no. of data points	experimental method	refs
		313.20−333.20	11.20−54.70	12	weight method	160
			total no.	**63**		
55	$[EMIM]^+[DCA]^-$	303.20−343.20	1.48−59.44	25	gravimetric microbalance method	142
56	$[EMIM]^+[DEPO_4]^-$	313.15−333.15	0.24−1.99	22	isochoric saturation method	164
57	$[EMIM]^+[eFAP]^-$	303.18−343.23	0.54−0.73	13	isochoric saturation method	198
		283.75−364.13	4.47−104.00	50	synthetic (bubble point) method	218
			total no.	**63**		
58	$[EMIM]^+[EtSO_4]^-$	313.15−333.15	14.36−94.61	21	weight method	17
		303.20−343.20	2.11−49.62	35	gravimetric microbalance method	142
		303.15−353.15	1.22−15.47	39	isochoric saturation method	219
		298.04−348.15	3.52−64.95	19	gravimetric microbalance method	220
			total no.	**114**		
59	$[EMIM]^+[MeSO_3]^-$	302.25−342.85	4.00−461.50	49	synthetic (bubble point) method	190
60	$[EMIM]^+[MDEGSO_4]^-$	303.20−343.20	8.54−67.10	30	gravimetric microbalance method	221
61	$[EMIM]^+[PF_6]^-$	308.14−366.03	14.90−971.00	73	synthetic (bubble point) method	222
62	$[EMIM]^+[Tf_2N]^-$	298.15−298.15	2.13−9.03	8	isochoric saturation method	62
		303.63−344.23	0.43−0.57	14	isochoric saturation method	223
		283.43−343.07	0.65−0.86	5	isochoric saturation method	205
		303.63−344.23	0.43−0.57	14	isochoric saturation method	162
		312.10−453.15	6.26−147.70	191	synthetic (bubble point) method	224
		292.75−344.55	12.20−432.00	78	synthetic (bubble point) method	168
		297.90−298.20	0.50−20.00	9	gravimetric microbalance method	152
		292.16−363.55	6.20−478.50	153	synthetic (bubble point) method	171
		298.15−343.15	12.35−147.94	21	synthetic (bubble point) method	216
		318.00−338.00	0.96−199.98	33	gravimetric microbalance method	203
			total no.	**526**		
63	$[EMIM]^+[TFA]^-$	298.10−298.10	0.10−20.00	9	gravimetric microbalance method	152
		298.10−348.20	0.10−20.00	27	gravimetric microbalance method	150
			total no.	**36**		
64	$[EMIM]^+[TfO]^-$	303.85−344.55	8.00−378.00	55	synthetic (bubble point) method	166
		303.20−343.20	1.80−58.84	30	gravimetric microbalance method	141
			total no.	**85**		
65	$[Et_3NBH_2MIM]^+[Tf_2N]^-$	298.1−298.15	0.03−2.99	9	gravimetric microbalance method	148
66	$[ETT]^+[eFAP]^-$	283.20−323.50	0.05−18.00	41	weight method	93
67	$[he]^+[Ac]^-$	303.00−323.00	0.89−10.08	24	isochoric saturation method	225
		298.15−328.15	1.16−15.24	18	isochoric saturation method	165
			total no.	**42**		
68	$[he]^+[FOR]^-$	303.00−323.00	0.44−10.01	27	isochoric saturation method	225
69	$[he]^+[L]^-$	303.00−323.00	7.80−100.90	24	isochoric saturation method	225
		298.15−328.15	1.24−15.56	18	isochoric saturation method	165
			total no.	**42**		
70	$[hea]^+[Ac]^-$	303.00−323.00	0.76−7.67	24	isochoric saturation method	225
71	$[hea]^+[FOR]^-$	303.00−323.00	0.66−8.92	21	isochoric saturation method	225
72	$[hea]^+[L]^-$	303.00−323.00	1.24−8.50	21	isochoric saturation method	225
73	$[HEMIM]^+[BF_4]^-$	303.15−353.15	1.14−11.94	44	isochoric saturation method	174
74	$[HEMIM]^+[PF_6]^-$	303.15−353.15	1.33−11.27	44	isochoric saturation method	226
75	$[HEMIM]^+[Tf_2N]^-$	303.15−353.15	0.97−11.14	30	isochoric saturation method	226
76	$[HEMIM]^+[TfO]^-$	303.15−353.15	1.01−12.80	30	isochoric saturation method	226
77	$[hheme]^+[Ac]^-$	298.15−328.15	1.24−15.42	18	isochoric saturation method	165
78	$[hheme]^+[L]^-$	298.15−328.15	1.54−15.35	18	isochoric saturation method	165
79	$[HMIM]^+[ACE]^-$	333.14−333.14	0.20−3.00	8	gravimetric microbalance method	148
80	$[HMIM]^+[BF_4]^-$	293.18−368.16	5.40−662.60	104	synthetic (bubble point) method	227
		298.15−298.15	3.12−8.99	8	isochoric saturation method	62
		307.55−322.15	21.30−86.40	44	weight method	194
		303.15−373.15	12.00−416.90	48	synthetic (bubble point) method	228
			total no.	**204**		
81	$[HMIM]^+[Br]^-$	333.15−333.15	30.90−148.91	12	synthetic (bubble point) method	229
82	$[HMIM]^+[eFAP]^-$	298.15−333.34	0.01−91.10	60	gravimetric microbalance method	148
		298.15−298.15	0.10−20.00	9	gravimetric microbalance method	152
		283.50−323.20	0.30−18.00	42	weight method	93
		298.13−343.08	0.59−0.73	12	isochoric saturation method	198

dx.doi.org/10.1021/cr300497a | Chem. Rev. 2014, 114, 1289−1326

Table 3. continued

no. of IL	ILs	T range (K)	P range (bar)	no. of data points	experimental method	refs
			total no.	**123**		
83	$[HMIM]^+[MeSO4]^-$	303.15−373.15	8.70−501.40	48	synthetic (bubble point) method	228
84	$[HMIM]^+[PF_6]^-$	298.31−363.58	6.40−946.00	98	synthetic (bubble point) method	172
		298.15−298.15	2.96−9.27	14	isochoric saturation method	62
		303.15−373.15	3.00−556.30	48	synthetic (bubble point) method	228
			total no.	**160**		
85	$[HMIM]^+[pFAP]^-$	298.15−333.12	0.01−12.90	39	gravimetric microbalance method	148
86	$[HMIM]^+[SAC]^-$	333.27−333.27	0.02−3.00	9	gravimetric microbalance method	148
87	$[HMIM]^+[TCB]^-$	283.56−364.04	2.71−123.36	62	synthetic (bubble point) method	230
88	$[HMIM]^+[Tf_2N]^-$	298.10−333.30	13.15−115.58	28	isochoric saturation method	155
		298.15−298.15	1.64−8.59	9	isochoric saturation method	62
		293.15−413.20	6.01−99.11	25	isochoric saturation method	231
		283.16−323.17	0.01−13.00	57	gravimetric microbalance method	148
		288.48−343.20	0.29−0.94	11	isochoric saturation method	232
		281.90−348.60	0.09−19.76	72	gravimetric microbalance method	151
		298.15−298.15	1.57−8.40	10	isochoric saturation method	119
		303.85−344.55	14.00−390.00	90	synthetic (bubble point) method	168
		297.30−297.40	0.09−19.75	9	gravimetric microbalance method	152
		298.15−343.15	8.00−247.08	26	synthetic (bubble point) method	216
		278.12−368.44	4.22−143.37	123	synthetic (bubble point) method	233
		303.15−373.15	4.20−452.80	64	synthetic (bubble point) method	228
			total no.	**524**		
89	$[HMIM]^+[TfO]^-$	313.23−313.39	14.94−84.23	6	isochoric saturation method	19
		303.85−344.55	12.50−363.00	70	synthetic (bubble point) method	166
		303.15−373.15	14.20−1001.20	64	synthetic (bubble point) method	228
			total no.	**140**		
90	$[HMMIM]^+[Tf_2N]^-$	298.20−333.30	14.97−118.04	29	isochoric saturation method	155
91	$[HMPY]^+[Tf_2N]^-$	283.18−323.15	0.01−13.00	56	gravimetric microbalance method	148
92	$[HMPYR]^+[Tf_2N]^-$	303.15−373.15	10.60−475.50	64	isochoric saturation method	234
93	$[HOC_3MIM]^+[NO_3]^-$	293.47−363.55	8.51−116.21	36	synthetic (bubble point) method	201
94	$[m\text{-}2\text{-}hea]^+[Ac]^-$	312.93−363.61	8.40−805.00	41	synthetic (bubble point) method	235
95	$[m\text{-}2\text{-}hea]^+[FOR]^-$	293.21−363.42	4.94−529.10	80	synthetic (bubble point) method	235
96	$[MDEA]^+[Cl]^-$	313.15−333.15	12.20−46.30	35	isochoric saturation method	236
97	$[MMIM]^+[DMPO_4]^-$	313.15−333.15	0.49−1.75	12	isochoric saturation method	164
98	$[MMIM]^+[MeSO_3]^-$	332.85−363.65	16.50−431.00	40	synthetic (bubble point) method	190
99	$[MMIM]^+[MP]^-$	313.15−373.15	34.00−250.00	26	synthetic (bubble point) method	189
100	$[N_{1,1,1,2\text{-}OH}]^+[Tf_2N]^-$	333.24−333.24	12.00−83.60	7	gravimetric microbalance method	148
101	$[N_{1,1,3,2\text{-}OH}]^+[Tf_2N]^-$	304.16−344.84	0.47−0.54	7	isochoric saturation method	162
102	$[N_{1,8,8,8}]^+[Tf_2N]^-$	313.20−323.20	80.80−205.60	8	isochoric saturation method	207
103	$[N_{2,1,1,3}]^+[Tf_2N]^-$	313.22−313.25	11.34−94.66	8	isochoric saturation method	19
104	$[N_{4,1,1,1}]^+[Tf_2N]^-$	333.23−333.23	15.60−80.90	6	isochoric saturation method	148
		282.93−343.07	0.36−0.89	12	isochoric saturation method	205
		313.20−323.20	85.80−196.30	8	isochoric saturation method	207
			total no.	**26**		
105	$[N_{4,4,4,1}]^+[Tf_2N]^-$	298.15−298.15	0.05−5.50	11	gravimetric microbalance method	16
106	$[N_{4,4,4,1}]^+[MeSO_4]^-$	338.35−368.63	10.09−115.28	28	synthetic (bubble point) method	237
107	$[N_{4,4,4,4}]^+[doc]^-$	333.46−333.46	20.10−91.70	6	isochoric saturation method	148
108	$[NMIM]^+[PF_6]^-$	293.15−298.15	8.60−35.40	11	isochoric saturation method	63
109	$[NMPYR]^+[Tf_2N]^-$	303.15−373.15	2.60−365.80	56	synthetic (bubble point) method	214
110	$[OMIM]^+[BF_4]^-$	313.15−333.15	15.61−93.73	21	weight method	17
		307.79−363.29	5.71−858.00	100	synthetic (bubble point) method	169
		307.55−322.15	41.70−87.20	32	weight method	194
			total no.	**153**		
111	$[OMIM]^+[PF_6]^-$	313.15−333.15	16.00−92.88	21	weight method	17
		303.15−353.15	1.29−18.50	42	isochoric saturation method	238
			total no.	**63**		
112	$[OMIM]^+[Tf_2N]^-$	298.20−333.30	13.26−114.69	22	isochoric saturation method	155
		297.55−344.55	6.80−348.00	96	synthetic (bubble point) method	168
		303.15−353.15	1.12−20.63	42	isochoric saturation method	239
		313.20−333.20	11.30−55.40	12	weight method	160
		303.15−353.15	1.12−20.63	42	isochoric saturation method	239

dx.doi.org/10.1021/cr300497a | Chem. Rev. 2014, 114, 1289−1326

Table 3. continued

no. of IL	ILs	T range (K)	P range (bar)	no. of data points	experimental method	refs
		313.20−333.20	9.60−55.00	11	weight method	240
			total no.	**225**		
113	$[OMIM]^+[TfO]^-$	303.85−344.55	6.80−340.00	65	synthetic (bubble point) method	166
114	$[OMPYR]^+[Tf_2N]^-$	303.15−373.15	5.10−359.20	72	isochoric saturation method	234
115	$[P_{1,4,4,4}]^+[MeSO_4]^-$	313.16−363.30	6.59−126.40	29	synthetic (bubble point) method	237
116	$[P_{1,4,4,4}]^+[TOS]^-$	323.15−323.15	0.00−13.00	34	gravimetric microbalance method	16
117	$[P_{4,4,4,4}]^+[FOR]^-$	298.00−298.20	0.10−20.00	9	gravimetric microbalance method	152
118	$[P_{6,6,6,14}]^+[Ala]^-$	298.15−298.15	0.51−1.46	2	isochoric saturation method	241
119	$[P_{6,6,6,14}]^+[Br]^-$	303.19−363.42	8.76−129.98	47	synthetic (bubble point) method	242
120	$[P_{6,6,6,14}]^+[C_{12}H_{25}PhSO_3]^-$	307.55−322.15	46.30−89.60	26	weight method	243
		303.15−363.15	3.90−113.70	112	synthetic (bubble point) method	199
			total no.	**138**		
121	$[P_{6,6,6,14}]^+[Cl]^-$	302.55−363.68	1.68−245.70	69	synthetic (bubble point) method	244
		313.20−323.20	82.10−207.10	8	isochoric saturation method	207
			total no.	77		
122	$[P_{6,6,6,14}]^+[DCA]^-$	271.11−363.35	3.04−902.48	105	synthetic (bubble point) method	242
123	$[P_{6,6,6,14}]^+[eFAP]^-$	303.17−343.30	0.68−0.79	15	isochoric saturation method	210
124	$[P_{6,6,6,14}]^+[Gly]^-$	295.15−295.15	0.01−1.30	14	isochoric saturation method	241
125	$[P_{6,6,6,14}]^+[Ile]^-$	295.15−295.15	0.01−1.01	7	isochoric saturation method	241
126	$[P_{6,6,6,14}]^+[Lys]^-$	295.15−295.15	0.00−1.17	11	isochoric saturation method	245
127	$[P_{6,6,6,14}]^+[MeSO_3]^-$	307.55−322.15	44.80−87.30	28	weight method	243
128	$[P_{6,6,6,14}]^+[phos]^-$	288.21−363.39	6.63−611.72	93	synthetic (bubble point) method	242
129	$[P_{6,6,6,14}]^+[Pro]^-$	283.15−373.15	0.00−1.22	89	isochoric saturation method	245
130	$[P_{6,6,6,14}]^+[Sar]^-$	298.15−298.15	0.00−1.11	4	isochoric saturation method	241
134	$[P_{6,6,6,14}]^+[Tau]^-$	298.15−298.15	0.01−1.16	6	isochoric saturation method	245
132	$[P_{6,6,6,14}]^+[Tf_2N]^-$	292.88−363.53	1.06−721.85	120	synthetic (bubble point) method	244
		293.35−375.35	5.30−222.00	90	isochoric saturation method	209
		313.20−323.20	80.90−201.70	8	isochoric saturation method	207
			total no.	**218**		
133	$[Py_2OH]^+[Tf_2N]^-$	298.15−333.15	6.80−50.44	27	isochoric saturation method	246
134	$[thea]^+[Ac]^-$	303.00−323.00	1.03−10.12	24	isochoric saturation method	225
135	$[thea]^+[L]^-$	303.00−323.00	9.60−84.70	21	isochoric saturation method	225
136	$[TMG]^+[L]^-$	308.05−327.46	4.90−101.80	27	weight method	179

4. CO_2 SOLUBILITY

Since the solubility data of CO_2 in $[BMIM]^+[PF_6]^-$ at 298.2 K and pressures up to 40 MPa was first measured by Blanchard et al.,[184] a large amount of solubility data of CO_2 in ILs has been published in the past decade. The solubility of CO_2 in ILs can be expressed on the basis of mole fraction (units dimensionless), molality (units mol $CO_2 \cdot kg^{-1}$ IL), and volume concentration (units mol $CO_2 \cdot L^{-1}$ IL). Among others, the mole fraction unit has been adopted by most of the references relevant to gas solubility in ILs because it can reflect the molecular interaction between gas and IL. Also, of interest is the different solubility expressions leading to different structure−property relations. Carvalho and Coutinho[185] claimed that CO_2 solubility expressed in molality is independent of the kinds of ILs with a few exceptions, but Ramdin et al.[186] thought that this conclusion is valid only for a limited number of ILs. Besides, it was found that under the same condition, as the alkyl chain length on the cations increases from $[BMIM]^+[BF_4]^-$ to $[HMIM]^+[BF_4]^-$ to $[OMIM]^+[BF_4]^-$, CO_2 solubility expressed in volume concentration is observed to decrease unexpectedly.[187,188] Therefore, in this review we have to use the mole fraction solubility uniformly, unless stated otherwise. In addition, we do not want to discuss the solubility of ILs in gases and agree with the viewpoint raised by the Brennecke group that no appreciable amount of IL is solubilized into the CO_2 phase.[17,20] Moreover, gas solubility data in a homogeneous liquid phase (VLE) rather than in a liquid−liquid phase (VLLE) are focused on in this review.

4.1. CO_2 Solubility in Single IL

Experimental CO_2 solubility data in single ILs are summarized in Table 3, including the kinds of IL, the operating temperature and pressure, the number of data points, and the experimental methods. Detailed values are given in Table S2, Supporting Information, involving about 9000 data points and 136 kinds of ILs.

4.1.1. Structure−Property Relation. Figure 6 shows the Henry's law constants of CO_2 in various ILs at 298.2 K collected from the references as well as predicted results by the UNIFAC and COSMO-RS models. It can be seen that they exhibit similar trends, but the predicted results by the UNIFAC model are quantitatively consistent with the experimental data, more accurate than the COSMO-RS model.

The Henry's law constants are influenced by the types of cations and anions. It is speculated by some authors that the anion plays a primary role in determining the CO_2 solubility in ILs, following the order of $[BF_4]^- < [TfO]^- < [TfA]^- < [PF_6]^- < [Tf_2N]^- < [methide]^- < [C_7F_{15}CO_2]^- < [eFAP]^- < [bFAP]^-$,[186] while the contribution of cations to CO_2 solubility is secondary. However, when the alkyl chain length on the cation increases to a certain extent, the situation may change. For example, with the same $[Tf_2N]^-$ anion, the Henry's law

dx.doi.org/10.1021/cr300497a | Chem. Rev. 2014, 114, 1289−1326

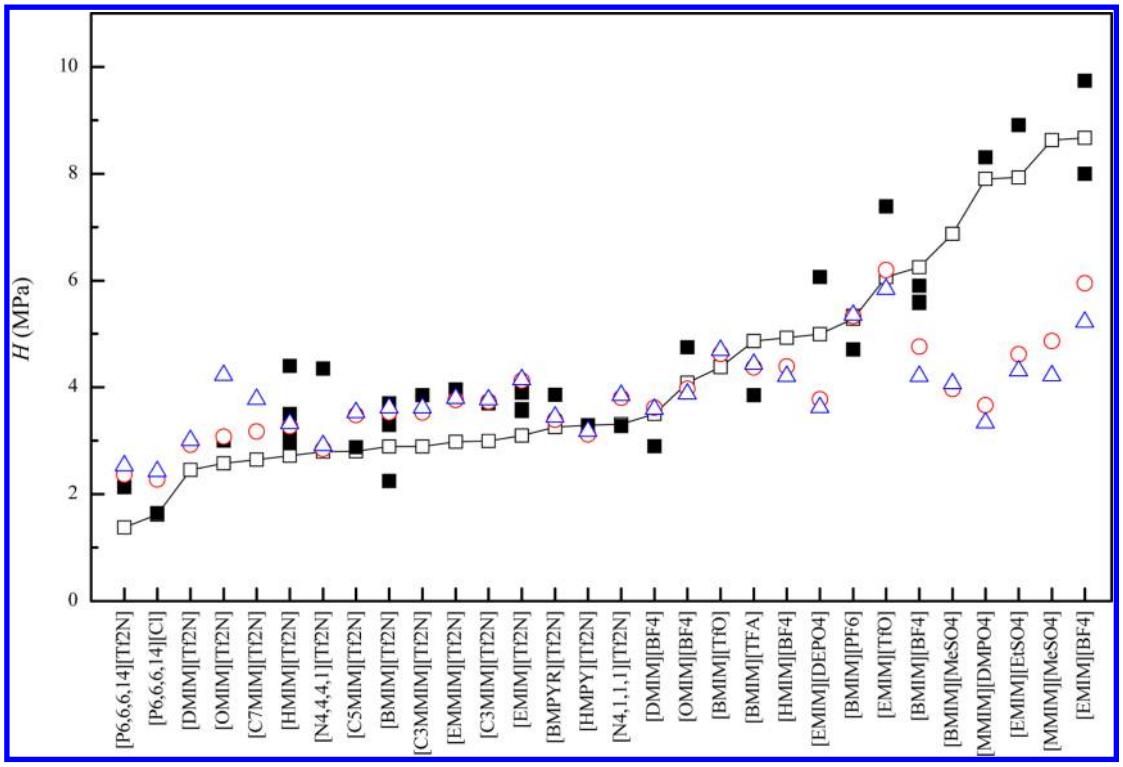

Figure 6. Henry's law constants of CO_2 in various ILs at T = 298.15 K: (□) predicted results by the UNIFAC model; red (○) predicted results by the COSMO-RS model (ADF combi2005); (blue △) predicted results by the COSMO-RS model (ADF combi1998); (■) experimental results from references.[16,35,106,141,148,151,156,157,159,164,171,173,175,192,194,200,205,219,232,248−250]

Table 4. Summary of Solubility Data of Mixed Gases in ILs

no.	mixed gases	ILs	T range (K)	P range (bar)	no. of data points	refs
1	CO_2/Ar	$[HMIM]^+[Tf_2N]^-$	333.00−573.00	50.00−70.00	3	256
2	CO_2/CH_4	$[HMIM]^+[Tf_2N]^-$	298.15−298.15	3.10−14.00	15	257
3	CO_2/H_2	$[BMIM]^+[BF_4]^-$	314.20−365.52	257.90−525.00	36	258
4	CO_2/H_2	$[BMIM]^+[PF_6]^-$	283.15−308.15	7.62−46.58	16	253
5	CO_2/H_2	$[HMIM]^+[Tf_2N]^-$	293.15−373.15	17.99−91.48	34	259
6	CO_2/H_2	$[HMIM]^+[Tf_2N]^-$	333.00−573.00	50.00−60.00	4	256
7	CO_2/N_2	$[HMIM]^+[Tf_2N]^-$	298.15−298.15	3.35−9.67	7	119
8	CO_2/O_2	$[HMIM]^+[Tf_2N]^-$	313.00−313.00	30.00−120.00	6	260
9	CO_2/O_2	$[HMIM]^+[Tf_2N]^-$	298.20−298.20	3.00−15.70	10	257
10	SO_2/N_2	$[HMIM]^+[Tf_2N]^-$	333.00−333.00	3.00−5.00	3	260
11	CO_2/N_2O	$[HMIM]^+[BF_4]^-$	296.50−315.30	4.74−6.46	20	261
12	CO_2/C_3H_8	$[HMIM]^+[Tf_2N]^-$	298.15−298.15	3.35−8.39	12	119
13	CO_2/H_2S	$[BMIM]^+[MeSO_4]^-$	295.80−315.30	2.25−4.87	20	262
14	CO_2/H_2S	$[BMIM]^+[PF_6]^-$	296.00−322.70	3.43−5.50	15	263
15	CO_2/H_2S	$[OMIM]^+[Tf_2N]^-$	303.15−343.15	1.72−12.08	27	239
16	CO_2/H_2S	$[OMIM]^+[PF_6]^-$	303.15−343.15	1.27−9.44	27	238
17	CO_2/SO_2	$[HMIM]^+[Tf_2N]^-$	294.5−322.10	1.05−4.19	23	153
18	CO_2/SO_2	$[BMIM]^+[MeSO_4]^-$	296.50−322.40	1.09−5.01	27	154
19	CO_2/SO_2	$[HMIM]^+[Tf_2N]^-$	333.00−333.00	5.00−10.0	2	260
20	H_2/Ar	$[HMIM]^+[Tf_2N]^-$	313.00−573.00	100.00−300.00	5	256

constant for $[N_{1,4,4,4}]^+$ is twice as high as that for $[P_{6,6,6,14}]^+$, the solubility difference being pronounced. For physical absorption, the structural factors such as fluorination on the cation and anion,[251] bromination on the anion,[95] long alkyl chains with branching or ether linkages on the cation,[115,148,252] and carbonyl or ester groups on the cation[148] do increase the CO_2 solubility relative to their alkyl analogues, while those structural factors such as C2 site substitution with a methyl group,[115,148,252] ether group,[160] hydroxyl group,[148] nitrile group,[114] and alkyne group[114] on the cation are unfavorable for increasing the CO_2 solubility. For chemical absorption, more details will be described in section 4.5.4.

The cloudy image of Henry's law constants of CO_2 in ILs with different combinations of cations and anions at 298.2 K as predicted by the COSMO-RS models is shown in Figure S1, Supporting Information, as well as those of solubility selectivity of H_2 to CO_2, CO to CO_2, N_2 to CO_2, CH_4 to CO_2, and O_2 to CO_2. Solubility selectivity is defined as

dx.doi.org/10.1021/cr300497a | Chem. Rev. 2014, 114, 1289−1326

Table 5. Summary of Solubility Data of CO_2 in ILs Containing Water

no.	ILs	T range (K)	P range (bar)	no. of data points	refs
1	$[bhea]^+[Ac]^-$	298.00−298.00	3.70−15.02	20	264
2	$[BMIM]^+[BF_4]^-$	298.00−298.00	3.44−15.11	20	264
3	$[BMIM]^+[PF_6]^-$	313.15−333.15	10.00−250.00	123	183
4	$[P_{6,6,6,14}]^+[Met]^-$	295.15−295.15	0.003−1.24	10	245
5	$[P_{6,6,6,14}]^+[Pro]^-$	295.15−295.15	0.01−0.96	19	245

$$S_{j/CO_2} = \frac{H_j}{H_{CO_2}} \tag{34}$$

It can be seen that the regions with high CO_2 solubility often correspond to low solubility selectivity, that is, the trends of solubility and solubility selectivity are roughly reverse except for H_2/CO_2, consistent with previous reports.[30,114,161,186] For gas separations, solubility and solubility selectivity will determine the amount of IL and the number of theoretical stages at a given product purity, respectively. Therefore, a compromise between solubility and solubility selectivity should be attained in selecting suitable ILs.

4.1.2. Influence of Other Gases and Water on Solubility. In the real situation, CO_2 often exists with other gases. In this case, the real selectivity (i.e., relative volatility) is defined as[153,253−255]

$$\alpha_{j/CO_2} = S_{j/CO_2} = \frac{y_j/x_j}{y_{CO_2}/x_{CO_2}} \tag{35}$$

where x and y represent the mole fractions of gases in liquid and vapor phases, respectively. Unfortunately, few solubility data of mixed gases in ILs are available from the references due to experimental difficulties, as summarized in Table 4. Toward the real separation, the solubility of mixed gases in ILs will be discussed in detail in section 6.8.

In general, the single-gas solubility in ILs follows the order SO_2 (H_2S) > CO_2 ≈ N_2O > C_2H_4 > C_2H_6 > CH_4 > Ar > O_2 > N_2 > CO > H_2 at the same temperature and pressure. In the case of CO_2 paired with other gases (e.g., CH_4, H_2, O_2, etc.) with lower solubility in ILs, CO_2 can enhance the other gas solubility at the same gas fugacity but reduce its own solubility as well.[257] On the contrary, in the case of CO_2 paired with other gases (e.g., SO_2 and H_2S) with higher solubility in ILs, other gases can enhance CO_2 solubility.[152,153,262,263] However, both cases lead to the real selectivity calculated by eq 35 being overestimated, since in the latter case CO_2 acts as a light component and SO_2 or H_2S as a heavy component. However, molecular simulation results do not support the solubility enhancement of O_2 in $[HMIM]^+[Tf_2N]^-$ in the presence of CO_2 and of CO_2 in $[HMIM]^+[Tf_2N]^-$ in the presence of SO_2.[260]

It is inevitable that the IL sometimes contains a little water due to its hygroscopic nature. Solubility data considering the effect of water content are summarized in Table 5. The influence of water on gas solubility in ILs is brought about in the following aspects.

(i) Degradation effect. It is known that ILs with $[PF_6]^-$ or $[BF_4]^-$ are unstable and easy to hydrolyze in the presence of water, with the fluoride-based impurities being formed.

(ii) Dilution effect. Water dilutes the ILs and inhibits dissolution of CO_2 in ILs in some degree because the affinity between water and CO_2 is very weak. Some authors[17,20,155] claimed that the influence of degradation and dilution effects on gas solubility in ILs is significant, which is the main reason leading to a large discrepancy among the solubility data coming from different sources. However, instead, other authors thought that water has only a minor influence on CO_2 solubility in ILs. For example, the Henry's law constant of CO_2 in $[OMIM]^+[Tf_2N]^-$ with a relative humidity of about 40% is very close to that in dried $[OMIM]^+[Tf_2N]^-$.[157] In the case of $[BMIM]^+[PF_6]^-$ with a water content from 0.0067 to 1.6 wt %, the average deviation in CO_2 solubility is only 6.7% at the same temperature and pressure.[183]

(iii) Enhancement effect. For chemical absorption with TSILs (i.e., $[pabim]^+[BF_4]^-$ and the ILs with $[Ac]^-$), the presence of water will promote complexation of CO_2 with amines to form carbamates[265,266] or with $[Ac]^-$ to form AB or AB_2 types of chemical complexation,[150,152,191] thus increasing the solubility of CO_2 in ILs.

4.1.3. Comparison of Solubility between Low and High Temperatures. Solubility diagrams of CO_2 in two common ILs, i.e., $[HMIM]^+[BF_4]^-$ and $[BMIM]^+[BF_4]^-$, from high to low temperatures are illustrated in Figure 7. It can be seen that the solubility of CO_2 increases significantly as temperature decreases. At low temperatures (below 273.15 K), the solubility is very high even at low pressures. For a given IL, operating at low temperatures will intensify both solubility and solubility selectivity for capturing CO_2. However, the solubility measurement of CO_2 in ILs at low temperatures is rarely conducted and should be emphasized in the future so as to open a wider temperature window for applications with respect to ILs.

4.1.4. Comparison among Different Models. CO_2 solubility data in ILs calculated by the UNIFAC model and two versions of the COSMO-RS model (ADF combi1998 and ADF combi2005) are given in Table S2, Supporting Information, where the relative deviation (RD) and average relative deviation (ARD) are defined as

$$\mathrm{RD} = \left|\frac{x_{pred} - x_{exp}}{x_{exp}}\right|, \quad \mathrm{ARD} = \frac{1}{N}\sum_{1}^{N}\left|\frac{x_{pred} - x_{exp}}{x_{exp}}\right| \tag{36}$$

where x_{exp} is the experimental CO_2 solubility data exhaustively collected from the references, x_{pred} is the predicted CO_2 solubility data by predictive models, and N is the number of data points. Evidently, in most cases the UNIFAC predicted results are close to experimental data with the ARDs for most of the IL-CO_2 systems being less than 20.00%, while two versions of the COSMO-RS model give rise to large deviations, with the ARDs sometimes more than 100%. Therefore, care

dx.doi.org/10.1021/cr300497a | Chem. Rev. 2014, 114, 1289−1326

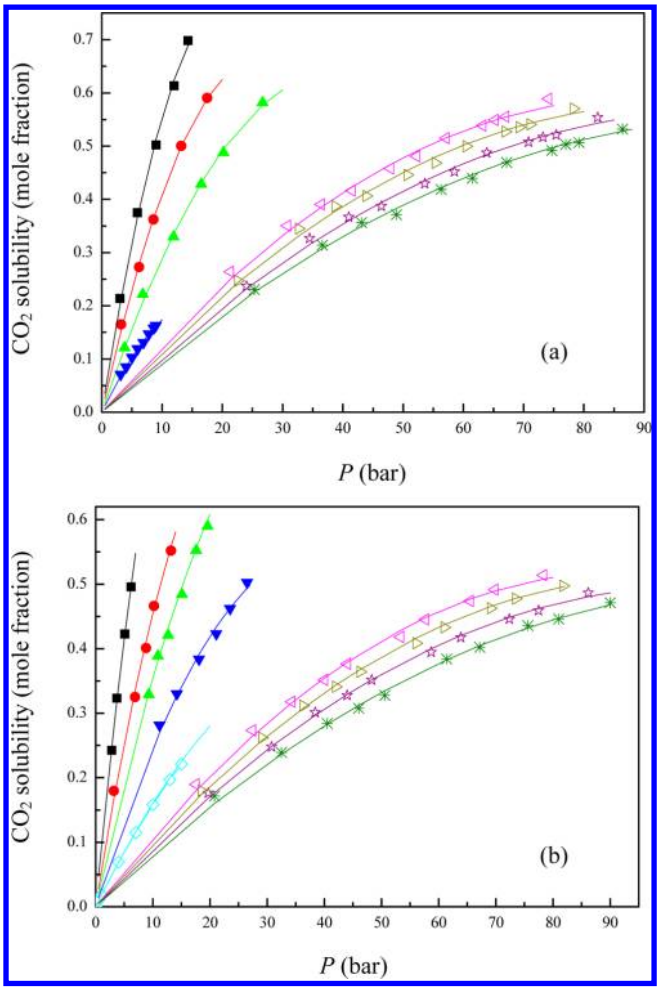

Figure 7. Solubility of CO_2 in $[HMIM]^+[BF_4]^-$ (a) and $[BMIM]^+[BF_4]^-$ (b) at different temperatures. (a) (■) 243.15,[158] (red ●) 258.15,[158] (green ▲) 273.15,[158] (blue ▼) 298.15,[62] (pink triangle pointing left) 307.55,[194] (olive triangle pointing right) 312.45,[194] (purple ☆) 317.45,[194] (green *) 322.15[194] K; (b) (■) 228.15,[158] (red ●) 243.15,[158]) (green ▲) 258.15,[158] (blue ▼) 273.15,[158] (light blue ◇) 298.20,[152] (pink triangle pointing left) 307.55,[194] (olive triangle pointing right) 312.45,[194] (purple ☆) 317.45,[194] (green *) 322.15 [194] K.

should be taken to use the COSMO-RS model at the risk of poor prediction for CO_2 solubility.

4.2. CO_2 Solubility in the Mixture of IL and IL

In comparison with CO_2 solubility in a single IL, the number of publications on CO_2 solubility in a mixture of IL and IL are fewer. Baltus et al.[157] first reported the Henry's law constant of CO_2 in a mixture of 58 mol % $[OMIM]^+[Tf_2N]^-$ and 42 mol % $[C_8F_{13}MIM]^+[Tf_2N]^-$ at 298.2 K and pressure close to 1 bar, which lies between the Henry's law constants in pure $[OMIM]^+[Tf_2N]^-$ and $[C_8F_{13}MIM]^+[Tf_2N]^-$. Finotello et al.[188] measured the solubility of CO_2, CH_4, and N_2 gases in a mixture of $[EMIM]^+[Tf_2N]^-$ and $[EMIM]^+[BF_4]^-$ at 313.2 K and 1 atm, which are present in the units of volume concentration. It is the first time for Lei et al.[160] to measure the solubility of CO_2 in binary mixtures of $[EMIM]^+[BF_4]^-$ + $[OMIM]^+[Tf_2N]^-$ and $[BMIM]^+[BF_4]^-$ + $[OMIM]^+[Tf_2N]^-$ with various mass fractions at high pressures up to 6.0 MPa for physical absorption, while Shiflett and Yokozeki[150] measured the solubility of CO_2 in an equimolar amount of $[EMIM]^+[Ac]^-$ and $[EMIM]^+[TFA]^-$ at temperatures of 298.1, 323.1, and 348.1 K and pressures up to 2.0 MPa, showing a combination of chemical and physical absorptions. The reasons why the mixed ILs are selected as separating agents for capturing CO_2 are attributed to the complementation of high viscosity with fluorinated IL and low viscosity with non-fluorinated IL, high solubility and high selectivity, or chemical and physical interactions.

Whether it is physical absorption or a combination of physical and chemical absorptions, the solubility of CO_2 in the mixture of IL and IL can be well predicted from those in individual ILs according to the following lever rule

$$x_1' = X_2 x_{1,2} + X_3 x_{1,3} \quad (37)$$

where X_2 and X_3 are mole fractions of individual ILs in the mixture on a CO_2-free basis and $x_{1,2}$ and $x_{1,3}$ are mole fractions (i.e., solubility) of CO_2 in pure ILs. Detailed solubility data of CO_2 in a mixture of two ILs are given in Table S16, Supporting Information.

4.3. CO_2 Solubility in the Mixture of Organic Solvent and IL

Although ILs have received popular attention due to their negligible vapor pressure, low toxicity, tunable structure, and high CO_2 solubility, the viscosity of pure ILs is often much higher than that of traditional organic solvents, which may limit their industrial applications. It is known that the viscosity of ILs can decrease sharply by adding a small amount of water or organic solvent.[268−271] Therefore, the mixture of IL and organic solvent as a new solvent for capturing CO_2 was also proposed combining the individual advantages of organic solvents and ILs.

Liu et al.[272] studied the viscosities and other thermodynamic properties of ILs at elevated pressures and reported only a few solubility data of CO_2 in the binary mixture of $[BMIM]^+[PF_6]^-$ and methanol at a temperature of 313.2 K and pressures of 7.15 and 10.00 MPa approaching the supercritical state. Mellein and Brennecke[19] and Aki et al.[20−22] investigated the ternary system phase behavior containing IL/organic solvent/CO_2 in which CO_2 was treated as an antisolvent to induce liquid−liquid phase splitting of homogeneous mixtures of organics and ILs, and the lowest critical end point pressure (LCEP) and the K-point pressure rather than CO_2 solubility were their main objectives. Hong et al.[223] reported the solubility of CO_2 in the binary mixture of $[EMIM]^+[Tf_2N]^-$ and acetonitrile (CH_3CN) at pressures close to atmospheric pressure and temperatures of 290−335 K and found that CO_2 solubility has a 50% reduction with the mole fraction of acetonitrile increasing from 0 to 0.77 at 303 K. Zhang et al.[273] studied the high-pressure phase behavior of the CO_2/acetone/$[BMIM]^+[PF_6]^-$ system at 313.15 K and showed that at pressures between 4.9 and 8.1 MPa a three-phase (LLV) region appears. Kühne et al.[274−276] presented the phase equilibria for ternary mixtures of $[BMIM]^+[BF_4]^-$, CO_2, and four organic solutes (4-isobutylacetophenone, 1-phenylethanol, acetophenone, and 1-(4-isobutylphenyl)ethanol) aiming to investigate the possibility of carrying out a reaction in a medium of IL/supercritical CO_2. Experimental results showed a higher solubility of CO_2 using a ketone as solute rather than an alcohol because the solute with a hydroxyl group (alcohol) may form hydrogen bonds with $[BF_4]^-$ and thus reduce the interaction between CO_2 and IL. A conclusion was also made that free volume in the IL/organic solvent mixture and interaction between solute and IL are important in determining the CO_2 solubility in the mixture of

dx.doi.org/10.1021/cr300497a | Chem. Rev. 2014, 114, 1289−1326

organic solvent and IL. Bogel-Łukasik et al.[217,277] measured the gas−liquid equilibrium at 313.15 K and pressure range of 9−12 MPa for ternary systems of CO_2 + IL + alcohol. Later, they studied the phase equilibrium for CO_2 + IL + organic acid systems at 313.15 K and found that formation of a stronger interaction in lactic acid reduces the CO_2 solubility when compared to propionic acid.[278] Ahn et al.[167] reported the solubility of CO_2 in a mixture of $[HMIM]^+[Tf_2N]^-$ and dimethyl carbonate (DMC) with different compositions at temperatures from 303.2 to 333.2 K and pressures up to 7.0 MPa. Ahmady et al.[279] and Sairi et al.[280] studied the solubility of CO_2 in mixtures of aqueous *N*-methyldiethanolamine (MDEA) + $[BMIM]^+[BF_4]^-$ and aqueous MDEA + TSIL ($[gua]^+[TfO]^-$). CO_2 solubility increases with an increase of $[BMIM]^+[BF_4]^-$ concentration; however, addition of $[gua]^+[TfO]^-$ into MDEA slightly lowers the CO_2 solubility, and the TSIL is believed to hinder the tertiary amine of MDEA and lessen the free space to absorb CO_2. Tian et al.[182] studied the solubility of CO_2 in the binary mixture $[BMIM]^+[BF_4]^-$ and *N*-methyl-2-pyrrolidone (NMP) with different concentrations at temperatures of 298.15−318.15 K. Taib and Murugesan[264] reported the CO_2 solubility in mixtures of aqueous IL and monoethanolamine (MEA) at pressures from 100 to 1600 kPa and found that pure or aqueous $[BMIM]^+[BF_4]^-$ has higher CO_2 solubility than that of $[bhea]^+[Ac]^-$ due to physical absorption, while the uptake of CO_2 in aqueous $[bhea]^+[Ac]^-$ + MEA solution is higher than that in $[BMIM]^+[BF_4]^-$ + MEA solution due to the reversible chemical reaction between $[bhea]^+[Ac]^-$ and CO_2, which could explain why the uptake of CO_2 is nearly constant with increasing temperature for aqueous $[bhea]^+[Ac]^-$ + MEA solution.

Recently, we measured the solubility of CO_2 in a mixture of IL (e.g., $[EMIM]^+[BF_4]^-$ and $[BMIM]^+[BF_4]^-$) and acetone,[181] demonstrating that CO_2 solubility in the mixture of acetone and $[BMIM]^+[BF_4]^-$ is higher than those in other binary mixtures of organic solvent and IL (e.g., acetone + $[EMIM]^+[BF_4]^-$,[159] DMC + $[HMIM]^+[Tf_2N]^-$, 4-isobutylacetophenone + $[BMIM]^+[BF_4]^-$,[274] acetophenone + $[BMIM]^+[BF_4]^-$,[275] 1-phenylethanol + $[BMIM]^+[BF_4]^-$,[275] and 1-(4-isobutylphenyl)-ethanol + $[BMIM]^+[BF_4]^-$[276]) at a fixed mole ratio of organic solvent to IL. Moreover, the solubility of CO_2 in the mixture of IL and organic solvent can be well predicted by the lever rule as mentioned above. Table S16, Supporting Information, lists detailed solubility data of CO_2 in a mixture of IL and organic liquid.

4.4. CO_2 Solubility in Poly(ionic liquid)s

Tang et al.[140,144−147,281,282] first observed that the poly(ionic liquid)s have higher CO_2 solubility than the corresponding IL monomers with faster absorption/desorption rates, and a series of poly(ionic liquid)s, e.g., PVBIT, PVBIH, PBIMT, P-$[MATMA]^+[BF_4]^-$, $P[VBTMA]^+[BF_4]^-$, was synthesized from their corresponding IL monomers. CO_2 absorption experiments were conducted by the authors. It was found that the poly(ionic liquid) $P[VBTMA]^+[BF_4]^-$ has a CO_2 absorption capacity of 10.2%, which is 6.6 times higher than that in the IL monomer $[BMIM]^+[BF_4]^-$ at the same temperature and pressure. In addition, poly(ionic liquid)s with ammonium-based monomers have much higher CO_2 absorption capacities than those with imidazolium-based monomers. The CO_2 absorption capacities of poly(ionic liquid)s with different cations decrease in the order ammonium > pyridinium > phosphnium > imidazolium, while for those with different anions the order becomes $[BF_4]^-$ > $[PF_6]^-$ ≫ $[Tf_2N]^-$, which is contrary to the solubility trend in common ILs.[186] A long alkyl substituent on the cation and cross-linking structure would decrease the CO_2 absorption capacity. Bara et al.[31−33] studied the separation selectivity of CO_2/N_2 and CO_2/CH_4, showing an ideal separation performance of poly(ionic liquid)s containing oligo(ethylene glycol) or nitrile-terminated alkyl substituents. However, most of the poly(ionic liquid)s are in the solid or polymeric state, which may be not suitable for a continuous operation in industry.

4.5. Solubility Mechanism

4.5.1. Anion Effect. The theory of anion effect speculates that the anion has a stronger effect on determining the CO_2 solubility in ILs than does the cation, as mentioned above. However, this theory cannot answer the following issues at least.

(i) The Henry's law constants of CO_2 in the ILs with long alkyl chain on the cations become very small (see Figure 6) provided that these ILs exist in the molten state at room temperature (e.g., $[P_{6,6,6,14}]^+[Tf_2N]^-$).

(ii) The Henry's law constants of CO_2 in $[OMIM]^+[Tf_2N]^-$ and $[C_8F_{13}MIM]^+[Tf_2N]^-$ at 298.2 K are 30 and 4.5 bar,[153] respectively, and significantly different from each other.

4.5.2. Free Volume Effect. More researchers are now cognizant of the pitfall of the anion effect and are beginning to support the theory of the free volume effect which should determine the CO_2 solubility in ILs. Then, from a microscopic viewpoint, where does the IL's free volume exist? The theory of anion effect speculates that free volume lies in the interstitial space near the alkyl chain on the cation, and a long alkyl chain is favorable for increasing free volume. However, recent molecular dynamic simulation and quantum chemical calculation[283,284] suggested that free volume lies in the interionic space between cation and anion, indicating that a weaker cation−anion interaction is favorable for increasing CO_2 solubility.

In classical thermodynamics, free volume is defined as the difference between the molar volume V_m and the van der Waals volume V_{vdw} of IL. Very recently, Shannon et al.[187] went a further step to introduce the concept of fractional free volume (FFV) to understand the physical dissolution of CO_2 in ILs, which is defined as

$$\mathrm{FFV} = \frac{V_m - 1.3V_{vdw}}{V_m} \tag{38}$$

where V_{vdw} can be calculated by the method suggested by Bond,[57] or by the COSMO-RS model as mentioned above.

The theory of the free volume effect can not only clarify the unsolved issues by the theory of anion effect but also provide insight into the following experimental phenomena at least.

(i) At a given temperature, the solubility of CO_2 in ILs first increases with increasing pressure but finally tends to level off at very high pressure where there is no available free volume occupied by CO_2 molecules. In other words, further addition of CO_2 molecules into IL is nearly impossible unless the strong cohesive structure of IL is broken.

(ii) The CO_2 solubility in ILs can be related with the molar volumes of ILs. The larger the molar volumes of ILs, the

dx.doi.org/10.1021/cr300497a | *Chem. Rev.* 2014, 114, 1289−1326

higher the CO_2 solubility. This is due to the larger molar volumes corresponding to the higher FFV, as confirmed by Shannon et al.[187] via the curve fitting over a series of imidazolium-based ILs. Herein, we like to extend this conclusion to other phosphonium- and ammonium-based ILs. It can be seen from Figure 8 that as molar volumes of ILs increase, CO_2 solubility also tends to increase, demonstrating the rationality of the free volume effect. Furthermore, as the alkyl chain length on the cations becomes long enough to make FFV of all ILs approach a common asymptotic value, one might speculate that the solubility of CO_2 in these ILs is the same, independent of the anions. However, no any experimental confirmation was done in this regard. Therefore, the theory of the free volume effect seems more promising than the theory of the anion effect.

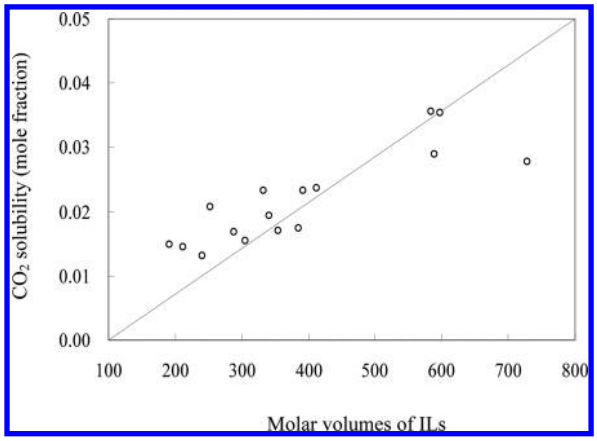

Figure 8. CO_2 solubility versus molar volumes of ILs for imidazolium-, phosphonium-, and ammonium-based ILs at 303.2 K and 1 atm. Data points come from ref 109 with permission. Copyright 2008 American Chemical Society.

4.5.3. Lewis Acid–Base Interaction. The theory originates from the experimental observation of ATR-IR spectroscopy,[285] which provides evidence of Lewis acid–base interaction between the anions (e.g., $[PF_6]^+$ and $[BF_4]^-$) and CO_2, and CO_2 acts as a Lewis acid and the anion as a Lewis base. However, the limitations of this theory are brought out in the following aspects.

(i) It cannot explain why the ILs with $[Tf_2N]^-$ generally have a higher CO_2 than those with $[PF_6]^+$ or $[BF_4]^-$, whereas the interaction between CO_2 and $[PF_6]^+$ (or $[BF_4]^-$) is stronger than between CO_2 and $[Tf_2N]^-$.[16,283]

(ii) Both MC simulation and quantum chemical calculation confirmed that the main molecular interaction between CO_2 and IL is van der Waals force instead of the Pearson's "hard and soft acid/base" principle.[95,96]

(iii) Unexpectedly, a higher CO_2 solubility in $[BMIM]^+[DCA]^-$ with $pK_a = 5.2$ as a basic anion was not obtained in comparison with the acetate anion with $pK_a = 4.75$,[170] which is in contradiction with the theory of Lewis acid–base interaction.

4.5.4. Chemical Interaction. The theory of chemical interaction is suitable for interpreting the solubility of CO_2 in ILs for chemical absorption, while the aforementioned three theories are only suitable for physical absorption. In this theory, a reversible chemical reaction between CO_2 and IL takes place in a similar way as that present in complex or reactive extractive distillation,[286,287] and the ILs are regenerated at the expense of high energy consumption by vacuum heating. The TSILs containing an amine or acetate moiety are commonly recommended.[266,288−293] Chemical absorption is suitable for dissolving CO_2 from flue gas at a relatively small partial pressure due to its large solubility in TSILs.

5. SO_2 SOLUBILITY

5.1. SO_2 Solubility in Single IL

Wu et al.[296−299] first proposed several kinds of TSILs (e.g., $[TMG]^+[L]^-$, $[MEA]^+[L]^-$), which may chemically react with SO_2 forming an intramolecular hydrogen bond to absorb SO_2 at temperatures of 313.2−367.2 K and ambient pressure, because TSILs have a much higher solubility than common ILs (e.g., $[RMIM]^+[PF_6]^-$ and $[RMIM]^+[BF_4]^-$) without basic functional groups. Anderson et al.[295] reported the solubility of SO_2 in ILs (i.e., $[HMIM]^+[Tf_2N]^-$ and $[HMPY]^+[Tf_2N]^-$) at temperatures from 298.2 to 333.2 K and pressures up to 4 bar, indicating that a large amount of SO_2 dissolves in ILs by simple physical absorption. Later, Yokozeki et al.[153,300] investigated the SO_2 solubility in imidazolium-based ILs with different anions (e.g., $[Tf_2N]^-$, $[Ac]^-$, and $[MeSO_4]^-$) over a temperature range of 283−348 K and pressure range of 0.005−0.3 MPa.

5.1.1. Structure–Property Relation. Manan et al.[42] showed that the solubility of SO_2 in imidazolium-based ILs with $[Tf_2N]^-$ anion decreases slowly with the increase of alkyl chain length on the cation. Solubility data of SO_2 in imidazolium- and pyridinium-based ILs with different anions at 298.15 K collected from refs 295 and 301 are illustrated in Figure 9. It can be seen that SO_2 solubility in ILs is extremely higher than CO_2 solubility, following the order $[BMIM]^+ < [EMIM]^+ < [HMIM]^+$ with the same anion $[BF_4]^-$, but their difference is very small. However, for ILs with $[Tf_2N]^-$ anion, SO_2 solubility follows the order $[HMIM]^+ < [BMIM]^+$. Anyway, the influence of alkyl chain length in imidazolium-based ILs on SO_2 solubility is not so apparent.

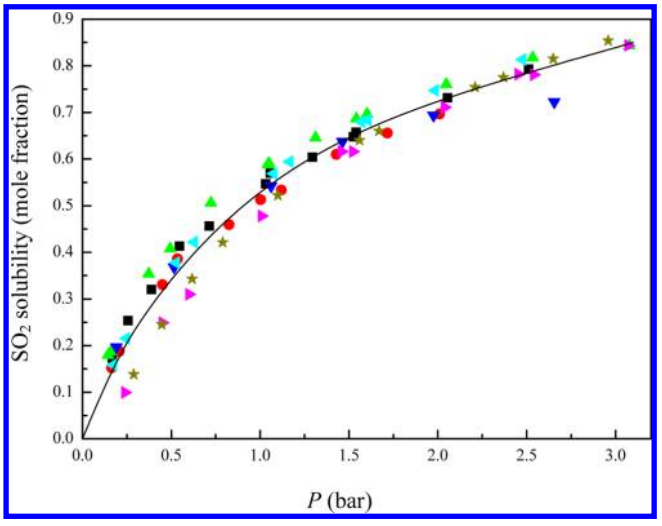

Figure 9. Solubility of SO_2 in imidazolium- and pyridinium-based ILs with different anions (i.e., $[BF_4]$, $[PF_6]$, and $[Tf_2N]$) at 298.15 K. (■) $[EMIM]^+[BF_4]^-$,[301] (red ●) $[BMIM]^+[BF_4]^-$,[301] (green ▲) $[HMIM]^+[BF_4]^-$,[301] (blue ▼) $[BMIM]^+[PF_6]^-$,[301] (light blue triangle pointing left) $[BMIM]^+[Tf_2N]^-$,[301] (pink triangle pointing right) $[HMIM]^+[Tf_2N]^-$,[295] (olive ★) $[HMPY]^+[Tf_2N]^-$.[295]

dx.doi.org/10.1021/cr300497a | Chem. Rev. 2014, 114, 1289−1326

Table 6. Summary of Solubility Data of SO_2 in ILs

no. of IL	ILs	T range (K)	P range (bar)	no. of data points	experimental method	refs
1	$[BMIM]^+[Ac]^-$	282.80−348.20	0.52−30.17	50	gravimetric microbalance method	300
2	$[BMIM]^+[BF_4]^-$	298.15−298.15	0.16−2.01	10	isochoric saturation method	301
		293.15−293.15	1.00−1.00	5	gravimetric microbalance method	302
			total no.	**15**		
3	$[BMIM]^+[MeSO_4]^-$	282.90−348.20	0.05−3.00	62	gravimetric microbalance method	300
4	$[BMIM]^+[PF_6]^-$	298.15−298.15	0.19−2.66	6	isochoric saturation method	301
5	$[BMIM]^+[Tf_2N]^-$	298.15−298.15	0.17−2.48	10	isochoric saturation method	301
		293.15−413.15	1.00−1.00	7	gravimetric microbalance method	302
			total no.	**17**		
6	$[EMIM]^+[BF_4]^-$	298.15−298.15	0.26−2.51	12	isochoric saturation method	301
7	$[HMIM]^+[BF_4]^-$	298.15−298.15	0.16−3.08	13	isochoric saturation method	301
8	$[HMIM]^+[Tf_2N]^-$	283.20−348.20	0.11−3.00	38	gravimetric microbalance method	153
		298.15−333.15	0.28−3.30	30	gravimetric microbalance method	295
			total no.	**68**		
8	$[HMPY]^+[Tf_2N]^-$	298.15−298.15	0.29−2.96	11	gravimetric microbalance method	295
9	$[MEA]^+[L]^-$	293.15−293.15	0.03−10.13	6	weight method	298
10	$[TMG]^+[L]^-$	293.15−293.15	0.03−10.13	6	weight method	298
11	$[TMGH]^+[BF_4]^-$	293.15−413.15	1.00−1.00	7	gravimetric microbalance method	302
12	$[TMGH]^+[Tf_2N]^-$	293.15−393.15	1.00−1.00	6	gravimetric microbalance method	302
13	$[TMGHB_2]^+[Tf_2N]^-$	293.15−393.15	1.00−1.00	6	gravimetric microbalance method	302
14	$[TMGHPO]^+[BF_4]^-$	293.15−413.15	1.00−1.00	7	gravimetric microbalance method	302
15	$[TMGHPO_2]^+[BF_4]^-$	293.15−413.15	1.00−1.00	7	gravimetric microbalance method	302

Solubility data of SO_2 in $[BMIM]^+[X]^-$ with different anions (i.e., $[BF_4]^-$, $[PF_6]^-$, and $[Tf_2N]^-$) almost overlap at pressures below 1.0 bar, and at high pressures SO_2 solubility in $[Tf_2N]^-$ is a little higher than the other two. However, more surprisingly, SO_2 solubility in $[HMIM]^+[Tf_2N]^-$ is even smaller than that in $[HMIM]^+[BF_4]^-$. Therefore, the influence of anions on SO_2 solubility is not predominant as much as CO_2 solubility. A similar conclusion is also obtained for TMG (1,1,3,3-tetramethylguanidinium)-based ILs, as reported by Huang et al.[302]

Although the thermodynamic properties of solvents can be tuned through combination of two kinds of ILs or with addition of organic liquid, intil now only SO_2 solubility data in single ILs have been reported. In further work, the solubility measurement of SO_2 in solvent mixtures should be addressed.

5.1.2. Comparison with COSMO-RS Model. In this review, solubility data of SO_2 in ILs exhaustively collected from the references are summarized in Table 6, and detailed values are listed in Table S3, Supporting Information, along with a comparison between experimental data and COSMO-RS-predicted results (by the ADF combi2005 and ADF combi1998 versions). In most cases, the COSMO-RS models underestimate the SO_2 solubility, indicating that the COSMO-RS models can only give a qualitative trend on the structure−property relation for SO_2 solubility in ILs but not a quantitative prediction. Unfortunately, other predictive thermodynamic models cannot be adopted for predicting the solubility of SO_2 in ILs due to the vacancy of model parameters. Therefore, there is an urgent demand for a reliable and an efficient predictive model to predict the solubility of SO_2 in ILs.

5.2. Solubility Mechanism

5.2.1. Physical Interaction. The solubility mechanism of SO_2 in common ILs is attributed to the physical interaction between SO_2 molecule and IL. SO_2 solubility is greatly dependent on pressure, exhibiting a similar trend as CO_2 solubility. Moreover, the absorbed SO_2 gas remains in the molecular state and can be readily desorbed from IL if only physical interaction dominates. Anderson et al.[295] showed that $[HMIM]^+[Tf_2N]^-$ and $[HMPY]^+[Tf_2N]^-$ can physically absorb a large amount of SO_2, and their Henry's constants are slightly higher than in $[TMG]^+[L]^-$. They also suggested that a high solubility could be achieved only by simply reducing the temperature slightly to avoid the problem of chemical complexation. Five kinds of ILs (i.e., $[BMIM]^+[BF_4]^-$, $[TMG]^+[BF_4]^-$, $[TMG]^+[BTA]^-$, $[BMIM]^+[BTA]^-$, and $[TMGB_2]^+[BTA]^-$) absorb SO_2 only physically without any chemical reaction, as evidenced by ^1H NMR and FT-IR spectroscopy.[303] The high SO_2 solubility in TMG-based ILs may be attributed to the interaction of a van der Waals type of bonding between the dissolved gas molecule and the delocalized π electrons on the cation.[302]

5.2.2. Chemical Interaction. It is believed that SO_2 dissolution by hydroxyl ammonium-based ILs, the ILs with acetate or methyl sulfate anion, and TSILs are based on both chemical and physical interactions. The mechanism of chemical interaction on SO_2 dissolution in TSIL (e.g., $[TMG]^+[L]^-$ and $[MEA]^+[L]^-$) has been verified by the FTIR spectrum that SO_2 reacts with the NH_2 group on the cation.[296−298] The hydroxyl ammonium ILs as proposed by Yuan et al.[304] mainly absorb SO_2 with chemical interaction where SO_2 reacts with the −NH group on the cation, and the mole ratio of IL to SO_2 is 1.0.[154,300]

Figure 10 shows the solubility data of SO_2 in three kinds of ILs with chemical interaction. It can be seen that at high pressures the predicted results by the COSMO-RS model are closer to the experimental data, indicating that physical interaction is predominant in this region, whereas a large deviation between experimental data and predicted results arises at low pressures, because in this case SO_2 dissolution is mainly based on chemical interaction which is not significantly influenced by pressure. SO_2 solubility increases with increasing pressure, and physical interaction takes a larger proportion at high pressures.

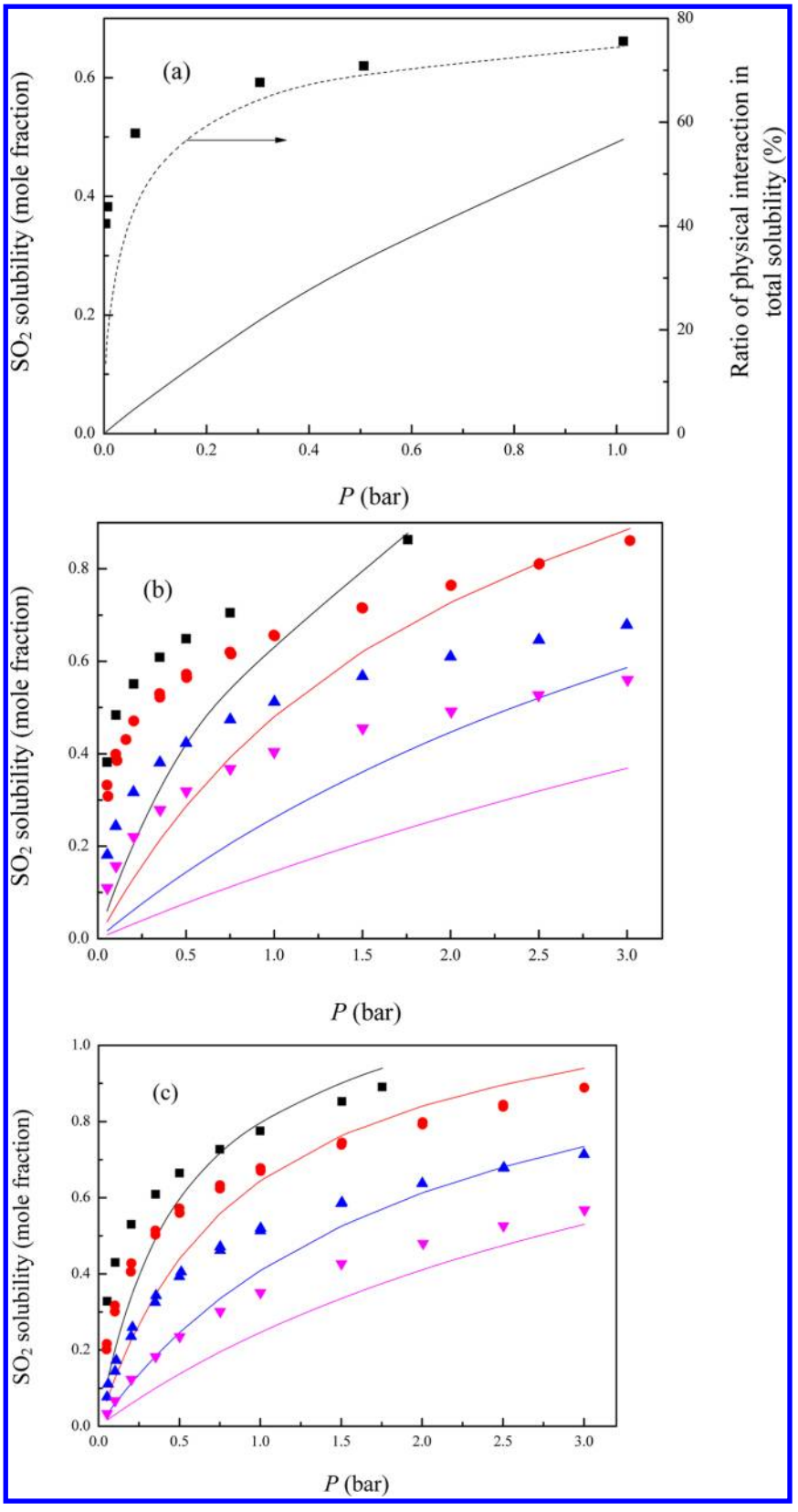

Figure 10. Solubility of SO_2 in ILs with chemical interaction. (Solid lines) Predicted results by the COSMO-RS model (ADF combi2005). (Scattered points) Experimental data. (a) $[TMG]^+[L]^-$ at 293.15 K;[298] (dashed lines) calculated ratio of physical interaction in total solubility. (b) $[BMIM]^+[Ac]^-$:[300] (■) 283.0, (red ●) 298.1, (blue ▲) 323.1, (pink ▼) 348.1 K. (c) $[BMIM]^+[MeSO_4]^-$:[300] (■) 283.0, (red ●) 298.1, (blue ▲) 323.1, (pink ▼)348.1 K.

dx.doi.org/10.1021/cr300497a | *Chem. Rev.* 2014, 114, 1289−1326

Table 7. Summary of Solubility Data of CO, N_2, O_2, and H_2 in ILs

no. of IL	ILs	gases	T range (K)	P range (bar)	no. of data points	experimental method	refs
1	$[BMIM]^+[BF_4]^-$	CO	283.18−343.04	0.80−0.90	9	isochoric saturation method	163
2	$[BMIM]^+[MeSO_4]^-$	CO	293.15−413.15	12.17−93.31	25	isochoric saturation method	311
3	$[BMIM]^+[PF_6]^-$	CO	293.20−373.15	7.76−91.67	36	isochoric saturation method	307
			283.16−343.27	0.81−0.91	8	isochoric saturation method	41
4	$[HMIM]^+[Tf_2N]^-$	CO	293.30−413.15	14.59−97.85	24	isochoric saturation method	308
			300.70−437.29	40.49−116.72	61	synthetic (bubble point) method	309
5	$[MDEA]^+[Cl]^-$	CO	313.15−333.15	25.10−86.20	35	isochoric saturation method	236
				total no.	**198**		
1	$[BMIM]^+[BF_4]^-$	N_2	283.20−243.14	0.51−0.92	12	isochoric saturation method	163
2	$[BMIM]^+[C_3F_7CO_2]^-$	N_2	303.15−333.15	22.00−84.20	20	isochoric saturation method	195
3	$[BMIM]^+[eFAP]^-$	N_2	303.17−343.20	0.91−1.03	20	isochoric saturation method	198
4	$[BMIM]^+[PF_6]^-$	N_2	283.27−343.15	0.42−0.89	13	isochoric saturation method	41
5	$[BMPYR]^+[eFAP]^-$	N_2	303.16−343.14	0.92−1.04	14	isochoric saturation method	210
6	$[HMPY]^+[Tf_2N]^-$	N_2	298.15−298.15	0.05−13.00	18	gravimetric microbalance method	251
7	$[MDEA]^+[Cl]^-$	N_2	313.15−333.15	21.50−74.70	40	isochoric saturation method	236
8	$[P_{6,6,6,14}]^+[eFAP]^-$	N_2	303.16−343.28	0.73−0.83	15	isochoric saturation method	210
9	$[TMG]^+[L]^-$	N_2	308.00−328.00	21.60−87.40	27	isochoric saturation method	313
				total no.	**179**		
1	$[BMIM]^+[BF_4]^-$	O_2	283.25−343.30	0.44−0.90	14	isochoric saturation method	163
			298.00−353.20	5.23−20.96	19	isochoric saturation method	196
2	$[BMIM]^+[C_3F_7CO_2]^-$	O_2	303.15−333.15	22.40−85.40	24	isochoric saturation method	195
3	$[BMIM]^+[PF_6]^-$	O_2	283.18−343.13	0.44−0.91	11	isochoric saturation method	41
			283.15−323.15	0.00−13.00	74	gravimetric microbalance method	156
			298.15−323.15	0.00−13.00	75	gravimetric microbalance method	16
			293.15−373.15	11.64−91.16	41	isochoric saturation method	314
4	$[BMIM]^+[PF_6]^-$	O_2	298.30−355.40	14.44−19.85	9	isochoric saturation method	196
5	$[BMIM]^+[Tf_2N]^-$	O_2	283.15−323.15	0.00−13.00	51	gravimetric microbalance method	16
			314.00−353.20	11.92−56.14	12	isochoric saturation method	196
6	$[BMPYR]^+[Tf_2N]^-$	O_2	283.15−323.15	0.00−13.00	52	gravimetric microbalance method	16
7	$[EMIM]^+[BF_4]^-$	O_2	314.09−344.54	0.20−0.88	7	isochoric saturation method	193
8	$[HMIM]^+[Tf_2N]^-$	O_2	293.25−413.20	7.24−91.04	22	isochoric saturation method	308
9	$[HMPY]^+[Tf_2N]^-$	O_2	283.15−323.15	0.02−10.00	101	gravimetric microbalance method	251
10	$[MDEA]^+[Cl]^-$	O_2	313.15−333.15	19.50−75.90	35	isochoric saturation method	236
11	$[N_{4,4,4,1}]^+[Tf_2N]^-$	O_2	283.15−323.15	0.00−11.50	45	gravimetric microbalance method	16
12	$[P_{1,4,4,4}]^+[TOS]^-$	O_2	323.15−323.15	0.00−13.00	34	gravimetric microbalance method	16
13	$[TMG]^+[L]^-$	O_2	308.00−328.00	11.80−97.20	30	isochoric saturation method	313
				total no.	**656**		
1	$[BMIM]^+[BF_4]^-$	H_2	278.20−343.11	0.46−0.90	16	isochoric saturation method	163
			314.09−365.86	218.00−552.00	31	synthetic (bubble point) method	258
2	$[BMIM]^+[C_3F_7CO_2]^-$	H_2	303.15−333.15	14.60−89.00	24	isochoric saturation method	195
3	$[BMIM]^+[MeSO_4]^-$	H_2	293.30−413.15	11.25−89.19	26	isochoric saturation method	311
4	$[BMIM]^+[PF_6]^-$	H_2	313.05−373.15	10.84−91.00	32	isochoric saturation method	315
			283.40−343.14	0.45−0.94	15	isochoric saturation method	41
5	$[BMIM]^+[Tf_2N]^-$	H_2	283.45−343.13	0.75−0.92	11	isochoric saturation method	205
			333.15−453.15	26.76−154.34	100	synthetic (bubble point) method	308
6	$[BMPY]^+[Tf_2N]^-$	H_2	293.00−413.00	13.65−89.45	24	isochoric saturation method	212
7	$[EMIM]^+[PF_6]^-$	H_2	298.00−356.40	26.82−32.51	6	isochoric saturation method	196
8	$[EMIM]^+[Tf_2N]^-$	H_2	282.98−343.07	0.43−0.90	13	isochoric saturation method	205
			312.14−452.42	57.14−143.05	52	synthetic (bubble point) method	322
9	$[HMIM]^+[Tf_2N]^-$	H_2	293.20−413.20	14.76−98.19	25	isochoric saturation method	316
			283.88−343.02	0.78−0.94	11	isochoric saturation method	232
			293.15−368.41	45.79−123.03	83	synthetic (bubble point) method	317
10	$[MDEA]^+[Cl]^-$	H_2	313.15−333.15	13.20−58.80	40	isochoric saturation method	236
11	$[N_{4,1,1,1}]^+[Tf_2N]^-$	H_2	282.93−343.02	0.46−0.93	13	isochoric saturation method	205
12	$[TMG]^+[L]^-$	H_2	308.00−328.00	12.60−99.10	30	isochoric saturation method	313
				total no.	**552**		

5.3. Capturing SO_2 and CO_2 Simultaneously

Although the topic on capturing SO_2 and CO_2 simultaneously with ILs is of great industrial interest, relevant references are very scarce. Jiang et al.[301] reported that the permeability of SO_2 in supported IL membranes is 9−19 times that of CO_2 when neglecting the interaction between SO_2 and CO_2. Shi and

dx.doi.org/10.1021/cr300497a | Chem. Rev. 2014, 114, 1289−1326

Table 8. Summary of Solubility Data of H_2S in ILs

no. of IL	ILs	T range (K)	P range (bar)	no. of data points	experimental method	refs
1	$[BMIM]^+[BF_4]^-$	303.15−343.15	0.61−8.36	42	isochoric saturation method	326
2	$[BMIM]^+[EtSO_4]^-$	303.15−353.15	1.14−12.70	36	isochoric saturation method	219
3	$[BMIM]^+[MeSO_4]^-$	298.10−298.10	0.11−7.51	8	gravimetric microbalance method	262
4	$[BMIM]^+[PF_6]^-$	298.15−403.15	0.69−96.30	39	weight method	325
		303.15−343.15	1.23−10.11	42	isochoric saturation method	326
5	$[BMIM]^+[Tf_2N]^-$	303.15−343.15	0.94−9.16	44	isochoric saturation method	326
6	$[EMIM]^+[PF_6]^-$	333.15−363.15	1.45−19.33	40	isochoric saturation method	324
7	$[EMIM]^+[Tf_2N]^-$	303.15−353.15	1.08−16.86	42	isochoric saturation method	324
8	$[HEMIM]^+[BF_4]^-$	303.15−353.15	1.21−10.66	51	isochoric saturation method	174
9	$[HEMIM]^+[PF_6]^-$	303.15−353.15	1.34−16.85	47	isochoric saturation method	328
10	$[HEMIM]^+[Tf_2N]^-$	303.15−353.15	1.56−18.32	41	isochoric saturation method	328
11	$[HEMIM]^+[TfO]^-$	303.15−353.15	1.06−18.39	41	isochoric saturation method	328
12	$[HMIM]^+[PF_6]^-$	303.15−343.15	1.11−11.00	67	isochoric saturation method	327
13	$[HMIM]^+[Tf_2N]^-$	303.15−353.15	0.69−20.17	57	isochoric saturation method	239
		303.15−343.15	0.97−10.50	30	isochoric saturation method	327
14	$[OMIM]^+[PF_6]^-$	303.15−353.15	0.85−19.58	48	isochoric saturation method	238
15	$[OMIM]^+[Tf_2N]^-$	303.15−353.15	0.94−19.12	47	isochoric saturation method	239
			total no.	**722**		

Maginn[260] studied the mixed gas absorption with ILs by MC simulation and showed that at low pressures two gases absorb independently while at high pressures they compete with each other. Yokozeki and Shiflett[153,154] developed a ternary RK (Redlich−Kwong) equation of state for describing the CO_2/SO_2/IL ($[HMIM]^+[Tf_2N]^-$ and $[BMIM]^+[MeSO_4]^-$) systems taking the interaction between SO_2 and CO_2 into consideration, and both the experimental and the calculated results indicated that the CO_2/SO_2 selectivity is significantly enhanced with addition of IL, and the strong absorption of CO_2 and SO_2 in ILs is favorable for simultaneous capture, but $[BMIM]^+[MeSO_4]^-$ is more pronounced than $[HMIM]^+[Tf_2N]^-$.

6. SOLUBILITY OF OTHER GASES IN ILS

Besides CO_2 and SO_2, other gases such as carbon monoxide (CO), nitrogen (N_2), oxygen (O_2), and so on are commonly contained in industrial gas mixtures, and thus, reliable knowledge on their solubility in ILs is indispensable for tailoring the suitable ILs and developing the process models. The subsections of this section are arranged in terms of the gas source and category.

6.1. Solubility of Carbon Monoxide, Nitrogen, Oxygen, and Hydrogen in ILs

6.1.1. Solubility of Carbon Monoxide (CO) in ILs. Anthony et al.[156] tried to measure the CO solubility in $[BMIM]^+[PF_6]^-$ using the gravimetric microbalance method; however, CO has solubility below the detection limit of their apparatus. Ohlin et al.[306] applied high-pressure ^{13}C NMR spectroscopy to measure the solubility of CO in ILs and found that CO solubility follows the order $[BF_4]^- < [PF_6]^- < [SbF_6]^- < [TFA]^- < [Tf_2N]^-$ with $[BMIM]^+$ cation; CO solubility increases with the increase of alkyl chain length on the cation for imidazolium- and pyridinium-based ILs. Many researchers believed that CO solubility decreases with increasing temperature, although the effect on temperature is not as significant as CO_2 or SO_2.[41,163,236,248,307−310] However, one paper reported that CO solubility in $[BMIM]^+[MeSO_4]^-$ increases with increasing temperature.[311] The discrepancy originated from the very small solubility of CO in ILs, which is difficult to be measured and highly prone to generating large errors in the experiment.

6.1.2. Solubility of Nitrogen (N_2) in ILs. Several researchers reported the N_2 solubility data in ILs, indicating that N_2 solubility increases with decreasing temperature;[41,163,313] however, Finotello et al.[250] used the semi-infinite volume method to measure the N_2 solubility, and an opposite trend was observed. Besides, N_2 solubility increases with the increase of alkyl chain length on the cation for imidazolium-based ILs and nitrile-functionalized ILs.[115] Moreover, N_2 solubility in oligo(ethylene glycol)-functionalized ILs[161] and benzyl-functionalized ILs[294] is smaller than in imidazolium-based ILs. IL membranes are suggested to separate CO_2 and N_2, while N_2 permeability follows the order $[Tf_2N]^- > [TfO]^- > [Cl]^- > [DCA]^-$.[35,39] It can be seen that fluorination on anion leads to the increase of N_2 solubility.

6.1.3. Solubility of Oxygen (O_2) in ILs. Solubility data of O_2 in ILs including $[BMIM]^+[BF_4]^-$, $[BMIM]^+[PF_6]^-$, $[BMIM]^+[Tf_2N]^-$, $[HMIM]^+[Tf_2N]^-$, $[HMPY]^+[Tf_2N]^-$, $[TMG]^+[L]^-$, and $[MDEA]^+[Cl]^-$ have been measured by the efforts of many researchers in recent years, with more than 650 effective data points (unreasonable negative data points excluded) reported. However, there is still a debate on the influence of temperature on the solubility of O_2 in ILs. The majority of researchers[16,41,163,236,251,308,313] agree that O_2 solubility in ILs decreases with increasing temperature; a few researchers[156,193] agree that O_2 solubility in ILs increases with increasing temperature; others support almost no influence of temperature on O_2 solubility in ILs.[314] Hert et al.[257] compared the solubility of O_2 in $[HMIM]^+[Tf_2N]^-$ for pure oxygen and mixed CO_2 and O_2 gases at 298.15 K and pressures up to 13 bar. It is surprising to find that the presence of CO_2 increases the O_2 solubility.

6.1.4. Solubility of Hydrogen (H_2) in ILs. The solubility of H_2 in ILs is remarkably lower than that of CO_2 or SO_2, showing an "inverse" temperature effect that H_2 solubility in ILs (e.g., $[BMIM]^+[PF_6]^-$,[41,248,315] $[HMIM]^+[Tf_2N]^-$,[316,317] $[BMIM]^+[MeSO_4]^-$,[311] and $[BMIM]^+[Tf_2N]^-$[318]) increases with increasing temperature. However, more intriguing, Jacquemin et al.[205] reported that H_2 solubility in $[N_{4,1,1,1}]^+[Tf_2N]^-$, $[BMIM]^+[Tf_2N]^-$, and $[EMIM]^+[Tf_2N]^-$

dx.doi.org/10.1021/cr300497a | Chem. Rev. 2014, 114, 1289−1326

Table 9. Summary of Solubility Data of N_2O in ILs

no. of IL	ILs	T range (K)	P range (bar)	no. of data points	experimental method	refs
1	$[(ETO)_2IM]^+[Tf_2N]^-$	302.05−363.45	6.10−240.40	102	synthetic (bubble point) method	329
2	$[(OH)_2IM]^+[Tf_2N]^-$	302.85−363.15	10.20−301.00	55	synthetic (bubble point) method	329
3	$[BMIM]^+[BF_4]^-$	292.45−373.55	11.40−133.30	45	synthetic (bubble point) method	329
		298.10−348.20	0.26−20.53	42	gravimetric microbalance method	261
4	$[BMIM]^+[eFAP]^-$	303.15−343.21	0.65−0.99	15	isochoric saturation method	198
5	$[BMIM]^+[SCN]^-$	293.05−373.30	10.30−184.90	49	synthetic (bubble point) method	329
6	$[BMIM]^+[Tf_2N]^-$	283.15−323.15	0.00−13.00	134	gravimetric microbalance method	16
7	$[BMPYR]^+[eFAP]^-$	303.15−343.22	0.60−0.77	15	isochoric saturation method	210
8	$[EMIM]^+[eFAP]^-$	303.15−343.23	0.50−0.64	14	isochoric saturation method	198
9	$[HMIM]^+[eFAP]^-$	303.16−343.26	0.50−0.69	15	isochoric saturation method	198
10	$[MMIM]^+[MP]^-$	292.35−373.15	21.00−164.50	42	synthetic (bubble point) method	329
11	$[P_{6,6,6,14}]^+[eFAP]^-$	303.15−343.23	0.59−0.78	15	isochoric saturation method	210
			total no.	**543**		

decreases with increasing temperature, and H_2 solubility in $[BMIM]^+[BF_4]^-$ [163] and $[EMIM]^+[EtSO_4]^-$[319] first increases with increasing temperature and then decreases at higher temperatures, exhibiting a maximum solubility in the temperature range from 283 to 343 K. With the same cation, H_2 solubility in $[BMIM]^+[X]^-$ follows the order $[PF_6]^- < [BF_4]^- < [SbF_6]^- \approx [TFA]^- < [Tf_2N]^-$.[320,321] In general, the solubility of CO, N_2, O_2, and H_2 in ILs is almost 1−2 orders of magnitude lower than that of CO_2 at the same temperature and pressure.

In summary, fluorination on the anion or the increase of alkyl chain length on cation is favorable for increasing the solubility of CO, N_2, O_2, and H_2. However, the effect of temperature on the solubility of CO, N_2, and O_2 is not as apparent as CO_2 or SO_2. For H_2, the solubility shows an "inverse" temperature effect. Thus, more works are still needed to explore the solubility mechanism and identify the structure−property relation.

Experimental solubility data of CO, N_2, O_2, and H_2 in ILs are summarized in Table 7, and detailed values are given through Tables S4−S7, Supporting Information. We do recognize that not all of the solubility data are fully trustable due to the resolution and error of the experimental apparatus, and even unreasonable values (negative mole fraction) are derived, as denoted in red in the Supporting Information.

6.2. Solubility of Hydrogen Sulfide in ILs

Pomelli et al.[323] first reported the solubility of hydrogen sulfide (H_2S) in $[BMIM]^+$-based ILs with different anions by NMR spectroscopy, and the observed solubility was even higher than CO_2, providing a significant opportunity for removal of H_2S using ILs. Afterward, a number of solubility data of H_2S in ILs have been measured (see Table S8, Supporting Information).[46,174,219,239,262,263,324−328] Table 8 gives a summary of experimental data obtained from the references including 722 data points.

The solubility of H_2S in ILs is a strong function of temperature and increases with the decrease of temperature. The cation has a moderate effect on solubility, and H_2S solubility increases with increasing alkyl chain length on the cation for imidazolium-based ILs.[323,324] Like the solubility trend of CO_2 in ILs, fluorination of the anion can improve the H_2S solubility, and H_2S solubility increases with the increase of the number of trifluoromethyl (CF_3) groups on the anion.[324,328] As a result, H_2S solubility follows the order $[HEMIM]^+[Tf_2N]^- > [HEMIM]^+[TfO]^- > [HEMIM]^+[PF_6]^- > [HEMIM]^+[BF_4]^-$. However, the influence of anion on H_2S solubility is debated. For $[BMIM]^+$-based ILs, some authors thought that H_2S solubility decreases in the order $[Cl]^- > [BF_4]^- > [TfO]^- > [Tf_2N]^- \gg [PF_6]^-$,[323] while other authors thought it follows the order $[Tf_2N]^- > [BF_4]^- > [PF_6]^-$ for $[BMIM]^+$-based ILs but $[BF_4]^- > [PF_6]^- \approx [Tf_2N]^-$ for $[HMIM]^+$-based ILs.[326,327]

6.3. Solubility of Nitrous Oxide in ILs

Anthony et al.[16] first reported nitrous oxide (N_2O) solubility in $[BMIM]^+[Tf_2N]^-$ at three temperatures (283.15, 298.15, and 323.15 K) and relative low pressures (up to 13.0 bar), showing that N_2O solubility is almost equal to CO_2 solubility at the same temperature, pressure, and IL. Revelli et al.[329] studied the solubility of N_2O in five imidazolium-based ILs at temperatures from 292 to 373 K and pressures up to 300 bar and claimed that the ILs of $[BMIM]^+[BF_4]^-$ and $[(ETO)_2IM]^+[Tf_2N]^-$ seem to be the most efficient solvent for capturing N_2O. Recently, Shiflett et al.[261,330] studied the N_2O solubility in $[BMIM]^+$-based ILs from 283 to 348 K and found that N_2O solubility is in the order $[Tf_2N]^- > [BF_4]^- > [N(CN)_2]^- > [Ac]^- > [SCN]^- > [NO_3]^-$.

Experimental solubility data of N_2O in ILs are summarized in Table 9, and detailed values as well as a comparison with COSMO-RS-predicted results are given in Table S9, Supporting Information.

6.4. Solubility of Methane and Gaseous Hydrocarbons in ILs

6.4.1. Solubility of Methane (CH_4) in ILs. CH_4 has much lower solubility than CO_2 in ILs but higher than H_2, CO, N_2, and O_2. Compared with other gaseous hydrocarbons (e.g., ethane, propane, and butane), CH_4 is significantly less soluble in ILs.[16,41,156,163,313,331] As expected, low temperature is favorable for increasing the solubility of CH_4 in ILs. Hert et al.[257] measured the solubility of CH_4 in $[HMIM]^+[Tf_2N]^-$ with and without CO_2 and found that the presence of CO_2 improves the CH_4 solubility. Kumełan et al.[312,332] reported the solubility data of CH_4 in $[BMIM]^+[MeSO_4]^-$ and $[HMIM]^+[Tf_2N]^-$ with a synthetic method at temperatures from 293.1 to 413.3 K and pressure up to 9.3 MPa and found that the solubility of CH_4 in $[BMIM]^+[MeSO_4]^-$ is much less than in $[HMIM]^+[Tf_2N]^-$. Increasing the alkyl chain length on the cation can improve the solubility of CH_4 in ILs.[114,250] For $[EMIM]^+$-based ILs, CH_4 solubility follows the order $[DCA]^- < [TfO]^- < [Tf_2N]^-$.[35]

6.4.2. Solubility of Other Gaseous Hydrocarbons in ILs. The solubility of other gaseous hydrocarbons, e.g., ethane

dx.doi.org/10.1021/cr300497a | Chem. Rev. 2014, 114, 1289−1326

Table 10. Summary of Solubility Data of CH_4 and Other Gaseous Hydrocarbons in ILs

no. of IL	ILs	gases	T range (K)	P range (bar)	no. of data points	experimental method	refs
1	$[BMIM]^+[BF_4]^-$	CH_4	283.05−343.09	0.49−0.98	13	isochoric saturation method	163
2	$[EMIM]^+[eFAP]^-$	CH_4	293.30−363.42	20.76−86.92	31	synthetic (bubble point) method	333
3	$[EMIM]^+[EtSO_4]^-$	CH_4	292.37−293.63	1.98−101.50	8	gravimetric microbalance method	220
4	$[BMIM]^+[MeSO_4]^-$	CH_4	293.15−413.20	13.63−88.53	24	isochoric saturation method	312
5	$[BMIM]^+[PF_6]^-$	CH_4	283.15−323.15	0.01−13.99	88	gravimetric microbalance method	156
			283.30−343.12	0.41−0.88	11	isochoric saturation method	41
6	$[BMIM]^+[Tf_2N]^-$	CH_4	300.31−453.15	15.01−161.05	82	synthetic (bubble point) method	331
7	$[HMIM]^+[Tf_2N]^-$	CH_4	293.30−413.25	8.86−93.00	24	isochoric saturation method	332
			298.15−333.15	0.20−9.88	51	gravimetric microbalance method	251
8	$[HMPY]^+[Tf_2N]^-$	CH_4	298.15−333.15	0.02−10.00	50	gravimetric microbalance method	251
9	$[TMG]^+[L]^-$	CH_4	308.00−328.00	10.40−100.40	30	isochoric saturation method	313
				total no.	**412**		
1	$[BMIM]^+[BF_4]^-$	C_2H_6	283.02−343.22	0.42−0.94	12	isochoric saturation method	163
2	$[BMIM]^+[eFAP]^-$	C_2H_6	303.26−343.33	0.94−1.08	15	isochoric saturation method	198
3	$[BMIM]^+[PF_6]^-$	C_2H_6	293.15−323.15	0.01−13.00	69	gravimetric microbalance method	156
			293.15−323.15	0.01−13.00	85	gravimetric microbalance method	16
			283.30−343.12	0.41−0.88	11	isochoric saturation method	41
4	$[BMIM]^+[Tf_2N]^-$	C_2H_6	283.15−323.15	0.01−13.00	65	gravimetric microbalance method	16
5	$[BMPYR]^+[eFAP]^-$	C_2H_6	303.26−343.25	0.71−0.92	7	isochoric saturation method	210
6	$[BMPYR]^+[Tf_2N]^-$	C_2H_6	304.24−344.69	0.39−0.44	5	isochoric saturation method	162
7	$[EMIM]^+[EtSO_4]^-$	C_2H_6	322.76−349.98	2.10−40.06	13	gravimetric microbalance method	220
8	$[EMIM]^+[Tf_2N]^-$	C_2H_6	304.14−344.70	0.44−0.50	9	isochoric saturation method	162
9	$[HMIM]^+[eFAP]^-$	C_2H_6	303.14−343.14	0.52−0.67	13	isochoric saturation method	198
10	$[HMIM]^+[Tf_2N]^-$	C_2H_6	283.32−343.21	0.44−0.99	10	isochoric saturation method	232
			293.17−368.40	3.88−130.70	108	synthetic (bubble point) method	335
11	$[HMPY]^+[Tf_2N]^-$	C_2H_6	298.15−333.15	0.01−10.00	54	gravimetric microbalance method	251
12	$[N_{1,1,3,2\text{-}OH}]^+[Tf_2N]^-$	C_2H_6	304.15−344.74	0.44−0.49	9	isochoric saturation method	162
13	$[P_{6,6,6,14}]^+[eFAP]^-$	C_2H_6	303.17−343.29	0.69−0.78	15	isochoric saturation method	210
				total no.	**500**		
1	$[BMIM]^+[Tf_2N]^-$	C_3H_8	279.98−339.97	1.00−12.18	23	isochoric saturation method	204
2	$[HMIM]^+[Tf_2N]^-$	C_3H_8	298.15−298.15	3.22−7.31	10	isochoric saturation method	119
				total no.	**33**		
1	$[BMIM]^+[Tf_2N]^-$	C_4H_{10}	280.00−340.00	0.21−3.51	16	isochoric saturation method	204
1	$[BMIM]^+[PF_6]^-$	C_2H_4	283.15−323.15	0.01−13.00	79	gravimetric microbalance method	156
			283.15−323.15	0.02−13.00	66	gravimetric microbalance method	16
2	$[BMIM]^+[Tf_2N]^-$	C_2H_4	283.15−323.15	0.02−13.00	53	gravimetric microbalance method	16
3	$[HMPY]^+[Tf_2N]^-$	C_2H_4	298.15−333.15	0.01−10.00	50	gravimetric microbalance method	251
				total no.	**248**		
1	$[BMIM]^+[Tf_2N]^-$	C_3H_6	279.98−339.97	0.88−10.62	16	isochoric saturation method	204
1	$[BMIM]^+[Tf_2N]^-$	C_4H_8	280.00−340.00	0.33−3.04	16	isochoric saturation method	204
1	$[BMIM]^+[BF_4]^-$	C_6H_6	283.15−323.15	0.00−0.20	51	gravimetric microbalance method	16

(C_2H_6), propane (C_3H_8), butane (C_4H_{10}), ethylene (C_2H_4), propylene (C_3H_6), 1-butene (C_4H_8), 1,3-butadiene (C_4H_6), and benzene vapor (C_6H_6) in ILs, has been measured recently. Their solubility decreases with increasing temperature, indicating that the dissolution process is exothermic.

Benzene vapor has the highest solubility and the strongest affinity with ILs among a series of gases, and C_2H_4 and C_2H_6 have a lower solubility than CO_2.[16] Alkene gases are more soluble in ILs than alkane gases.[16,156] The solubility of gaseous hydrocarbons together with CO_2 in ILs generally follows the order $CH_4 < C_2H_6 < C_2H_4 < C_3H_8 < CO_2 < C_3H_6 < C_4H_{10} < C_4H_8 < C_4H_6 < C_6H_6$.[16,41,162,163,204,232,251,334,335] The solubility of some gases (C_2H_4, C_3H_6, C_4H_6, C_4H_8, CO_2, etc.) in five phosphonium-based ILs was studied, and the results showed that their solubility follows the order $[P_{14,4,4,4}]^+[DBS]^- < [P_{2,4,4,4}]^+[DEP]^- < [P_{14,6,6,6}]^+[DCA]^- < [P_{14,6,6,6}]^+[Cl]^- < [P_{14,6,6,6}]^+[Tf_2N]^-$.[334] For C_2H_6, it was found to be more soluble in the pyrrolidinium-based ILs than in the ammonium-based ILs.[162]

Experimental solubility data of these gases in ILs are summarized in Table 10; detailed values as well as a comparison with COSMO-RS-predicted results are given in Table S10, Supporting Information. The COSMO-RS model can correctly predict the general trend for the solubility of these gases in ILs.

6.5. Solubility of Inert Gases in ILs

The solubility of inert gases, i.e., argon (Ar), krypton (Kr), and xenon (Xe), in ILs has been studied. Anthony et al.[16,156] investigated the solubility of Ar in $[BMIM]^+[PF_6]^-$ at low pressures (below 13 bar) and concluded that Ar has extraordinary weak interaction with IL, and thus, a very low solubility similar to oxygen was obtained. Later, Jacquemin et al.[41,163] reported the solubility of Xe in $[BMIM]^+[PF_6]^-$ and $[BMIM]^+[BF_4]^-$ as a function of temperature ranged from 283 to 343 K at pressures close to atmospheric pressure and found

dx.doi.org/10.1021/cr300497a | Chem. Rev. 2014, 114, 1289−1326

Table 11. Summary of Solubility Data of Inert Gases (Ar, Kr and Xe) in ILs

no. of IL	ILs	gases	T range (K)	P range (bar)	no. of data points	experimental method	refs
1	$[BMIM]^+[BF_4]^-$	Ar	283.01−343.02	0.80−0.99	9	isochoric saturation method	163
2	$[BMIM]^+[PF_6]^-$	Ar	283.15−283.15	4.00−11.50	13	gravimetric microbalance method	156
			298.15−298.15	1.00−13.00	25	gravimetric microbalance method	156
			323.15−323.15	0.01−10.00	14	gravimetric microbalance method	156
3	$[BMIM]^+[PF_6]^-$	Ar	298.15−298.15	1.00−13.00	25	gravimetric microbalance method	16
			323.15−323.15	0.00−10.00	15	gravimetric microbalance method	16
4	$[BMIM]^+[PF_6]^-$	Ar	283.40−343.15	0.49−0.95	11	isochoric saturation method	41
				total no.	**112**		
1	$[EMIM]^+[Ac]$-	Kr	283.40−343.15	0.47−0.95	11	isochoric saturation method	196
2	$[EMIM]^+[Tf_2N]$-	Kr	303.20−353.30	9.15−67.95	14	isochoric saturation method	196
1	$[BMIM]^+[MeSO_4]^-$	Xe	293.10−413.15	11.94−112.85	24	isochoric saturation method	312
2	$[HMIM]^+[Tf_2N]^-$	Xe	293.30−413.30	14.76−95.63	25	isochoric saturation method	332

that the solubility decreases with increasing temperature. Ar is more soluble in $[BMIM]^+[PF_6]^-$ than $[BMIM]^+[BF_4]^-$ at the same temperature and pressure.

Kumełan et al.[312,332] measured the solubility of CH_4 and Xe in $[BMIM]^+[MeSO_4]^-$ and $[HMIM]^+[Tf_2N]^-$ at temperatures between 293 and 413 K. In both ILs, Xe shows a significantly higher solubility than CH_4, and the solubility in $[HMIM]^+[Tf_2N]^-$ is higher than that in $[BMIM]^+[MeSO_4]^-$. Thus, it can be deduced that Xe is more soluble than Ar in ILs. Recently, Afzal et al.[196] measured the solubility of Kr in $[EMIM]^+[Ac]^-$ and $[EMIM]^+[Tf_2N]^+$ using the isochoric saturation method over the temperature range from 303 to 353 K and at pressures up to 67 bar.

Experimental solubility data of Ar, Kr, and Xe in ILs are summarized in Table 11, and detailed values as well as a comparison with COSMO-RS-predicted results are given in Table S11, Supporting Information.

6.6. Solubility of Hydrofluorocarbons in ILs

The phase behavior of the fluoroform (CHF_3, R-23) and $[EMIM]^+[PF_6]^-$ system was first studied, fluoroform being in the supercritical state.[336] Shiflett and Yokozeki reported the solubility of several hydrofluorocarbons (HFCs) from methane and ethane series and vinyl fluoride (C_2H_3F, R-1141) in different ILs.[26,27,337−340] Pison et al.[341] measured the solubility of totally fluorinated alkanes, i.e., CF_4 (R-14), C_2F_6 (R-116), and C_3F_8 (R-216), in $[P_{6,6,6,14}]^+[Tf_2N]^-$ at temperatures between 303 and 343 K and close to atmospheric pressure and found that the solubility is in the order $CF_4 < C_2F_6 < C_3F_8$, which is in accordance with the solubility trend of gaseous hydrocarbons in ILs. For HFCs series, the solubility in the same IL follows R-32 > R-152 > R-23 > R-134a > R-125 > R-143a. Kumełan et al.[342] presented the CF_4 solubility in $[HMIM]^+[Tf_2N]^-$ at pressures up to 9.6 MPa and made a comparison of the solubility with other gases, showing that the solubility sequence is $CO_2 > Xe > CH_4 > CF_4 > H_2$.

The solubility of HFCs in ILs increases with increasing alkyl chain length on the cation.[343,344] Fluorination on the anion enhances the interaction between HFC and IL because the hydrogen−fluorine interaction plays an important role in determining the HFC solubility. An increase in the length of fluoroalkyl chain increases the HFC solubility. For different anions, the solubility of HFCs follows the order $[SCN]^- < [MeSO_4]^- < [Ac]^- < [BF_4]^- < [HFPS]^- < [PF_6]^- < [TPES]^- < [TFES]^- < [Tf_2N]^- < [BEI]^-$.

Eexperimental solubility data of HFCs in ILs are summarized in Table 12, and detailed values as well as a comparison with COSMO-RS-predicted results are given in Table S12, Supporting Information.

6.7. Solubility of Ammonia and Water in ILs

6.7.1. Solubility of Ammonia (NH_3) in ILs. NH_3 not only has an extremely high solubility in ILs at room temperature but also can be almost completely desorbed by lowering the pressure or heating.[25,302,346] Shi and Maginn[347] investigated the NH_3 absorption in ILs by osmotic ensemble MC simulation at temperatures from 298 to 348 K and explained the reason for the amazing high solubility. It is conceivable that NH_3 through the nitrogen atom forms a strong hydrogen bond with the ring hydrogen atoms on the cation. However, the anion has much less effect on the solubility, which is different from the solubility mechanism of CO_2 in ILs. The solubility of NH_3 in a series of $[C_nMIM]^+[BF_4]^-$ was measured to explore the effect of alkyl chain length on the cation on NH_3 solubility. As expected, the longer the alkyl chain length on the cation, the higher the NH_3 solubility in ILs.[348] Palomar et al.[349,350] used the COSMO-RS model to seek the optimum IL for absorption of NH_3 and proposed the TSIL, i.e., $[choline]^+[Tf_2N]^-$, which has the highest efficiency and is the most suitable solvent for NH_3 absorption.

6.7.2. Solubility of Water (H_2O) in ILs. Solubility data of H_2O vapor in ILs are very scarce. Jureviciute et al.[351] suggested that H_2O is more soluble in $[BF_4]^-$-based ILs than $[PF_6]^-$-based ILs. This is consistent with the previous finding by Anthony et al.[352] that the solubility of H_2O vapor in $[OMIM]^+[BF_4]^-$ is higher than that in $[OMIM]^+[PF_6]^-$. Moreover, the solubility of H_2O in ILs decreases with increasing alkyl chain length on the cation, which is reverse to the solubility trend of NH_3 in ILs.

Experimental solubility data of NH_3 and H_2O in ILs are summarized in Table 13, and detailed values as well as a comparison with COSMO-RS-predicted results are given in Tables S13 and S14, Supporting Information.

6.8. Solubility of Gas Mixture in ILs

Compared to the solubility data of pure gas in ILs, solubility data of mixed gases in ILs are scarcely reported, which, however, are important for developing real processes because the gas solubility may be significantly influenced by the presence of another gas. Experimental solubility data of gas mixture in ILs are collected in Table S17, Supporting Information.

Solinas et al.[353] studied the influence of the presence of CO_2 in the IL $[EMIM]^+[Tf_2N]^+$ on the H_2 solubility by means of high-pressure NMR and found that there is a significant

dx.doi.org/10.1021/cr300497a | Chem. Rev. 2014, 114, 1289−1326

Table 12. Summary of Solubility Data of Hydrofluorocarbons in ILs

no. of IL	ILs	gases	T range (K)	P range (bar)	no. of data points	experimental method	refs
1	$[EMIM]^+[Tf_2N]^-$	R-114	283.00−348.10	0.01−0.15	21	gravimetric microbalance method	339
2	$[BMIM]^+[DCA]^-$	R-1141	298.00−373.20	1.20−42.62	18	gravimetric microbalance method	340
3	$[BMIM]^+[HFPS]^-$	R-1141	297.90−372.70	1.12−37.35	16	gravimetric microbalance method	340
4	$[BMPY]^+[BF_4]^-$	R-1141	277.90−373.20	1.25−42.27	27	gravimetric microbalance method	340
5	$[EMIM]^+[Tf_2N]^-$	R-1141	279.90−348.10	0.25−20.01	70	gravimetric microbalance method	340
6	$[EMIM]^+[TfO]^-$	R-1141	278.00−372.60	1.62−42.07	26	gravimetric microbalance method	340
7	$[OMIM]^+[TFES]^-$	R-1141	277.90−373.20	1.37−47.59	27	gravimetric microbalance method	340
8	$[EMIM]^+[Tf_2N]^-$	R-114a	283.10−348.10	0.01−0.15	22	gravimetric microbalance method	339
9	$[P_{6,6,6,14}]^+[Tf_2N]^-$	R-116	303.19−343.23	1.09−1.31	8	isochoric saturation method	341
10	$[EMIM]^+[Tf_2N]^-$	R-124	283.00−348.10	0.01−0.30	26	gravimetric microbalance method	339
11	$[EMIM]^+[Tf_2N]^-$	R-124a	283.10−348.10	0.01−0.30	26	gravimetric microbalance method	339
12	$[BMIM]^+[PF_6]^-$	R-134	283.11−348.16	0.10−3.51	30	gravimetric microbalance method	27
13	$[EMIM]^+[Tf_2N]^-$	R-134	282.90−348.10	0.01−0.35	31	gravimetric microbalance method	339
14	$[BMIM]^+[HFPS]^-$	R-134a	283.10−348.10	0.10−3.51	32	gravimetric microbalance method	337
15	$[BMIM]^+[TPES]^-$	R-134a	283.05−348.10	0.10−3.51	32	gravimetric microbalance method	337
16	$[BMIM]^+[TTES]^-$	R-134a	282.10−348.15	0.10−3.51	32	gravimetric microbalance method	337
17	$[EMIM]^+[BEI]^-$	R-134a	283.10−348.10	0.10−3.51	32	gravimetric microbalance method	337
18	$[EMIM]^+[Tf_2N]^-$	R-134a	282.70−348.10	0.01−0.35	31	gravimetric microbalance method	339
19	$[HMIM]^+[BF_4]^-$	R-134a	298.15−348.15	0.81−143.30	20	synthetic (bubble point) method	345
20	$[HMIM]^+[PF_6]^-$	R-134a	298.15−348.15	0.81−128.80	23	synthetic (bubble point) method	345
21	$[HMIM]^+[Tf_2N]^-$	R-134a	298.15−348.15	0.42−43.20	31	synthetic (bubble point) method	345
22	$[P_{4,4,4,14}]^+[HFPS]^-$	R-134a	283.05−348.10	0.10−3.50	31	gravimetric microbalance method	337
23	$[P_{6,6,6,14}]^+[TPFS]^-$	R-134a	282.80−348.10	0.10−3.51	32	gravimetric microbalance method	337
24	$[HMIM]^+[Tf_2N]^-$	R-14	293.30−413.30	11.27−90.06	27	isochoric saturation method	342
25	$[P_{6,6,6,14}]^+[Tf_2N]^-$	R-14	303.41−343.49	1.05−1.24	13	isochoric saturation method	341
26	$[BMIM]^+[TfO]^-$	R-152a	273.22−348.13	0.54−8.79	24	isochoric saturation method	343
27	$[EMIM]^+[TfO]^-$	R-152a	273.22−348.16	0.40−8.48	24	isochoric saturation method	343
28	$[BMIM]^+[PF_6]^-$	R-161	283.06−348.16	0.10−7.01	30	gravimetric microbalance method	27
29	$[P_{6,6,6,14}]^+[Tf_2N]^-$	R-218	303.43−343.70	0.41−1.20	10	isochoric saturation method	341
30	$[BMIM]^+[PF_6]^-$	R-23	303.20−363.42	5.80−410.00	160	synthetic (bubble point) method	202
31	$[EMIM]^+[PF_6]^-$	R-23	308.04−367.54	16.02−516.40	155	synthetic (bubble point) method	336
32	$[BMIM]^+[Ac]^-$	R-32	298.05−298.25	0.10−10.00	8	gravimetric microbalance method	338
33	$[BMIM]^+[FS]^-$	R-32	298.15−298.15	0.10−10.01	8	gravimetric microbalance method	338
34	$[BMIM]^+[HFPS]^-$	R-32	298.15−298.15	0.10−10.00	8	gravimetric microbalance method	338
35	$[BMIM]^+[MeSO_4]^-$	R-32	298.15−298.15	0.10−10.01	8	gravimetric microbalance method	338
36	$[BMIM]^+[SCN]^-$	R-32	298.15−298.15	0.10−9.99	8	gravimetric microbalance method	338
37	$[BMIM]^+[TFES]^-$	R-32	298.15−298.15	0.10−9.99	8	gravimetric microbalance method	338
38	$[BMIM]^+[TfO]^-$	R-32	273.13−348.24	0.98−9.02	26	isochoric saturation method	343
39	$[BMIM]^+[TPES]^-$	R-32	298.15−298.15	0.10−9.99	8	gravimetric microbalance method	338
40	$[BMIM]^+[TTES]^-$	R-32	298.15−298.15	0.10−9.99	8	gravimetric microbalance method	338
41	$[BMPY]^+[Tf_2N]^-$	R-32	298.15−298.15	0.10−10.00	8	gravimetric microbalance method	338
42	$[C_3MMIM]^+[methide]^-$	R-32	283.15−348.05	0.10−10.01	30	gravimetric microbalance method	338
43	$[C_3MMIM]^+[Tf_2N]^-$	R-32	298.05−298.15	0.10−10.01	8	gravimetric microbalance method	338
44	$[C_3MPY]^+[Tf_2N]^-$	R-32	283.15−348.05	0.10−10.00	30	gravimetric microbalance method	338
45	$[DMIM]^+[TFES]^-$	R-32	298.15−298.15	0.10−10.01	8	gravimetric microbalance method	338
46	$[EMIM]^+[BEI]^-$	R-32	283.15−348.05	0.10−10.01	31	gravimetric microbalance method	338
47	$[EMIM]^+[Tf_2N]^-$	R-32	283.15−348.05	0.10−10.01	31	gravimetric microbalance method	338
48	$[EMIM]^+[TFES]^-$	R-32	298.05−298.15	0.10−10.02	8	gravimetric microbalance method	338
49	$[EMIM]^+[TfO]^-$	R-32	273.14−348.16	0.97−8.57	27	isochoric saturation method	343
50	$[HMIM]^+[TFES]^-$	R-32	298.15−298.15	0.10−0.98	8	gravimetric microbalance method	338
51	$[BMIM]^+[PF_6]^-$	R-41	283.09−348.18	0.10−20.00	34	gravimetric microbalance method	27
				total no.	**1400**		

increase of H_2 solubility in the presence of CO_2. Later, Hert et al.[257] reported that the presence of CO_2 increases the solubility of O_2 and CH_4 in $[HMIM]^+[Tf_2N]^-$ at 298.15 K and pressures up to 13 bar due to CO_2 cosolubilizing the sparsely soluble gas via favorable dispersion interactions. However, Shi and Maginn[260] showed that the mixed gas solubilities are nearly ideal, with little enhancement or competition between the two solutes for mixtures of CO_2/O_2 and SO_2/N_2 using molecular simulation. Yokozeki et al.[253] proposed using the IL $[BMIM]^+[PF_6]^-$ for hydrogen purification from CO_2/H_2 mixtures, and the results quantitatively demonstrated the high selectivity for CO_2/H_2 separation under the operating conditions. Toussaint et al.[258] showed that addition of CO_2 to the binary system of H_2 and $[BMIM]^+[BF_4]^-$ would increase

dx.doi.org/10.1021/cr300497a | Chem. Rev. 2014, 114, 1289−1326

Table 13. Summary of Solubility Data of NH_3 and H_2O in ILs

no. of IL	ILs	gases	T range (K)	P range (bar)	no. of data points	experimental method	refs
1	$[BMIM]^+[BF_4]^-$	NH_3	282.20−355.10	0.91−25.70	36	isochoric saturation method	346
		NH_3	293.15−333.15	0.70−8.30	25	isochoric saturation method	348
2	$[BMIM]^+[PF_6]^-$	NH_3	283.40−355.80	1.38−27.00	29	isochoric saturation method	346
3	$[EMIM]^+[BF_4]^-$	NH_3	293.15−333.15	1.10−6.30	25	isochoric saturation method	348
4	$[EMIM]^+[Tf_2N]^-$	NH_3	283.30−347.60	1.14−28.60	30	isochoric saturation method	346
5	$[HMIM]^+[BF_4]^-$	NH_3	293.15−333.15	1.40−7.10	25	isochoric saturation method	348
6	$[HMIM]^+[Cl]^-$	NH_3	283.10−347.90	0.44−24.90	30	isochoric saturation method	346
7	$[OMIM]^+[BF_4]^-$	NH_3	293.15−333.15	1.00−6.10	25	isochoric saturation method	348
				total no.	**225**		
1	$[HMIM]^+[PF_6]^-$	H_2O	283.15−323.15	0.00−0.05	65	gravimetric microbalance method	16

the H_2 solubility at lower temperatures (below 330 K) but decrease the solubility at higher temperatures (above 340 K). In general, the very soluble gas acts as cosolvent for the sparsely soluble gas in ILs.

Shiflett et al.[153,154,253,261−263] reported a series of simultaneous solubility of two very soluble gases in ILs, i.e., CO_2 and N_2O in $[BMIM]^+[BF_4]^-$, CO_2 and H_2S in $[BMIM]^+[MeSO_4]^-$, CO_2 and H_2S in $[BMIM]^+[PF_6]^-$, CO_2 and SO_2 in $[OMIM]^+[PF_6]^-$, and CO_2 and SO_2 in $[BMIM]^+[MeSO_4]^-$. They observed an antisolvent effect of H_2S and SO_2 on CO_2 solubility. Kim et al.[119] presented the experimental results on the simultaneous solubility of two very soluble gases, i.e., CO_2 and C_3H_8 in $[HMIM]^+[Tf_2N]^-$ at 298.15 K and up to 1 MPa. Ortiz et al.[354] studied the separation of propene and propane, which are of both chemical and physical solubility in $[BMIM]^+[BF_4]^-$ acting as reactive solvent. Recently, Fallanza et al.[355] used the COSMO-RS model to select the most suitable and effective IL for separation of propane and propylene by reactive absorption.

Only one paper reported the solubilities of two sparsely soluble gases (H_2 and Ar) in $[HMIM]^+[Tf_2N]^-$ at 313−573 K and 100−300 bar using molecular simulation, and the results showed that in this case the solubilities of these two gases are not significantly influenced by one another.[256] As a whole, the solubility mechanism and specific interaction between mixed gases and IL are still debated by different authors. Further work should be addressed to provide deeper theoretical insight into the solubility of gas mixture in ILs.

7. CONCLUSIONS

In this review, solubility data of a series of important gases such as CO_2, SO_2, CO, N_2, O_2, and H_2 are exhaustively collected over a wide temperature and pressure range and provided as Supporting Information for the readers to use conveniently. With respect to this topic, chemists and chemical engineers will be encountered with a lot of challenges in the near future, including the following points at least. (i) Solubility data of gases except for CO_2 in ILs are still limited and should be complemented especially at low temperatures. (ii) Solubility data of mixed gases in ILs are also scarce, which can provide fundamental knowledge for developing the actual processes because one gas solubility may be significantly influenced by the presence of another gas. (iii) Predictive molecular thermodynamic models are still needed to be advanced so as to improve the prediction accuracy and thus reduce the amount of experimental work in measuring the solubility data due to numerous combinations of cations and anions and extreme operating conditions (low temperature and very high pressure). The present COSMO-RS model is often not sufficient to accurately predict the solubility of gases in ILs as mentioned above. Therefore, we have to resort to other predictive models (e.g., UNIFAC model), and thus, more group parameters are required to fill into the current parameter matrixes. (iv) The solubility of gases in ILs may be improved by combing the advantages of ILs with other new types of materials, e.g., metal−organic frameworks (MOFs), not limited to other commercially available ILs and organic solvents.

Despite the insufficiency of solubility data obtained so far, it can be concluded that ILs not only have high solubility for some single gases but also can selectively dissolve some gas mixtures. It is entirely likely to replace the volatile organic solvents with ILs without changing the main flowsheet and equipment in many industrial processes. In view of the potential advantages of ILs, we are encouraged to carry out fundamental research in this field.

ASSOCIATED CONTENT

Supporting Information

Complete database on the solubility of gases in ILs as a spreadsheet file, including abbreviations and full names for IL anions and cations, their chemical structures, gas/IL systems with more than 16 000 gas solubility data points, experimental methods, Henry's law constants, predicted results by predictive thermodynamic models, and corresponding cited references. This material is available free of charge via the Internet at http://pubs.acs.org.

AUTHOR INFORMATION

Corresponding Author

*Phone: +86 10 64433695. E-mail: chenbh@mail.buct.edu.cn.

Notes

The authors declare no competing financial interest.

Biographies

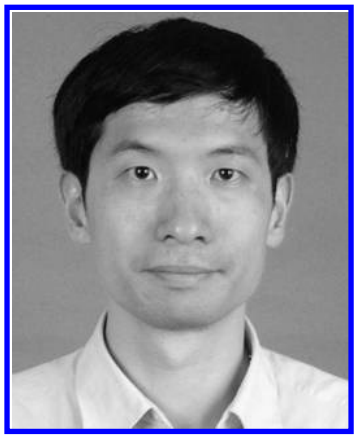

Zhigang Lei was born in Hubei province (China) in 1973. He received his B.S. degree in 1995 from Wuhan Institute of Technology and Ph.D. degree in 2000 from Tsinghua University. Later, he was a postdoctoral member in Beijing University of Chemical Technology working with Professor Chengyue Li. In 2003−2005, he worked as a researcher in the Research Center of Supercritical Fluid Technology (Tohoku University, Sendai, Japan). In 2005−2006 he received the world-famous Humboldt Fellowship and carried out his research in the Chair of Separation Science and Technology (Universität Erlange-Nürnberg, Erlangen, Germany). In 2006, he came back to China. He is now a professor in the State Key Laboratory of Chemical Resource Engineering (BUCT, China). His current research interests include process intensification in chemical engineering and predictive molecular thermodynamics. He has contributed to more than 70 papers in international journals and one book entitled *Special Distillation Processes* published by Elsevier B.V. (2005).

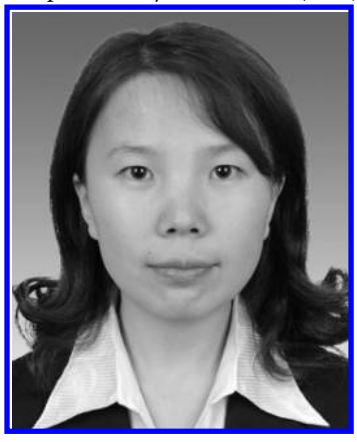

Chengna Dai was born in Hebei province (China) in 1984. She received her doctor degree in 2013 from Beijing University of Chemical Technology under the supervision of Professor Zhigang Lei. Her current research interest is separation science with ionic liquids, and she has contributed to 10 papers in international journals.

Biaohua Chen was born in Jiangxi province (China) in 1963. He received his Ph.D. degree in 1996 from China University of Petroleum (Beijing). In 2000, he was a visiting scholar at Washington University in St. Louis and the University of Washington. He has received two National Science and Technology Progress Prizes (second class), two provincial or ministerial level Science and Technology Progress Prizes (first class), and one Natural Science Progress Prize. He is currently a member of the Standing Committee of Beijing Chemical Industry Association and the Editorial Board of the *Journal of Petrochemical Universities* (China). His main research interests are environmental and green chemistry. He has contributed to more than 100 papers in international journals.

ACKNOWLEDGMENTS

This work was financially supported by the National Nature Science Foundation of China under Grant Nos. 21121064 and 21076008.

REFERENCES

(1) Battino, R.; Clever, H. L. *Chem. Rev.* **1966**, *4*, 395.
(2) Wilhelm, E.; Battino, R.; Wilcock, R. J. *Chem. Rev.* **1977**, *77*, 219.
(3) Welton, T. *Chem. Rev.* **1999**, *99*, 2071.
(4) Wasserscheid, P.; Welton, T. *Ionic Liquids in Synthesis*; Wiley-VCH: Weinheim, 2003.
(5) Marsh, K. N.; Boxall, J. A.; Lichtenthaler, R. *Fluid Phase Equilib.* **2004**, *219*, 93.
(6) Dong, Q.; Muzny, C. D.; Kazakov, A.; Diky, V.; Magee, J. W.; Widegren, J. A.; Chirico, R. D.; Marsh, K. N.; Frenkel, M. *J. Chem. Eng. Data* **2007**, *52*, 1151.
(7) Diedenhofen, M.; Klamt, A. *Fluid Phase Equilib.* **2010**, *294*, 31.
(8) Lei, Z.; Chen, B.; Li, C.; Liu, H. *Chem. Rev.* **2008**, *108*, 1419.
(9) Seiler, M.; Jork, C.; Kavarnou, A.; Arlt, W.; Hirsch, R. *AIChE J.* **2004**, *50*, 2439.
(10) Marciniak, A. *Fluid Phase Equilib.* **2010**, *294*, 213.
(11) Haumann, M.; Riisager, A. *Chem. Rev.* **2008**, *108*, 1474.
(12) Jutz, F.; Andanson, J. M.; Baiker, A. *Chem. Rev.* **2011**, *111*, 322.
(13) Hallett, J. P.; Welton, T. *Chem. Rev.* **2011**, *111*, 3508.
(14) Wasserscheid, P.; Keim, W. *Angew. Chem., Int. Ed.* **2000**, *39*, 3773.
(15) Xu, H.; Zhao, D.; Xu, P.; Liu, F.; Gao, G. *J. Chem. Eng. Data* **2005**, *50*, 133.
(16) Anthony, J. L.; Anderson, J. L.; Maginn, E. J.; Brennecke, J. F. *J. Phys. Chem. B* **2005**, *109*, 6366.
(17) Blanchard, L. A.; Gu, Z.; Brennecke, J. F. *J. Phys. Chem. B* **2001**, *105*, 2437.
(18) Camper, D.; Becker, C.; Koval, C.; Noble, R. *Ind. Eng. Chem. Res.* **2006**, *45*, 445.
(19) Mellein, B. R.; Brennecke, J. F. *J. Phys. Chem. B* **2007**, *111*, 4837.
(20) Aki, S. N. V. K.; Scurto, A. M.; Brennecke, J. F. *Ind. Eng. Chem. Res.* **2006**, *45*, 5574.

(21) Scurto, A. M.; Aki, S.; Brennecke, J. F. *J. Am. Chem. Soc.* **2002**, *124*, 10276.
(22) Scurto, A. M.; Aki, S.; Brennecke, J. F. *Chem. Commun.* **2003**, 572.
(23) Dong, L.; Zheng, D.; Wu, X. *Ind. Eng. Chem. Res.* **2012**, *51*, 4741.
(24) Yokozeki, A.; Shiflett, M. B. *Ind. Eng. Chem. Res.* **2010**, *49*, 9496.
(25) Yokozeki, A.; Shiflett, M. B. *Appl. Energy* **2007**, *84*, 1258.
(26) Shiflett, M. B.; Yokozeki, A. *AIChE J.* **2006**, *52*, 1205.
(27) Shiflett, M. B.; Yokozeki, A. *Ind. Eng. Chem. Res.* **2006**, *45*, 6375.
(28) Bara, J. E.; Camper, D. E.; Gin, D. L.; Noble, R. D. *Acc. Chem. Res.* **2010**, *43*, 152.
(29) Bara, J. E.; Carlisle, T. K.; Gabriel, C. J.; Camper, D.; Finotello, A.; Gin, D. L.; Noble, R. D. *Ind. Eng. Chem. Res.* **2009**, *48*, 4739.
(30) Bara, J. E.; Gabriel, C. J.; Carlisle, T. K.; Camper, D.; Finotello, A.; Gin, D. L.; Noble, R. D. *Chem. Eng. J* **2009**, *147*, 43.
(31) Bara, J. E.; Lessmann, S.; Gabriel, C. J.; Hatakeyama, E. S.; Noble, R. D.; Gin, D. L. *Ind. Eng. Chem. Res.* **2007**, *46*, 5397.
(32) Bara, J. E.; Kaminski, A. K.; Noble, R. D.; Gin, D. L. *J. Membr. Sci.* **2007**, *288*, 13.
(33) Bara, J. E.; Gabriel, C. J.; Hatakeyama, E. S.; Carlisle, T. K.; Lessmann, S.; Noble, R. D.; Gin, D. L. *J. Membr. Sci.* **2008**, *321*, 3.
(34) Bara, J. E.; Gin, D. L.; Noble, R. D. *Ind. Eng. Chem. Res.* **2008**, *47*, 9919.
(35) Camper, D.; Bara, J.; koval, C.; Noble, R. *Ind. Eng. Chem. Res.* **2006**, *45*, 6279.
(36) Lodge, T. P. *Science* **2008**, *321*, 50.
(37) Scovazzo, P.; Havard, D.; McShea, M.; Mixon, S.; Morgan, D. *J. Membr. Sci.* **2009**, *327*, 41.
(38) Scovazzo, P. *J. Membr. Sci.* **2009**, *343*, 199.
(39) Scovazzo, P.; Kieft, J.; Finan, D. A.; Koval, C.; DuBois, D.; Noble, R. *J. Membr. Sci.* **2004**, *238*, 57.
(40) Scovazzo, P.; Visser, A. E.; Davis, J. H., Jr.; Rogers, R. D.; Koval, C. A.; DuBois, D. L.; Noble, R. D. In *Industrial Applications of Ionic Liquids*; Rogers, R. D., Seddon, K. R., Eds.; American Chemical Society: Washington, DC, 2002.
(41) Jacquemin, J.; Husson, P.; Majer, V.; Gomes, M. F. C. *Fluid Phase Equilib.* **2006**, *240*, 87.
(42) Manan, N. A.; Hardacre, C.; Jacquemin, J.; Rooney, D. W.; Youngs, T. G. A. *J. Chem. Eng. Data* **2009**, *54*, 2005.
(43) Eslamimanesh, A.; Gharagheizi, F.; Mohammadi, A. H.; Richon, D. *Chem. Eng. Sci.* **2011**, *66*, 3039.
(44) *The Rectisol Process*; http://uicgroupecho.wikispaces.com/file/view/B_0308e_Rectisol.pdf (accessed Sept 30, 2013).
(45) Hochgesand, G. *Ind. Eng. Chem. Res.* **1970**, *62*, 37.
(46) Heintz, Y. J.; Sehabiaue, L.; Morsi, B. I.; Jones, K. L.; Luebke, J. D.; Pennline, H. W. *Energy Fuels* **2009**, *23*, 4822.
(47) Kato, R.; Gmehling, J. *J. Chem. Thermodyn.* **2005**, *37*, 603.
(48) Lei, Z.; Zhang, J.; Li, Q.; Chen, B. *Ind. Eng. Chem. Res.* **2009**, *48*, 2697.
(49) Santiago, R. S.; Santos, G. R.; Aznar, M. *Fluid Phase Equilib.* **2010**, *295*, 93.
(50) Santiago, R. S.; Aznar, M. *Fluid Phase Equilib.* **2011**, *303*, 111.
(51) Alevizou, E. I.; Pappa, G. D.; Voutsas, E. C. *Fluid Phase Equilib.* **2009**, *284*, 99.
(52) Nebig, S.; Bolts, R.; Gmehling, J. *Fluid Phase Equilib.* **2007**, *258*, 168.
(53) Nebig, S.; Gmehling, J. *Fluid Phase Equilib.* **2010**, *294*, 206.
(54) Nebig, S.; Liebert, V.; Gmehling, J. *Fluid Phase Equilib.* **2009**, *277*, 61.
(55) Nebig, S.; Gmehling, J. *Fluid Phase Equilib.* **2011**, *302*, 220.
(56) Kato, R.; Gmehling, J. *Fluid Phase Equilib.* **2005**, *231*, 38.
(57) Bondi, A. *Physical Properties of Molecular Liquids, Crystals and Glasses*; Wiley: New York, 1968.
(58) Kikic, I.; Fermeglia, M.; Rasmussen, P. *Chem. Eng. Sci.* **1991**, *46*, 2775.
(59) Macedo, E. A.; Skovborg, P.; Rasmussen, P. *Chem. Eng. Sci.* **1990**, *45*, 875.
(60) Achard, C.; Dussap, C. G.; Gros, J. B. *Fluid Phase Equilib.* **1994**, *98*, 71.
(61) Yan, W.; Topphoff, M.; Rose, C.; Gmehling, J. *Fluid Phase Equilib.* **1999**, *162*, 97.
(62) Kim, Y. S.; Choi, W. Y.; Jang, J. H.; Yoo, K. P.; Lee, C. S. *Fluid Phase Equilib.* **2005**, *228*−*229*, 439.
(63) Kim, J. E.; Lim, J. S.; Kang, J. W. *Fluid Phase Equilib.* **2011**, *306*, 251.
(64) Breure, B.; Bottini, S. B.; Witkamp, G. J.; Peters, C. J. *J. Phys. Chem. B* **2007**, *111*, 14265.
(65) Bermejo, M. D.; Martin, A.; Foco, G.; Cocero, M. J.; Bottini, S. B.; Peters, C. J. *J. Supercrit. Fluids* **2009**, *50*, 112.
(66) Chávez-Islas, L. M.; Vasquez-Medrano, R.; Flores-Tlacuhuac, A. *Ind. Eng. Chem. Res.* **2011**, *50*, 5153.
(67) Domanska, U.; Mazurowska, L. *Fluid Phase Equilib.* **2004**, *221*, 73.
(68) Domanska, U. *Fluid Phase Equilib.* **1989**, *46*, 223.
(69) Valderrama, J. O.; Zarricueta, K. *Fluid Phase Equilib.* **2009**, *275*, 145.
(70) Paduszynski, K.; Domanska, U. *Ind. Eng. Chem. Res.* **2012**, *51*, 591.
(71) Ye, C.; Shreeve, J. M. *J. Phys. Chem. A* **2007**, *111*, 1456.
(72) Palomar, J.; Ferro, V. R.; Torrecilla, J. S.; Rodriguez, F. *Ind. Eng. Chem. Res.* **2007**, *46*, 6041.
(73) Banerjee, T.; Singh, M. K.; Sahoo, R. K.; Khanna, A. *Fluid Phase Equilib.* **2005**, *234*, 64.
(74) Alvarez, V. H.; Aznar, M. *J. Taiwan Inst. Chem. E.* **2008**, *39*, 353.
(75) Santiago, R. S.; Santos, G. R.; Aznar, M. *Fluid Phase Equilib.* **2009**, *278*, 54.
(76) Delley, B. *Mol. Simul.* **2006**, *32*, 117.
(77) Gemehling, J.; Rasmussen, P.; Fredenslund, A. *Ind. Eng. Chem. Process Des. Dev.* **1982**, *21*, 118.
(78) Nocon, G.; Weidlich, U.; Gmehling, J.; Menke, J.; Onken, U. *Fluid Phase Equilib.* **1983**, *13*, 381.
(79) Kleiber, M. *Fluid Phase Equilib.* **1995**, *107*, 161.
(80) Lei, Z.; Dai, C.; Liu, X.; Xiao, L.; Chen, B. *Ind. Eng. Chem. Res.* **2012**, *51*, 12135.
(81) Klamt, A.; Eckert, F. *Fluid Phase Equilib.* **2000**, *172*, 43.
(82) Klamt, A. *J. Phys. Chem.* **1995**, *99*, 2224.
(83) Klamt, A.; Jonas, V.; Burger, T.; Lohrenz, J. C. *J. Phys. Chem. A* **1998**, *102*, 5074.
(84) Diedenhofen, M.; Eckert, F.; Klamt, A. *J. Chem. Eng. Data* **2003**, *48*, 475.
(85) Klamt, A.; Eckert, F.; Diedenhofen, M. *Fluid Phase Equilib.* **2009**, *285*, 15.
(86) Eckert, F.; Klamt, A. *Fluid Phase Equilib.* **2003**, *210*, 117.
(87) Klamet, A.; Eckert, F. *AIChE J.* **2002**, *48*, 369.
(88) Banerjee, T.; Khanna, A. *J. Chem. Eng. Data* **2006**, *51*, 2170.
(89) Varma, N. R.; Ramalingam, A.; Banerjee, T. *Chem. Eng. J.* **2011**, *166*, 30.
(90) Lei, Z.; Chen, B.; Li, C. *Chem. Eng. Sci.* **2007**, *62*, 3940.
(91) Grensemann, H.; Gmehling, J. *Ind. Eng. Chem. Res.* **2005**, *44*, 1610.
(92) Anantharaj, R.; Banerjee, T. *Fuel Process. Technol.* **2011**, *92*, 39.
(93) Zhang, X.; Liu, Z.; Wang, W. *AIChE J.* **2008**, *54*, 2717.
(94) Maiti, A. *Chem. Sus. Chem.* **2009**, *2*, 628.
(95) Palomar, J.; Gonzalez-Miquel, M.; Polo, A.; Rodriguez, F. *Ind. Eng. Chem. Res.* **2011**, *50*, 3452.
(96) Zhang, X.; Hun, F.; Liu, Z.; Wang, W.; Shi, W.; Maginn, E. J. *J. Phys. Chem. B* **2009**, *113*, 7591.
(97) Shah, J. K.; Maginn, E. J. *J. Phys. Chem. B* **2005**, *109*, 10395.
(98) Heintz, A. *J. Chem. Thermodyn.* **2005**, *37*, 525.
(99) Cadena, C.; Anthony, J. L.; Shah, J. K.; Morrow, T. I.; Brennecke, J. F.; Maginn, E. J. *J. Am. Chem. Soc.* **2004**, *126*, 5300.
(100) Huang, X.; Margulis, C. J.; Li, Y.; Berne, B. J. *J. Am. Chem. Soc.* **2005**, *127*, 17842.
(101) Lin, S. T.; Sandler, S. I. *Ind. Eng. Chem. Res.* **2002**, *41*, 899.
(102) Banerje, T.; Singh, M. K.; Khanna, A. *Ind. Eng. Chem. Res.* **2006**, *45*, 3207.

(103) Pye, C. C.; Ziegler, T.; van Lenthe, E.; Louwen, J. N. *Can. J. Chem.* **2009**, *87*, 790.
(104) *ADF COSMO-RS Manual*; http://www.scm.com/Doc/Doc2010/CRS/CRS/page18.html (accessed Sept 30, 2013).
(105) Shimoyama, Y.; Ito, A. *Fluid Phase Equilib.* **2010**, *297*, 178.
(106) Camper, D.; Scovazzo, P.; Koval, C.; Noble, R. *Ind. Eng. Chem. Res.* **2004**, *43*, 3049.
(107) Scovazzo, P.; Camper, D.; Kieft, J.; Poshusta, J.; Koval, C.; Noble, R. *Ind. Eng. Chem. Res.* **2004**, *43*, 6855.
(108) Hildebrand, J. H.; Scott, R. L. *The Solubility of Nonelectrolytes*, 3rd ed.; Dover Publications: New York, 1964.
(109) Kilaru, P. K.; Condemarin, R. A.; Scovazzo, P. *Ind. Eng. Chem. Res.* **2008**, *47*, 900.
(110) Prausnitz, J. M.; Lichtenthaler, R. N.; de Azvedo, E. G. *Molecular Thermodynamics of Fluid-Phase Equilibria*, 3rd ed.; Prentice Hall: Upper Saddle River, NJ, 1999.
(111) Camper, D.; Becker, C.; Koval, C.; Noble, R. *Ind. Eng. Chem. Res.* **2005**, *44*, 1928.
(112) Kilaru, P. K.; Scovazzo, P. *Ind. Eng. Chem. Res.* **2008**, *47*, 910.
(113) Moganty, S. S.; Baltus, R. E. *Ind. Eng. Chem. Res.* **2010**, *49*, 5846.
(114) Carlisle, T. K.; Bara, J. E.; Gabriel, C. J.; Noble, R. D.; Gin, D. L. *Ind. Eng. Chem. Res.* **2008**, *47*, 7005.
(115) Bara, J. E.; Carlisle, T. K.; Gabriel, C. J.; aCamper, D.; Finotello, A.; Gin, D. L.; Noble, R. D. *Ind. Eng. Chem. Res.* **2009**, *48*, 2739.
(116) You, S. S.; Yoo, K. P.; Lee, C. S. *Fluid Phase Equilib.* **1994**, *93*, 193.
(117) You, S. S.; Yoo, K. P.; Lee, C. S. *Fluid Phase Equilib.* **1994**, *93*, 215.
(118) Park, B. H.; Yoo, K. P.; Lee, C. S. *Fluid Phase Equilib.* **2003**, *212*, 175.
(119) Kim, Y. S.; Jang, J. H.; Lim, B. D.; Kang, J. W.; Lee, C. S. *Fluid Phase Equilib.* **2007**, *256*, 70.
(120) Skjold-Jørgensen, S. *Fluid Phase Equilib.* **1984**, *16*, 317.
(121) Skjold-Jørgensen, S. *Ind. Eng. Chem. Res.* **1988**, *27*, 110.
(122) Gross, J.; Sadowski, G. *Ind. Eng. Chem. Res.* **2001**, *40*, 1244.
(123) Karakatsani, E. K.; Spyriouni, T.; Economou, I. G. *AIChE J.* **2005**, *51*, 2328.
(124) Karakatsani, E. K.; Economou, I. G. *J. Phys. Chem. B* **2006**, *110*, 9252.
(125) Kroon, M. C.; Karakatsani, E. K.; Economou, I. G.; Witkamp, G. J.; Peters, C. J. *J. Phys. Chem. B* **2006**, *110*, 9262.
(126) Karakatsani, E. K.; Economou, I. G.; Kroon, M. C.; Peters, C. J.; Witkamp, G. J. *J. Phys. Chem. B* **2007**, *111*, 15487.
(127) Andreu, J. S.; Vega, L. F. *J. Phys. Chem. B* **2008**, *112*, 15398.
(128) Andreu, J. S.; Vega, L. F. *J. Phys. Chem. B* **2007**, *111*, 16028.
(129) Vega, L. F.; Vilaseca, O.; Llovell, F.; Andreu, J. S. *Fluid Phase Equilib.* **2010**, *294*, 15.
(130) Adidharma, H.; Radosz, M. *Ind. Eng. Chem. Res.* **1998**, *37*, 4453.
(131) Ji, X.; Adidharma, H. *Ind. Eng. Chem. Res.* **2007**, *46*, 4667.
(132) Ji, X.; Adidharma, H. *Ind. Eng. Chem. Res.* **2006**, *45*, 7719.
(133) Ji, X.; Adidharma, H. *Chem. Eng. Sci.* **2009**, *64*, 1985.
(134) Ji, X.; Adidharma, H. *Fluid Phase Equilib.* **2010**, *293*, 141.
(135) Lei, Z.; Ohyabu, H.; Sato, Y.; Inomata, H.; Smith, R. L., Jr. *J. Supercrit. Fluids* **2007**, *40*, 452.
(136) Sato, Y.; Fujiwara, K.; Takikawa, T.; Sumarno; Takishima, S.; Masuoka, H. *Fluid Phase Equilib.* **1999**, *162*, 261.
(137) Sato, Y.; Yurugi, M.; Yamabiki, T.; Takishima, S.; Masuoka, H. *J. Appl. Polym. Sci.* **2001**, *79*, 1134.
(138) Sato, Y.; Takikawa, T.; Sorakubo, A.; Takishima, S.; Masuoka, H.; Imaizumi, M. *Ind. Eng. Chem. Res.* **2000**, *39*, 4813.
(139) *NIST Chemistry WebBook*; http://webbook.nist.gov/chemistry/ (accessed Sept 30, 2013).
(140) Blasig, A.; Tang, J.; Hu, X.; Tan, S. P.; Shen, Y.; Radosz, M. *Ind. Eng. Chem. Res.* **2007**, *46*, 5542.
(141) Soriano, A. N.; Doma, B. T., Jr.; Li, M. H. *J. Chem. Thermodyn.* **2009**, *41*, 525.
(142) Soriano, A. N.; Doma, B. T., Jr.; Li, M. H. *J. Taiwan Inst. Chem. E.* **2009**, *40*, 387.
(143) Soriano, A. N.; Doma, B. T., Jr.; Li, M. H. *J. Chem. Eng. Data* **2008**, *53*, 2550.
(144) Tang, J.; Shen, Y.; Radosz, M.; Sun, W. *Ind. Eng. Chem. Res.* **2009**, *48*, 9113.
(145) Tang, J.; Tang, H.; Sun, W.; Radosz, M.; Shen, Y. *Polymer* **2005**, *46*, 12460.
(146) Tang, J.; Tang, H.; Sun, W.; Radosz, M.; Shen, Y. *J. Polym. Sci. A: Polym. Chem.* **2005**, *43*, 5477.
(147) Blasig, A.; Tang, J.; Hu, X.; Shen, Y.; Radosz, M. *Fluid Phase Equilib.* **2007**, *256*, 75.
(148) Muldoon, M. J.; Aki, S. N. V. K.; Anderson, J. L.; Dixon, J. K.; Brennecke, J. F. *J. Phys. Chem. B* **2007**, *111*, 9001.
(149) Shiflett, M. B.; Yokozeki, A. *Ind. Eng. Chem. Res.* **2005**, *44*, 4453.
(150) Shiflett, M. B.; Yokozeki, A. *J. Chem. Eng. Data* **2009**, *54*, 108.
(151) Shiflett, M. B.; Yokozeki, A. *J. Phys. Chem. B* **2007**, *111*, 2070.
(152) Yokozeki, A.; Shiflett, M. B.; Junk, C. P.; Grieco, L. M.; Foo, T. *J. Phys. Chem. B* **2008**, *112*, 16654.
(153) Yokozeki, A.; Shiflett, M. B. *Energy Fuel* **2009**, *23*, 4701.
(154) Shiflett, M. B.; Yokozeki, A. *Energy Fuel* **2010**, *24*, 1001.
(155) Aki, S. N. V. K.; Mellein, B. R.; Saurer, E. M.; Brennecke, J. F. *J. Phys. Chem. B* **2004**, *108*, 20355.
(156) Anthony, J. L.; Maginn, E. J.; Brennecke, J. F. *J. Phys. Chem. B* **2002**, *106*, 7315.
(157) Baltus, R. E.; Culbertson, B. H.; Dai, S.; Luo, H.; DePaoli, D. W. *J. Phys. Chem. B* **2004**, *108*, 721.
(158) Dai, C.; Lei, Z.; Wang, W.; Xiao, L.; Chen, B. *AIChE J.* **2013**, *59*, 4399.
(159) Lei, Z.; Yuan, J.; Zhu, J. *J. Chem. Eng. Data* **2010**, *55*, 4190.
(160) Lei, Z.; Han, J.; Zhang, B.; Li, Q.; Zhu, J.; Chen, B. *J. Chem. Eng. Data* **2012**, *57*, 2153.
(161) Bara, J. E.; Gabriel, C. J.; Lessmann, S.; Carlisle, T. K.; Finotello, A.; Gin, D. L.; Noble, R. D. *Ind. Eng. Chem. Res.* **2007**, *46*, 5380.
(162) Hong, G.; Jacquemin, J.; Deetlefs, M.; Hardacre, C.; Husson, P.; Costa Gomes, M. F. *Fluid Phase Equilib.* **2007**, *256*, 27.
(163) Jacquemin, J.; Costa Gomes, M. F.; Husson, P.; Majer, V. *J. Chem. Thermodyn.* **2006**, *38*, 490.
(164) Palgunadi, J.; Kang, J. E.; Nguyen, D. Q.; Kim, J. H.; Min, B. K.; Lee, S. D.; Kim, H.; Kim, H. S. *Thermochim. Acta* **2009**, *494*, 94.
(165) Kurnia, K. A.; Harris, F.; Wilfred, C. D.; Mutalib, M. I. A.; Murugesan, T. *J. Chem. Thermodyn.* **2009**, *41*, 1069.
(166) Shin, E. K.; Lee, B. C. *J. Chem. Eng. Data* **2008**, *53*, 2728.
(167) Ahn, J. Y.; Lee, B. C.; Lim, J. S.; Yoo, K. P.; Kang, J. W. *Fluid Phase Equilib.* **2010**, *290*, 75.
(168) Shin, E. K.; Lee, B. C.; Lim, J. S. *J. Supercrit. Fluids* **2008**, *45*, 282.
(169) Gutkowski, K. I.; Shariati, A.; Peters, C. J. *J. Supercrit. Fluids* **2006**, *39*, 187.
(170) Carvalho, P. J.; Alvarez, V. H.; Marrucho, I. M.; Aznar, M.; Coutinho, J. A. P. *J. Supercrit. Fluids* **2009**, *50*, 105.
(171) Carvalho, P. J.; Alvarez, V. H.; Machado, J. J. B.; Pauly, J.; Daridon, J. L.; Marrucho, I. M.; Aznar, M.; Coutinho, J. A. P. *J. Supercrit. Fluids* **2009**, *48*, 99.
(172) Shariati, A.; Peters, C. J. *J. Supercrit. Fluids* **2004**, *30*, 139.
(173) Hou, Y.; Baltus, R. E. *Ind. Eng. Chem. Res.* **2007**, *46*, 8166.
(174) Shokouhi, M.; Adibi, M.; Jalili, A. H.; Hosseini-Jenab, M.; Mehdizadeh, A. *J. Chem. Eng. Data* **2010**, *55*, 1663.
(175) Zhang, J.; Zhang, Q.; Qiao, B.; Deng, Y. *J. Chem. Eng. Data* **2007**, *52*, 2277.
(176) Valderrama, J. O.; Reategui, A.; Sanga, W. W. *Ind. Eng. Chem. Res.* **2008**, *47*, 8416.
(177) Alvarez, V.; Aznar, M. *Open Thermodyn.* **2008**, *2*, 25.
(178) Kamps, Á. P.; Tuma, D.; Xia, J.; Maurer, G. *J. Chem. Eng. Data* **2003**, *48*, 746.
(179) Zhang, S.; Yuan, X.; Chen, Y.; Zhang, X. *J. Chem. Eng. Data* **2005**, *50*, 1582.

(180) Kroon, M. C.; Shariati, A.; Costantini, M.; van Spronsen, J.; Witkamp, G. J.; Sheldon, R. A.; Peters, C. J. *J. Chem. Eng. Data* **2005**, *50*, 173.
(181) Lei, Z.; Qi, X.; Zhu, J.; Li, Q.; Chen, B. *J. Chem. Eng. Data* **2012**, *57*, 3458.
(182) Tian, S.; Hou, Y.; Wu, W.; Ren, S.; Pang, K. *J. Chem. Eng. Data* **2012**, *57*, 756.
(183) Fu, D.; Sun, X.; Pu, J.; Zhao, S. *J. Chem. Eng. Data* **2006**, *51*, 371.
(184) Blanchard, L. A.; Hancu, D.; Beckman, E. J.; Brennecke, J. F. *Nature* **1999**, *399*, 28.
(185) Carvalho, P. J.; Coutinho, J. A. P. *J. Phys. Chem. Lett.* **2010**, *1*, 774.
(186) Ramdin, M.; de Loos, T. W.; Vlugt, T. J. H. *Ind. Eng. Chem. Res.* **2012**, *51*, 8149.
(187) Shannon, M. S.; Tedstone, J. M.; Danielsen, S. P. O.; Hindman, M. S.; Irvin, A. C.; Bara, J. E. *Ind. Eng. Chem. Res.* **2012**, *51*, 5565.
(188) Finotello, A.; Bara, J. E.; Narayan, S.; Camper, D.; Noble, R. D. *J. Phys. Chem. B* **2008**, *112*, 2335.
(189) Revelli, A. L.; Mutelet, F.; Jaubert, J. N. *J. Phys. Chem. B* **2010**, *114*, 12908.
(190) Jung, Y. H.; Jung, J. Y.; Jin, Y. R.; Lee, B. C.; Baek, I. H.; Kim, S. H. *J. Chem. Eng. Data* **2012**, *57*, 3321.
(191) Shiflett, M. B.; Kasprzak, D. J.; Junk, C. P.; Yokozeki, A. *J. Chem. Thermodyn.* **2008**, *40*, 25.
(192) Carvalho, P. J.; Álvarez, V. H.; Schröder, B.; Gil, A. M.; Marrucho, I. M.; Aznar, M.; Santos, L. M. N. B. F.; Coutinho, J. A. P. *J. Phys. Chem. B* **2009**, *113*, 6803.
(193) Husson-Borg, P.; Majer, V.; Gomes, M. F. C. *J. Chem. Eng. Data* **2003**, *48*, 480.
(194) Chen, Y.; Zhang, S.; Yuan, X. *Thermochim. Acta* **2006**, *441*, 42.
(195) Zhou, L.; Fan, J.; Shang, X.; Wang, J. *J. Chem. Thermodyn.* **2013**, *59*, 28.
(196) Afzal, W.; Liu, X.; Prausnitz, J. M. *J. Chem. Thermodyn.* **2013**, *63*, 88.
(197) Jang, S.; Cho, D. W.; Im, T.; Kim, H. *Fluid Phase Equilib.* **2010**, *299*, 216.
(198) Almantariotis, D.; Stevanovic, S.; Fandiño, O.; Pensado, A. S.; Padua, A. A. H.; Coxam, J. Y.; Costa Gomes, M. F. *J. Phys. Chem. B* **2012**, *116*, 7728.
(199) Chen, Y.; Mutelet, F.; Jaubert, J. *Fluid Phase Equilib.* **2013**, *354*, 191.
(200) Kumełan, J.; Kamps, Á. P.; Tuma, D.; Maurer, G. *J. Chem. Eng. Data* **2006**, *51*, 1802.
(201) Bermejo, M. D.; Montero, M.; Saez, E.; Florusse, L. J.; Kotlewska, A. J.; Cocero, M. J.; van Rantwijk, F.; Peters, C. J. *J. Phys. Chem. B* **2008**, *112*, 13532.
(202) Shariati, A.; Gutkowski, K.; Peters, C. J. *AIChE J.* **2005**, *51*, 1532.
(203) Karadas, F.; Köz, B.; Jacquemin, J.; Deniz, E.; Rooney, D.; Thompson, J.; Yavuz, C. T.; Khraisheh, M.; Aparicio, S.; Atihan, M. *Fluid Phase Equilib.* **2013**, *351*, 74.
(204) Lee, B. C.; Outcalt, S. L. *J. Chem. Eng. Data* **2006**, *51*, 892.
(205) Jacquemin, J.; Husson, P.; Majer, V.; Gomes, M. F. C. *J. Solution Chem.* **2007**, *36*, 967.
(206) Raeissi, S.; Peters, C. J. *J. Chem. Thermodyn.* **2009**, *54*, 382.
(207) Manic, M. S.; Queimada, A. J.; Macedo, E. A.; Najdanovic-Visak, V. *J. Supercrit. Fluids* **2012**, *65*, 1.
(208) Stevanovic, S.; Podgorsek, A.; Moura, L.; Santini, C. C.; Padua, A. A. H.; Costa Gomes, M. F. *Int. J. Greenhouse Gas Control* **2013**, *17*, 78.
(209) Song, H. N.; Lee, B. C.; Lim, J. S. *J. Chem. Eng. Data* **2010**, *55*, 891.
(210) Stevanovic, S.; Costa Gomes, M. F. *J. Chem. Thermodyn.* **2013**, *59*, 65.
(211) Yim, J. H.; Song, H. N.; Yoo, K. P.; Lim, J. S. *J. Chem. Eng. Data* **2011**, *56*, 1197.
(212) Kumełan, J.; Tuma, D.; Kamps, Á. P.; Maurer, G. *J. Chem. Eng. Data* **2010**, *55*, 167.
(213) Sharma, P.; Choi, S. H.; Park, S. D.; Baek, I. H.; Lee, G. S. *Chem. Eng. J.* **2012**, *181*−*182*, 834.
(214) Kim, S. A.; Yim, J. K.; Lim, J. S. *Fluid Phase Equilib.* **2012**, *332*, 28.
(215) Kodama, D.; Kanakubo, M.; Kokubo, M.; Ono, T.; Kawanami, H.; Yokoyama, T.; Nanjo, H.; Kato, M. *J. Supercrit. Fluids* **2010**, *52*, 189.
(216) Ren, W.; Sensenich, B.; Scurto, A. M. *J. Chem. Thermodyn.* **2010**, *42*, 305.
(217) Bogel-Łukasik, R.; Matkowska, D.; Bogel-Łukasik, E.; Hofman, T. *Fluid Phase Equilib.* **2010**, *293*, 168.
(218) Althuluth, M.; Mota-Martinez, M. T.; Kroon, M. C.; Peters, C. J. *J. Chem. Eng. Data* **2012**, *57*, 3422.
(219) Jalili, A. H.; Mehdizadeh, A.; Shokouhi, M.; Ahmadi, A. N.; Hosseini-Jenab, M.; Fateminassab, F. *J. Chem. Thermodyn.* **2010**, *42*, 1298.
(220) Bermejo, M. D.; Fieback, T. M.; Martín, Á. *J. Chem. Thermodyn.* **2013**, *58*, 237.
(221) Soriano, A. N.; Doma, B. T., Jr.; Li, M. H. *J. Chem. Thermodyn.* **2008**, *40*, 1654.
(222) Shariati, A.; Peters, C. J. *J. Supercrit. Fluids* **2004**, *29*, 43.
(223) Hong, G.; Jacquemin, J.; Husson, P.; Costa Gomes, M. F.; Deetlefs, M.; Nieuwenhuyzen, M.; Sheppard, O.; Hardacre, C. *Ind. Eng. Chem. Res.* **2006**, *45*, 8180.
(224) Schilderman, A. M.; Raeissi, S.; Peters, C. J. *Fluid Phase Equilib.* **2007**, *260*, 19.
(225) Yuan, X.; Zhang, S.; Liu, J.; Lu, X. *Fluid Phase Equilib.* **2007**, *257*, 195.
(226) Jalili, A. H.; Mehdizadeh, A.; Shokouhi, M.; Sakhaeinia, H.; Taghikhani, V. *J. Chem. Thermodyn.* **2010**, *42*, 787.
(227) Costantini, M.; Toussaint, V. A.; Shariati, A.; Peters, C. J.; Kikic, I. *J. Chem. Eng. Data* **2005**, *50*, 52.
(228) Yim, J. H.; Lim, J. S. *Fluid Phase Equilib.* **2013**, *352*, 67.
(229) Nwosu, S. O.; Schleicher, J. C.; Scurto, A. M. *J. Supercrit. Fluids* **2009**, *51*, 1.
(230) Mota-Martinez, M. T.; Althuluth, M.; Kroon, M. C.; Peters, C. J. *Fluid Phase Equilib.* **2012**, *332*, 35.
(231) Kumełan, J.; Kamps, Á. P.; Tuma, D.; Maurer, G. *J. Chem. Thermodyn.* **2006**, *38*, 1396.
(232) Gomes, M. F. C. *J. Chem. Eng. Data* **2007**, *52*, 472.
(233) Raeissi, S.; Florusse, L.; Peters, C. J. *J. Supercrit. Fluids* **2010**, *55*, 825.
(234) Yim, J. H.; Song, H. N.; Lee, B. C.; Lim, J. S. *Fluid Phase Equilib.* **2011**, *308*, 147.
(235) Mattedi, S.; Carvalho, P. J.; Coutinho, J. A. P.; Alvarez, V. H.; Iglesias, M. *J. Supercrit. Fluids* **2011**, *56*, 224.
(236) Zhao, Y.; Zhang, X.; Dong, H.; Zhen, Y.; Li, G.; Zeng, S.; Zhang, S. *Fluid Phase Equilib.* **2011**, *302*, 60.
(237) Ramdin, M.; Vlugt, T. J. H.; de Loos, T. W. *J. Chem. Eng. Data* **2012**, *57*, 2275.
(238) Safavi, M.; Ghotbi, C.; Taghikhani, V.; Jalili, A. H.; Mehdizadeh, A. *J. Chem. Thermodyn.* **2013**, *65*, 220.
(239) Jalili, A. H.; Safavi, M.; Ghotbi, C.; Mehdizadeh, A.; Hosseini-Jenab, M.; Taghikhani, V. *J. Phys. Chem. B* **2012**, *116*, 2758.
(240) Lei, Z.; Zhang, B.; Zhu, J.; Gong, W.; Lü, J.; Li, Y. *Chin. J. Chem. Eng.* **2013**, *21*, 310.
(241) Goodrich, B. F.; de la Fuente, J. C.; Gurkan, B. E.; Zadigian, D. J.; Price, E. A.; Huang, Y.; Brennecke, J. F. *Ind. Eng. Chem. Res.* **2011**, *50*, 111.
(242) Ramdin, M.; Olasagasti, T. Z.; Vlugt, T. J. H.; de Loos, T. W. *J. Supercrit. Fluids* **2013**, *82*, 41.
(243) Zhang, S.; Chen, Y.; Ren, R. X. F.; Zhang, Y.; Zhang, J.; Zhang, X. *J. Chem. Eng. Data* **2005**, *50*, 230.
(244) Carvalhoa, P. J.; Álvarezb, V. H.; Marruchoa, I. M.; Aznarb, M.; Coutinho, J. A. P. *J. Supercrit. Fluids* **2010**, *52*, 258.

(245) Goodrich, B. F.; de la Fuente, J. C.; Gurkan, B. E.; Lopez, Z. K.; Price, E. A.; Huang, Y.; Brennecke, J. F. *J. Phys. Chem. B* **2011**, *115*, 9140.
(246) Makino, T.; Kanakubo, M.; Umecky, T.; Suzuki, A. *Fluid Phase Equilib.* **2013**, *357*, 64.
(247) Mahurin, S. M.; Yeary, J. S.; Baker, S. N.; Jiang, D.; Dai, S.; Baker, G. A. *J. Membr. Sci.* **2012**, *401*−*402*, 61.
(248) Urukova, I.; Vorholz, J.; Maurer, G. *J. Phys. Chem. B* **2005**, *109*, 12154.
(249) Kerlé, D.; Ludwig, R.; Geiger, A.; Paschek, D. *J. Phys. Chem. B* **2009**, *113*, 12727.
(250) Finotello, A.; Bara, J. E.; Camper, D.; Noble, R. D. *Ind. Eng. Chem. Res.* **2008**, *47*, 3453.
(251) Anderson, J. L.; Dixon, J. K.; Brennecke, J. F. *Acc. Chem. Res.* **2007**, *40*, 1208.
(252) Beckman, E. J. *Chem. Commun.* **2004**, 1885.
(253) Yokozeki, A.; Shiflett, M. B. *Appl. Energy* **2007**, *84*, 351.
(254) Yokozeki, A.; Shiflett, M. B. *Ind. Eng. Chem. Res.* **2008**, *47*, 8389.
(255) Peng, X.; Wang, W.; Xue, R.; Shen, Z. *AIChE J.* **2006**, *52*, 994.
(256) Shi, W.; Sorescu, D. C.; Luebke, D. R.; Keller, M. J.; Wickramanayake, S. *J. Phys. Chem. B* **2010**, *114*, 6531.
(257) Hert, D. G.; Anderson, J. L.; Aki, S. N. V. K.; Brennecke, J. F. *Chem. Commun.* **2005**, 2603.
(258) Toussaint, V. A.; Kühne, E.; Shariati, A.; Peters, C. J. *J. Chem. Thermodyn.* **2013**, *59*, 239.
(259) Kumełan, J.; Tuma, D.; Maurer, G. *Fluid Phase Equilib.* **2011**, *311*, 9.
(260) Shi, W.; Maginn, E. J. *J. Phys. Chem. B* **2008**, *112*, 16710.
(261) Shiflett, M. B.; Niehaus, A. M. S.; Yokozeki, A. *J. Phys. Chem. B* **2011**, *115*, 3478.
(262) Shiflett, M. B.; Niehaus, A. M. S.; Yokozeki, A. *J. Chem. Eng. Data* **2010**, *55*, 4785.
(263) Shiflett, M. B.; Yokozeki, A. *Fluid Phase Equilib.* **2010**, *294*, 105.
(264) Taib, M. M.; Murugesan, T. *Chem. Eng. J.* **2012**, *181*−*182*, 56.
(265) Hasib-ur-Rahman, M.; Siaj, M.; Larachi, F. *Chem. Eng. Process.* **2010**, *49*, 313.
(266) Bates, E. D.; Mayton, R. D.; Ntai, I.; Davis, J. H., Jr. *J. Am. Chem. Soc.* **2002**, *124*, 926.
(267) Pinto, A. M.; Rodríguez, H.; Colón, Y. J.; Arce, A., Jr.; Arce, A.; Soto, A. *Ind. Eng. Chem. Res.* **2013**, *52*, 5975.
(268) Wang, J. J.; Tian, Y.; Zhao, Y.; Zhuo, K. L. *Green Chem.* **2003**, *5*, 618.
(269) Zhou, Q.; Wang, L. S.; Chen, H. P. *J. Chem. Eng. Data* **2006**, *51*, 905.
(270) Fendt, S.; Padmanabhan, S.; Blanch, H. W.; Prausnitz, J. M. *J. Chem. Eng. Data* **2011**, *56*, 31.
(271) Ciocirlan, O.; Croitoru, O.; Iulian, O. *J. Chem. Eng. Data* **2011**, *56*, 1526.
(272) Liu, Z.; Wu, W.; Han, B.; Dong, Z.; Zhao, G.; Wang, J.; Jiang, T.; Yang, G. *Chem.—Eur. J.* **2003**, *9*, 3897.
(273) Zhang, Z.; Wu, W.; Wang, B.; Chen, J.; Shen, D.; Han, B. *J. Supercit. Fluids* **2007**, *40*, 1.
(274) Kühne, E.; Perez, E.; Witkamp, G. J.; Peres, C. J. *J. Supercit. Fluids* **2008**, *45*, 27.
(275) Kühne, E.; Santarossa, S.; Perez, E.; Witkamp, G. J.; Peres, C. J. *J. Supercit. Fluids* **2008**, *46*, 93.
(276) Kühne, E.; Perez, E.; Witkamp, G. J.; Peres, C. J. *J. Supercit. Fluids* **2008**, *45*, 293.
(277) Bogel-Łukasik, R.; Najdanovic-Visak, V.; Barreiros, S.; da Ponte, M. N. *Ind. Eng. Chem. Res.* **2008**, *47*, 4473.
(278) Bogel-Łukasik, R.; Matkowska, D.; Zakrzewska, M. E.; Bogel-Łukasik, E.; Hofman, T. *Fluid Phase Equilib.* **2010**, *295*, 177.
(279) Ahmady, A.; Hashim, M. A.; Aroua, M. K. *Chem. Eng. J.* **2011**, *172*, 763.
(280) Sairi, N. A.; Yusoff, R.; Alias, Y.; Aroua, M. K. *Fluid Phase Equilib.* **2011**, *300*, 89.
(281) Tang, J.; Sun, W.; Tang, H.; Radosz, M.; Shen, Y. *Macromolecules* **2005**, *38*, 2037.
(282) Tang, J.; Sun, W.; Tang, H.; Plancher, H.; Radosz, M.; Shen, Y. *Chem. Commun.* **2005**, 3325.
(283) Babarao, R.; Dai, S.; Jiang, D. *J. Phys. Chem. B* **2011**, *115*, 9789.
(284) Zhang, X.; Liu, X.; Yao, X.; Zhang, S. *Ind. Eng. Chem. Res.* **2011**, *50*, 8323.
(285) Kazarian, S. G.; Briscoe, B. J.; Welton, T. *Chem. Commun.* **2000**, 2047.
(286) Lei, Z.; Zhang, J.; Chen, B. *J. Chem. Technol. Biotechnol.* **2002**, *77*, 1251.
(287) Lei, Z.; Li, C.; Li, Y.; Chen, B. *Sep. Purif. Technol.* **2004**, *36*, 131.
(288) Davis, J. H., Jr. *Chem. Lett.* **2004**, *33*, 1072.
(289) Gutowski, K. E.; Maginn, E. J. *J. Am. Chem. Soc.* **2008**, *130*, 14690.
(290) Gurkan, B. E.; de la Fuente, J.; Mindrup, E. M.; Ficke, L. E.; Goodrich, B. F.; Price, E. A.; Schneider, W. F.; Brennecke, J. F. *J. Am. Chem. Soc.* **2010**, *132*, 2116.
(291) Camper, D.; Bara, J. E.; Gin, D. L.; Noble, R. D. *Ind. Eng. Chem. Res.* **2008**, *47*, 8496.
(292) Wang, C.; Luo, H.; Jiang, D.; Li, H.; Dai, S. *Angew. Chem.* **2010**, *122*, 6114.
(293) Yu, G.; Zhang, S.; Yao, X.; Zhang, J.; Dong, K.; Dai, W.; Mori, R. *Ind. Eng. Chem. Res.* **2006**, *45*, 2875.
(294) Mahurin, S. M.; Dai, T.; Yeary, J. S.; Luo, H.; Dai, S. *Ind. Eng. Chem. Res.* **2011**, *50*, 14061.
(295) Anderson, J. L.; Dixon, J. K.; Maginn, E. J.; Brennecke, J. F. *J. Phys. Chem. B* **2006**, *110*, 15059.
(296) Wu, W.; Han, B.; Gao, H.; Liu, Z.; Jiang, T.; Huang, J. *Angew. Chem., Int. Ed.* **2004**, *43*, 2415.
(297) Ren, S.; Hou, Y.; Wu, W.; Liu, Q.; Xiao, Y.; Chen, X. *J. Phys. Chem. B* **2010**, *114*, 2175.
(298) Jin, M.; Hou, Y.; Wu, W.; Ren, S.; Tian, S.; Xiao, L.; Lei, Z. *J. Phys. Chem. B* **2011**, *115*, 6585.
(299) Ren, S.; Hou, Y.; Wu, W.; Jin, M. *Ind. Eng. Chem. Res.* **2011**, *50*, 998.
(300) Shiflett, M. B.; Yokozeki, A. *Ind. Eng. Chem. Res.* **2010**, *49*, 1370.
(301) Jiang, Y. Y.; Zhou, Z.; Jiao, Z.; Li, L.; Wu, Y. T.; Zhang, Z. B. *J. Phys. Chem. B* **2007**, *111*, 5058.
(302) Huang, J.; Riisager, A.; Berg, R. W.; Fehrmann, R. *J. Mol. Catal. A: Chem* **2008**, *279*, 170.
(303) Huang, J.; Riisager, A.; Wasserscheid, P.; Fehrmann, R. *Chem. Commun.* **2006**, 4027.
(304) Yuan, X. L.; Zhang, S. J.; Lu, X. M. *J. Chem. Eng. Data* **2007**, *52*, 596.
(305) Ghobadi, A. F.; Taghikhani, V.; Elliott, J. R. *J. Phys. Chem. B* **2011**, *115*, 13599.
(306) Ohlin, C. A.; Dyson, P. J.; Laurenczy, G. *Chem. Commun.* **2004**, 1070.
(307) Kumełan, J.; Kamps, Á. P.; Tuma, D.; Maurer, G. *Fluid Phase Equilib.* **2005**, *228*−*229*, 207.
(308) Kumełan, J.; Kamps, Á. P.; Tuma, D.; Maurer, G. *J. Chem. Eng. Data* **2009**, *54*, 966.
(309) Florusse, L. J.; Raeissi, S.; Peters, C. J. *J. Chem. Eng. Data* **2011**, *56*, 4797.
(310) Sharma, A.; Julcour, C.; Kelkar, A. A.; Deshpande, R. M.; Delmas, H. *Ind. Eng. Chem. Res.* **2009**, *48*, 4075.
(311) Kumełan, J.; Kamps, Á. P.; Tuma, D.; Maurer, G. *Fluid Phase Equilib.* **2007**, *260*, 3.
(312) Kumełan, J.; Kamps, Á. P.; Tuma, D.; Maurer, G. *J. Chem. Eng. Data* **2007**, *52*, 2319.
(313) Yuan, X.; Zhang, S.; Chen, Y.; Lu, X.; Dai, W.; Mori, R. *J. Chem. Eng. Data* **2006**, *51*, 645.
(314) Kumełan, J.; Kamps, Á. P.; Urukova, I.; Tuma, D.; Maurer, G. *J. Chem. Thermodyn.* **2005**, *37*, 595.
(315) Kumełan, J.; Kamps, Á. P.; Tuma, D.; Maurer, G. *J. Chem. Eng. Data* **2006**, *51*, 11.

(316) Kumełan, J.; Kamps, Á. P.; Tuma, D.; Maurer, G. *J. Chem. Eng. Data* **2006**, *51*, 1364.
(317) Raeissi, S.; Florusse, L. J.; Peters, C. J. *J. Chem. Eng. Data* **2011**, *56*, 1105.
(318) Raeissi, S.; Peters, C. J. *AIChE J.* **2012**, *58*, 3553.
(319) Jacquemin, J.; Husson, P.; Majer, V.; Padua, A. A. H.; Gomes, M. F. C. *Green Chem.* **2008**, *10*, 944.
(320) Berger, A.; de Souza, R. F.; Delgado, M. R.; Dupont, J. *Tetrahedron: Asymmetry* **2001**, *12*, 1825.
(321) Dyson, P. J.; Laurenczy, G.; Ohlin, C. A.; Vallance, J.; Welton, T. *Chem. Commun.* **2003**, 2418.
(322) Raeissi, S.; Schilderman, A. M.; Peters, C. J. *J. Supercrit. Fluids* **2013**, *73*, 126.
(323) Pomelli, C. S.; Chiappe, C.; Vidis, A.; Laurenczy, G.; Dyson, P. J. *J. Phys. Chem.* **2007**, *111*, 13014.
(324) Sakhaeinia, H.; Jalili, A. H.; Taghikhani, V.; Safekordi, A. A. *J. Chem. Eng. Data* **2010**, *55*, 5839.
(325) Jou, F. Y.; Mather, A. E. *Int. J. Thermophys.* **2007**, *28*, 490.
(326) Jalili, A. H.; Rahmati-Rostami, M.; Ghotbi, C.; Hosseini-Jenab, M.; Ahmadi, A. N. *J. Chem. Eng. Data* **2009**, *54*, 1844.
(327) Rahmati-Rostami, M.; Ghotbi, C.; Hosseini-Jenab, M.; Ahmadi, A. N. *J. Chem. Thermodyn.* **2009**, *41*, 1052.
(328) Sakhaeinia, H.; Taghikhani, V.; Jalili, A. H.; Mehdizadeh, A.; Safekordi, A. A. *Fluid Phase Equilib.* **2010**, *298*, 303.
(329) Revelli, A. L.; Mutelet, F.; Jaubert, J. N. *J. Phys. Chem. B* **2010**, *114*, 8199.
(330) Shiflett, M. B.; Niehaus, A. M. S.; Elliott, B. A.; Yokozeki, A. *Int. J. Thermophys.* **2012**, *33*, 412.
(331) Raeissi, S.; Peters, C. J. *Fluid Phase Equilib.* **2010**, *294*, 67.
(332) Kumełan, J.; Kamps, Á. P.; Tuma, D.; Maurer, G. *Ind. Eng. Chem. Res.* **2007**, *46*, 8236.
(333) Althuluth, M.; Kroon, M. C.; Peters, C. J. *Ind. Eng. Chem. Res.* **2012**, *51*, 16709.
(334) Ferguson, L.; Scovazzo, P. *Ind. Eng. Chem. Res.* **2007**, *46*, 1369.
(335) Florusse, L. J.; Raeissi, S.; Peters, C. J. *J. Chem. Eng. Data* **2008**, *53*, 1283.
(336) Shariati, A.; Peters, C. J. *J. Supercrit. Fluids* **2003**, *25*, 109.
(337) Shiflett, M. B.; Harmer, M. A.; Junk, C. P.; Yokozeki, A. *Fluid Phase Equilib.* **2006**, *242*, 220.
(338) Shiflett, M. B.; Harmer, M. A.; Junk, C. P.; Yokozeki, A. *J. Chem. Eng. Data* **2006**, *51*, 483.
(339) Shiflett, M. B.; Yokozeki, A. *J. Chem. Eng. Data* **2007**, *52*, 2007.
(340) Shiflett, M. B.; Elliott, B. A.; Yokozeki, A. *Fluid Phase Equilib.* **2012**, *316*, 147.
(341) Pison, L.; Lopes, J. N. C.; Rebelo, L. P. N.; Padua, A. A. H.; Gomes, M. F. C. *J. Phys. Chem. B* **2008**, *112*, 12394.
(342) Kumełan, J.; Kamps, Á. P.; Tuma, D.; Yokozeki, A.; Shiflett, M. B.; Maurer, G. *J. Phys. Chem. B* **2008**, *112*, 3040.
(343) Dong, L.; Zheng, D.; Sun, G.; Wu, X. *J. Chem. Eng. Data* **2011**, *56*, 3663.
(344) Dong, L.; Zheng, D.; Wu, X. *Ind. Eng. Chem. Res.* **2012**, *51*, 4741.
(345) Ren, W.; Scurto, A. M. *Fluid Phase Equilib.* **2009**, *286*, 1.
(346) Yokozeki, A.; Shiflett, M. B. *Ind. Eng. Chem. Res.* **2007**, *46*, 1605.
(347) Shi, W.; Maginn, E. *AIChE J.* **2009**, *55*, 2414.
(348) Li, G.; Zhou, Q.; Zhang, X.; Wang, L.; Zhang, S.; Li, J. *Fluid Phase Equilib.* **2010**, *297*, 34.
(349) Palomar, J.; Gonzalez-Miquel, M.; Bedia, J.; Rodriguez, F.; Rodriguez, J. J. *Sep. Purif. Technol.* **2011**, *82*, 43.
(350) Bedia, J.; Palomar, J.; Gonzalez-Miquel, M.; Rodriguez, F.; Rodriguez, J. J. *Sep. Purif. Technol.* **2012**, *95*, 188.
(351) Jureviciute, I.; Bruckenstein, S.; Hillman, A. R. *J. Electroanal. Chem.* **2000**, *488*, 73.
(352) Anthony, J. L.; Maginn, E. J.; Brennecke, J. F. *J. Phys. Chem. B* **2001**, *105*, 10942.
(353) Solinas, M.; Pfaltz, A.; Cozzi, P. G.; Leitner, W. *J. Am. Chem. Soc.* **2004**, *126*, 16142.
(354) Ortiz, A.; Galan, L. M.; Gorri, D.; de Haan, A. B.; Ortiz, I. *Ind. Eng. Chem. Res.* **2010**, *49*, 7227.
(355) Fallanza, M.; González-Miquel, M.; Ruiz, E.; Ortiz, A.; Gorri, D.; Palomar, J.; Ortiz, I. *Chem. Eng. J.* **2013**, *220*, 284.